Multivariate statistical modelling and analysis of compound events

Emanuele Bevacqua

PhD thesis

to obtain the academic degree

Doctor of Natural Sciences (Dr. rer. nat.)

submitted to the

Faculty of Natural Sciences
Department of Physics
University of Graz

First referee
Prof. Douglas Maraun
University of Graz, Austria

Second referee
Dr. Martin Widmann
University of Birmingham, UK

2019

Supervisor
Prof. Douglas Maraun
University of Graz, Austria

Co-supervisor
Dr. Martin Widmann
University of Birmingham, UK

Abstract

PhD Thesis
by Emanuele Bevacqua

Many extreme geophysical impacts result from compound events (CEs), i.e. from the joint occurrence of underlying contributing events. Here, a conceptual model is developed, which allows for assessing the CE hazard in present day and future climate. The model is implemented via pair-copula constructions and includes physical predictors which (i) provides insight into the processes underlying CEs, as well as into the temporal variability of CEs, and (ii) allows for statistical downscaling of CEs. Based on this model, (1) compound flooding (CF), that happens along low-lying coastal areas when a storm surge obstructs the precipitation runoff into the sea, and (2) soil moisture drought are studied.

(1) The results show that, in the present, the European locations experiencing the highest CF probability are mostly located along the Mediterranean Sea. In the future (RCP8.5 scenario), the CF probability will increase over Northern Europe, mostly due to an intensification of precipitation extremes. It is highlighted that local CF risk assessment should consider the dependence between CF drivers to avoid potential risk underestimation. In the future, CF should be considered as a potential hazard aggravating the risk caused by mean sea level rise in several European regions.

(2) Soil moisture drought is studied as a CE of precipitation and potential evapotranspiration (PET) in Europe during summer. Precipitation is found to be the main driver of soil moisture drought. In dry climates, where evapotranspiration (ET) is moisture limited in summer, PET does not improve the estimation of soil moisture. Thus, drought indices including PET should be interpreted carefully, within the context of the climate in which they are applied.

Also, based on this conceptual model, long compound hot and dry conditions in Europe are studied, and multi-site daily precipitation on Austrian river catchments are statistically downscaled. Thus, the model could be used for studying other CE types.

Zusammenfassung

Doktorarbeit
vorgelegt von Emanuele Bevacqua

Viele Naturkatastrophen resultieren aus *compound events* (CEs), d.h. aus gemeinsam auftretenden Gefährdungsereignissen. Es wird deshalb ein konzeptionelles Modell entwickelt, das die Beurteilung der CE-Gefahr ermöglicht. Das Modell ist via *pair-copula constructions* entwickelt und beinhaltet physische Prädiktoren, die (i) Einblicke in die Prozesse und in die zeitliche Variabilität der CEs liefern, und (ii) eine statistische Herunterskalierung der CEs ermöglichen. Basierend auf diesem Modell werden (1) Überflutungen (*compound flooding*, CF), die sich entlang der Küstengebiete ereignen, wenn eine Sturmflut den Niederschlagsfluss ins Meer verhindert und (2) Bodentrockenheit untersucht.

(1) Im ersten Fall wird gezeigt, dass in Europa die höchsten CF-Wahrscheinlichkeiten überwiegend entlang der Mittelmeerküsten auftreten. In der Zukunft (RCP8.5 Szenario) wird die CF-Wahrscheinlichkeit, vor allem aufgrund einer Intensivierung der Niederschläge, in Nordeuropa zunehmen. Um eine mögliche Unterschätzung des Risikos zu vermeiden, sollte eine lokale CF-Risikobewertung die Abhängigkeit zwischen den CF-Treibern berücksichtigen. In Zukunft sollte CF als potentielle Gefahr betrachtet werden, da sie das Risiko eines mittleren Meeresspiegelanstiegs verschärft.

(2) Im zweiten Fall wird die Bodentrockenheit als CE von Niederschlägen und potentieller Evapotranspiration (PET) in Europa im Sommer untersucht. Es ergibt sich, dass Niederschläge der Haupttreiber für Bodentrockenheit sind. In trockenen Klimazonen, in denen die Evapotranspiration (ET) im Sommer begrenzt ist, verbessert PET zur Abschätzung der Bodenfeuchte nicht. Eine sorgfältige Interpretation von Trockenheitsindizes einschließlich PET im Kontext des jeweiligen Klimas ist notwendig.

Auf der Grundlage dieses konzeptionellen Modells wurden lange, heiße und trockene Bedingungen untersucht und tägliche Niederschläge statistisch herunterskaliert. In weiterer Folge könnte das Modell für das Studium anderer CE-Typen verwendet werden.

Acknowledgements

I have wished to actively conduct scientific research in the field of climate science since I was very young. Thus, working on this PhD has represented a very important life achievement for me. I am really thankful to all who have supported me during the PhD.

At first place, I want to thank my supervisor Prof. Douglas Maraun. I would like to express my sincere appreciation to Douglas for supporting me, and providing guidance whenever I needed it, but also for providing me with freedom when it was important. I am happy and proud that I could work with Douglas and learn through his supervision during these years. I hope we will actively continue having fruitful and stimulating scientific discussions in the future.

As a PhD student, I have been involved in the international research project CE:LLO, therefore, I want to express my thanks to the other people who - officially or not - have taken part in the project. Everyone has been helpful whenever it was necessary, and I could learn a lot discussing with the project members. I hope that collaborations with them will continue in the future as well. I thank Dr. Mathieu Vrac, who was a very helpful and friendly mentor during my research stay in the beautiful Paris. Similarly, I thank Dr. Ingrid Hobæk Haff and Prof. Arnoldo Frigessi for hosting me during my short research stay at the Norwegian Computing Center in Oslo. Ingrid was always very open to sharing her deep expertise on multivariate statistical modelling. I thank also the people from Birmingham: Dr. Martin Widman and (almost Dr.) Colin Manning. In these years, I could share with Colin several offices and lot of funny experiences worldwide; and I also find working and discussing very stimulating with him. I would also like to thank the other colleagues from the Joint Research Centre (JRC) in Ispra, especially Dr. Michalis Vousdoukas and Evangelos Voukouvalas. I am very grateful to the Volkswagen Foundation for funding the CE:LLO project (Az.: 88468) and, therefore, my PhD.

Throughout my PhD, I could work at GEOMAR in Kiel (Germany) and at LSCE in Paris (France), while I am currently working at Wegener Center in Graz (Austria). The working environment in GEOMAR, LSCE, and Wegener Center is very stimulating, and I am happy that I could discuss with so many interesting and pleasant people there. At GEOMAR I shared the office with Dr. Edmund Meredith and Dr. Claudia Volosciuk, who made for a very nice working environment. In Paris I had a great time thanks to many amazing people I met there! The Wegener Center of Graz is a stimulating and friendly environment directed by Prof. Gottfried Kirchengast with exemplary passion and commitment. I thank everyone from Wegener Center, for example, Karin Eisner, Bettina Schlager, and Sabine Tschuertz from the administration staff: they have always been really professional and funny! A huge thanks goes to the Reloclim group members for the friendly atmosphere and for sharing their knowledge during exciting discussions. I thank my office colleagues Dr. Thomas Mendlik, Dr. Martin Jury, Laurin Herbsthofer, and David Kohlfuerst for the friendly working environment and for helping whenever necessary.

Furthermore, I really thank all the other people who crossed my way during these years both in the academic and non-academic environments. With some of these people I had fun and/or discussions that definitely inspired me to improve as a person and scientist. I really enjoyed discussing with people from several disciplines that I met during conferences, workshops, and Skype calls. On this topic, I thank Dr. Jakob Zscheischler and ETH Zurich for guesting me at the "Workshop on addressing the challenge of compound events", and the people of the *compound event community* for stimulating discussions. Also, I thank Dr. Erich Fischer and Prof. Reto Knutti for fruitful and inspiring chats.

I am thankful to other people of the scientific community who contributed to the achievement of the results of this thesis. I thank the reviewers who constructively commented on our manuscripts to improve their quality, and the people who recognised the value of our work during these years. I am grateful to the community that contributes to model, software, and data set developments. In particular, I thank the developers of Linux, the free software environment R, and Latex. I acknowledge the FLUXNET community, the Italian National Institute for Environmental Protection and Research (ISPRA), and Arpae Emilia-Romagna for providing important data. I acknowledge the World Climate Research Programs Working Group on Coupled Modelling, which is responsible for CMIP, and the climate modeling groups for producing and making available their model output. I thank European Centre for Medium-Range Weather Forecasts (ECMWF) for providing ERA-Interim reanalysis data. I acknowledge FES2012 which was produced by Noveltis, Legos and CLS Space Oceanography Division and distributed by Aviso, with support from Cnes. I acknowledge the E-OBS dataset from the EU-FP6 project ENSEMBLES and the data providers in the ECA&D project.

Last but not least, special thanks go to my family and to the *Kielerin* Sonja for their constant support.

To Franca and Pino...

Contents

1 Introduction 3

2 Modelling of compound events 9
- 2.1 A changing climate . . . 9
- 2.2 Climate models, downscaling, and impact models . . . 11
- 2.3 Compound events . . . 13
  - 2.3.1 Compound flooding (CF) . . . 14
    - 2.3.1.1 Modelling CF . . . 15
  - 2.3.2 Soil moisture droughts . . . 18
    - 2.3.2.1 Modelling of soil moisture . . . 19
- 2.4 Advantages and limitations of statistical modelling of compound events . 20

3 Methods 23
- 3.1 Conceptual conditional model for compound events . . . 23
- 3.2 Statistical methods . . . 25
  - 3.2.1 Copulas . . . 27
  - 3.2.2 Tail dependence . . . 27
  - 3.2.3 Pair-Copula Constructions . . . 28
    - 3.2.3.1 Sampling and conditional sampling from vines . . . 29
- 3.3 Multivariate return periods . . . 30

4 Multivariate statistical modelling of CF in Ravenna (Italy) 33
- 4.1 Introduction . . . 33
- 4.2 Data . . . 35
- 4.3 Model development . . . 35
  - 4.3.1 Impact function . . . 37
  - 4.3.2 Meteorological Predictor Selection . . . 37
- 4.4 Results . . . 41
  - 4.4.1 Unconditional (3-dimensional) model . . . 41
  - 4.4.2 Conditional (5-dimensional) model . . . 42
- 4.5 Discussion and conclusions . . . 45

5 Higher CF probability in Europe under anthropogenic climate change 49
- 5.1 Introduction . . . 49
- 5.2 Data and Methods . . . 50
- 5.3 Results . . . 54
- 5.4 Discussion and conclusions . . . 56

6 Soil moisture drought in Europe: a compound event of precipitation and potential evapotranspiration on multiple timescales 59
6.1 Introduction 59
6.2 Data 60
6.3 Model development 61
6.3.1 Meteorological predictor selection 62
6.3.2 Model evaluation metrics 64
6.4 Results 64
6.4.1 Model performance 65
6.4.2 Assessment of contributing variables to soil moisture 65
6.4.3 Assessing the relevance of the dependence between the contributing variables 69
6.4.4 Relevance of PET over short and long integration periods 72
6.5 Discussion and conclusions 73

7 Conclusions 77
7.1 Summary and implications 77
7.2 Outlook: future steps in the compound event research 82

A Appendix 87
A.1 Homogenisation of river level data 87
A.2 CDVineCopulaConditional: an R-package for sampling from conditional C- and D-vine copulas 87
A.3 Vines and sampling procedure 88
A.4 Statistical inference of the joint pdf 91
A.4.1 Selected pair-copula families 94
A.5 Model and return periods uncertainty estimation via parametric bootstrap 94
A.6 Incorporation of the AR(1) in the unconditional model 96
A.7 Brier score for extreme values 97
A.8 Cross-validation procedure 98

B Appendix 99
B.1 Relative sea level rise influence on extreme sea level 99
B.2 Bivariate validation 99
B.3 Supplementary figures 101

C Appendix 109
C.1 Statistical inference of the multivariate probability density function 109

List of Figures 110

List of Tables 113

List of Acronyms 115

Bibliography 117

Preface

This thesis is based on works which have been published, submitted, or otherwise are in preparation for publication. These works, including the associated information about - mostly - my individual contributions, are listed below. Information about the contribution of other authors, which was clearly very important, may be found in the published papers.

1. **Bevacqua, E.**, Maraun, D., Haff, I. H., Widmann, M., and Vrac, M. (2017). "Multivariate statistical modelling of compound events via pair-copula constructions: analysis of floods in Ravenna (Italy)". Hydrology and Earth System Sciences, 21, 2701-2723, DOI:10.5194/hess-21-2701-2017.

   Contribution. EB developed the study, the statistical model, carried out the analysis, interpreted the results, and wrote the paper, with contributions from the coauthors. DM had the initial idea for the study.

2. **Bevacqua, E.** (2017). "CDVineCopulaConditional: an R-package for conditional sampling from multivariate copula decomposed via C- and D-vines". R-package.

   Contribution. EB developed and implemented the algorithms of the package, and wrote the package documentation.

3. Manning, C., Widmann, M., **Bevacqua, E.**, Van Loon, A. F., Maraun, D., and Vrac, M. (2018). "Soil moisture drought in Europe: a compound event of precipitation and potential evapotranspiration on multiple timescales". Journal of Hydrometeorology, Journal of Hydrometeorology, DOI:10.1175/JHM-D-18-0017.1.

   Contribution. EB contributed to the design of the study, to the development and implementation of the statistical model, to interpret the results, and to the writing process.

4. **Bevacqua, E.**, Maraun, D., Vousdoukas, M. I., Evangelos, V., Vrac, M., Mentaschi, L., and Widmann, M. (2019). "Higher probability of compound flooding from precipitation and storm surge in Europe under anthropogenic climate

change". Science Advances, Vol. 5, no. 9, eaaw5531, DOI: 10.1126/sciadv.aaw5531. (This paper was under review at the time of the thesis submission.)

Contribution. EB conceived the study and designed the work, with DM. EB carried out the data analysis and performed the astronomical tide simulations. EB wrote the paper with contributions from the coauthors. All authors discussed the results and commented on the manuscript.

5. Switanek, M. B., Maraun, D., and **Bevacqua, E.** (2018). "Stochastic downscaling of gridded precipitation to spatially coherent sub-grid precipitation fields using a transformed Gaussian model". In preparation.

   Contribution. EB has contributed to the model development, to the design of the study, and to the writing process.

6. Manning, C., Widmann, M., **Bevacqua, E.**, Van Loon, A. F., Maraun, D.,and Vrac, M. (2019). "Increased probability of compound long-duration dry & hot events in Europe during summer (1950-2013)". Environ. Res. Lett. 14 094006. DOI: 10.1088/1748-9326/ab23bf. (This paper was under review at the time of the thesis submission.)

   Contribution. EB has contributed to conceiving and designing the study, to developing the statistical model, and to interpreting the results.

1. Introduction

"Although there may be no immediate cause for alarm about the consequences of carbon dioxide increase in the atmosphere, there is certainly need for further study. We need to have a better assessment of where the carbon dioxide goes after it has been dispersed from our chimneys [...] The development of increasingly sophisticated numerical simulation of the global climate seems the only possible approach in spite of the effort involved"[139]

- John Stanley Sawyer, Nature (1972)

The evidence of anthropogenic climate change continues to strengthen[153], and the associated changes in extreme weather and climate events threat the society. To reduce the impacts arising from climate change, societies can adapt to the changing risk and/or mitigate greenhouse gas emission causing anthropogenic climate change. The planning of adaptation and mitigation measures is mostly based on model projections of the future climate. However, climate models are numerical representations of our current knowledge of the climate system, and model simulations are affected by uncertainties which are partially irreducible because driven by the chaotic behaviour of the climate system. But another part of the uncertainties is driven by climate model errors, which can be reduced through a better understanding of the climate system. Thus, such a better understanding would contribute providing more credible future climate projections, with unevaluable benefit to society. The climate community has done much effort to increase our knowledge of the climate system, however, many challenges still need to be addressed. One of these challenges is the understanding of many of the extreme impacts that are driven by multiple events.

On the 6^{th} of February 2015, a low-pressure system that developed over the north of Spain moved across the Island of Corsica into Italy. The low pressure itself (Figure 1.1) and the associated southeasterly winds drove a storm surge along the northern Adriatic coast, especially in Ravenna (Italy). There, alongside the storm surge, large amounts of precipitation fell in the surrounding area causing high values of discharge in small rivers

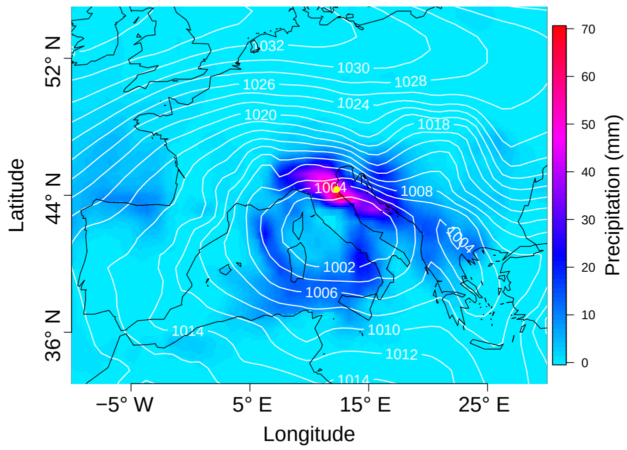

Figure 1.1: **Atmospheric conditions during a compound flooding (CF) in Ravenna.** Sea level pressure and total precipitation on 6^{th} February 2015, when the coastal area of Ravenna (indicated by the yellow dot) was hit by a CF.

near the coast. These river discharges were partially obstructed from draining into the sea by the storm surge, which then contributed to major flooding along the coast. Such a *compound flood (CF)* is a typical example of a *compound event (CE)*. CEs result from a combination of multiple events (represented by the *contributing variables*), which in isolation might not be extreme themselves, but when occurring simultaneously or in rapid succession have an extreme impact[199] (i.e. the *CE impact*). Likewise, the temporal persistence of known extreme events can strongly exacerbate the induced impacts. Understanding CEs is a complex undertaking[84], as it requires the understanding of multiple phenomena, and how these interact to drive the extreme CE impact. In addition to (1) CF, other examples of CEs are: (2) soil moisture drought, which can have a negative impact on agriculture, and it is driven both by scarcity of precipitation and by the evapotranspiration; (3) persistent concurrent meteorological drought and heatwave conditions, whose combination can increase the likelihood of wildfires, threaten vegetation health, e.g., prompting tree mortality, and negatively affect the global economy[46,103,150,207,214].

Despite many extreme geophysical impacts are caused by CEs, and the associated major economic and human losses[215], climatological studies have mostly focused on univariate and individual, mostly short-term, events; such an approach may lead to an underestimation of the risk associated with extreme events. Furthermore, when the impact is addressed as compound, the dependencies among the contributing variables often are not taken explicitly, or not taken at all, into account during the risk assessments, which may lead to serious risk underestimation[19,20,214]. Studies have only started focussing on CEs, as underlined by the Intergovernmental Panel on Climate Change (IPCC), and more research addressing this class of events is required[147]. For understanding the risk associated with CEs in present and future climate, some questions are critical: (1) Which are the contributing variables (and the associated physical drivers) defining CEs? (2) How is the CE risk assessment influenced by the dependence of the CE contributing variables? (3) Both for present and future climate, which are the locations most prone to a given CE impact? Furthermore, as climate models are crucial tools for understanding how CEs will change in the future, the following questions are relevant: (4) How do existing models represent the CE contributing variables and the associated physical drivers? (5) How are these CE physical drivers expected to change in the future? Thus, (6) what is the probability of CEs to occur in future climate and what are the associated uncertainties?

This thesis aims to advance the research by developing the first conceptual model for CEs, implemented via multivariate statistical methods, that allows for answering the mentioned questions for a given CE type. Based on this model, we study CF and soil moisture drought. This thesis thereby addresses some of the key challenges identified in the World Climate Research Programme (WCRP) Grand Challenges on Weather and Climate Extremes, which highlighted the relevance of CEs to climate science[207].

Multivariate statistical modelling of CEs offers many advantages, however no statistical models have been developed for CEs, and here we aim to close this research gap. Statistical modelling of CE can be employed for (1) downscaling of CEs, which is required to extend the CEs risk assessment to the past or future climate, where climate models either do not simulate realistic values of the local variables driving the extreme events or do not simulate them at all. In general, downscaling of CE is possible both via dynamical models and with a combination of dynamical and statistical models; but employing statistical models often is a valid and computationally less expensive alternative to dynamical models. Furthermore, statistical and dynamical modelling of CEs are exchangeable only to some extent, indeed statistical models are useful for (2) validating the output of the dynamical models themselves[70], e.g. for validating the covariabity of the contributing variables of CEs[20]. Also, multivariate statistical modelling of CEs allows for: (3) understanding the physical drivers of CEs and of their changes through, e.g., conditional sensitivity analysis[19,20,93,94]. (4) Extrapolating statistical estimates of extreme events, e.g. return periods, where purely empirical estimates are likely biased due to the rarity of the extreme events; statistical modelling also allows for (5) obtaining uncertainty ranges around such estimates.

However, due to the complex dependence structure between the CE contributing variables, advanced statistical models are necessary to statistically model the multivariate probability density function (pdf) of the CE variables. In this thesis, we employ Pair-copula constructions (PCCs). These have been recently introduced in climate science[70,86,125] and are a very promising tool for modelling CEs. Modelling CEs employing a standard multivariate Gaussian distribution would not provide satisfactory results. The Gaussian distribution would assume that the dependencies between all the variable pairs are of the same type and without any dependence of the extreme events, and that all of the marginal distributions are Gaussian. To solve the latter problems, the use of copulas has been introduced in geophysics and climate science[135,141], and it is now widely used when studying CEs[198,214]. However, multivariate parametric copulas lack flexibility when modelling systems with high dimensionality, where heterogeneous dependencies exist among the different pairs[1]. This lack of flexibility of copulas would be a limitation for many types of CEs. Thus, here we use PCCs, which decompose the dependence structure into bivariate copulas and give greater flexibility in modelling generic high-dimensional systems compared to multivariate parametric copulas[1,2,15,67].

In this context, the objectives of this thesis can be divided into four parts.

- **Conceptual model development.** Develop a conceptual model for CEs in two versions. A non-conditional version, which allows for resampling the observed CE characteristics, and get robust risk estimates, including risk uncertainties. A conditional version, which allows - in addition - for simulating the CE impact given predictors, e.g., large-scale meteorological processes that provide insight both into the past and future temporal variability of CEs and in the involved physical mechanisms. As described below, the model will be employed for studying CEs, thus the model performances will be extensively assessed. In particular, to implement the model, we will use PCCs and test their efficiency for modelling CEs. The conceptual model has been presented in Bevacqua et al.[19], and the routines to sample from conditional pdfs decomposed via PCCs were published within the *CDVineCopulaConditional* R-package[18].

Based on the developed model, we will study:

- **CF in Ravenna (Italy).** Driven by the event of the 6^{th} of February 2015, we study CF in Ravenna. To explicitly quantify the flooding probability, we define the CF impact, i.e. the water level driven by sea and river levels. We use meteorological predictors to extend the analysis to the past, and get a more robust hazard assessment. We quantify the CF return periods including uncertainty estimates, and the effect of the dependence between the contributing variables on the final return period estimate. This part of the work is presented in Bevacqua et al.[19].
- **Present and future CF probability along the European coast.** Despite the CF relevance, a comprehensive CF assessment beyond individual locations at the country scale is missing. Furthermore, extreme precipitation[123], river flooding[65],

and extreme sea levels[57,64,195] are expected to increase under future climate change. Therefore it is likely that also the CF probability will increase along with these driving processes. However, future CF probabilities, taking into account future changes of precipitation, storm surges, waves, and astronomical tides, have not been assessed yet. In Bevacqua et al.[20], based on climate model simulations, we estimate the CF probability along the European coast both in the present and in future climate under the business-as-usual (RCP8.5) scenario. Our study identifies regions potentially facing CF, and detect the physical drivers leading to future changes in the CF hazard. Furthermore, here the conceptual model is also used to evaluate how climate models represent the CF drivers.

- **The contribution of potential evapotranspiration (PET) and precipitation to soil moisture drought in Europe.** Soil moisture observations are sparse, and an explicit representation of soil moisture via physically based land surface models is difficult. Thus, drought indices incorporating precipitation and temperature through PET are often employed as proxies of soil moisture[35,187]. However, the question remains whether such indices can provide an adequate representation of soil moisture drought[58]. Understanding the contribution of PET and precipitation to soil moisture in different climates can help in the interpretation of soil moisture future changes as depicted by drought indices. In Manning et al.[93], we have analysed soil moisture drought in wet, transitional and dry climates in Europe during summer as a CE of precipitation and PET. We assessed the individual roles of these two variables (integrated on multiple timescales) and that of their dependence structure to the estimation of soil moisture.

Furthermore, this conceptual model has been employed for multivariate statistical downscaling of the precipitation field in Switanek et al.[166]. Also, the framework has been used for studying persistent concurrent drought and heatwave conditions over Europe in Manning et al.[94]. These two works will be only briefly discussed in the conclusions of the thesis (chapter 7).

How to read the thesis. In chapter 2, I provide a general description of CEs in the context of the climate system, including a review of the typical modelling approaches used for CF and soil moisture drought. In chapter 3, I present the conceptual model and the main statistical methods that will be used in the thesis; this part is important to understand the next chapters, where the conceptual model will be employed. The studies of CF in Ravenna, CF along the European coast, and soil moisture drought in Europe are presented in chapters 4, 5, and 6, respectively. These three chapters are independent of each other, and each of them includes a final discussion and conclusions.

The conclusions of the thesis, including a summary of the results, and an outlook on possible future research will be given in chapter 7. In the text, sometimes, the reader will be directed to the appendices for more technical details.

2. Modelling of compound events

In this chapter, I give a brief overview of the modelling approaches used in climate science in the context of climate change. Then, I introduce compound events (CEs), focussing on the description of compound flooding and soil moisture drought, and on how these two CEs have been modelled in the literature so far. The last section of the chapter provides a discussion of advantages and limitations of statistical modelling of CEs. Part of the content of this chapter can be found in Bevacqua et al.[19,20] and Manning et al.[93].

2.1 A changing climate

Climate is usually defined as *the "average weather", or more rigorously, as the statistical description in terms of the mean and variability of relevant quantities over a period of time ranging from months to thousands or millions of years*[32]. The classical period is 30 years, as defined by the World Meteorological Organization (WMO)[32].

Climate changes both because of natural and anthropogenic reasons[95]. In general, climate variations may result from internal interactions between the components of the climate system, such as the interaction between atmosphere and ocean in the tropical Pacific that leads to the Niño-Southern Oscillation (ENSO) (Fig. 2.1c). Furthermore, climate can vary because of external forcings such as volcanic eruptions and changes in solar irradiation. In addition to these naturally-driven external forcings, the last century has seen anomalous greenhouse gas (GHG) emissions that has led to an average global warming[128]. The accepted evidence of the current climate change is based on multiple indicators, such as increasing surface temperature (Fig. 2.1a), which in turn leads to ice melting (Fig. 2.1b), and increasing precipitation extremes[44], sea level[57,64,195], and upper-ocean heat content[153]. Both models and theory agree on attributing much of global warming to anthropogenic GHG emission: the current average global temperature would have been substantially lower without anthropogenic GHG emission (Fig. 2.2).

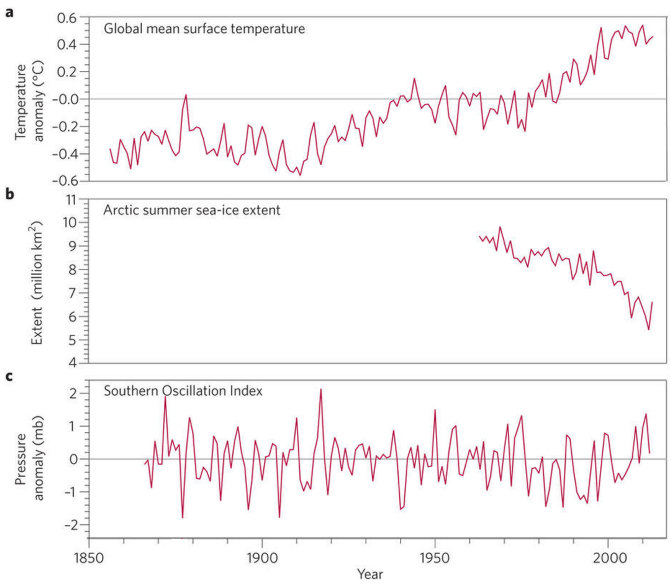

Figure 2.1: **Physical evidence of climate change.** **(a)** Global annual mean surface temperature anomaly. **(b)** Arctic summer sea-ice extent. **(c)** Annual mean Southern Oscillation (El Niño/Southern Oscillation) Index derived from surface pressure measurements at Tahiti and Darwin. Reprinted and adapted from Shepherd [153].

Climate change is one of the major threats to humanity of the 21st century. Without adaptation to or mitigation of climate change, human and economic losses will be intolerable by society. For example, without adaptation to sea level rise, 0.2-4.6 % (depending on the future GHG emissions) of the global population is expected to be flooded annually in 2100, therefore, although very expensive, adaptation will be widespread to overcome damages which would otherwise be intolerable [64]. To contribute addressing the climate change challenge, the IPCC was set up in 1988 by the World Meteorological Organization (WMO) and United Nations Environment Programme (UNEP). The IPCC provides policymakers with reports of the current scientific knowledge about climate change and its impacts, and with options for adaptation and mitigation.

To assess the climate change impacts, models are employed to obtain projections of the future climate. Such projections are climate predictions conditional on plausible scenarios of future GHG concentration trends. The IPCC Fifth Assessment Report has adopted four scenarios, namely the Representative Concentration Pathways RCP2.6, RCP4.5, RCP6, and RCP8.5, whose definition is based on the concept of radiative forcing. The radiative forcing is "the rate of energy change per unit area (W/m^2) of the globe as measured at the top of the atmosphere" [131], and it is used as a measure of the influence that GHG concentration has in altering the balance of incoming and outgoing energy in the Earth-atmosphere system.

The RCP scenarios prescribe a range of plausible future radiative forcings (Fig. 2.3). For example, the RCP8.5 corresponds to a radiative forcing increase of 8.5 W/m^2 in

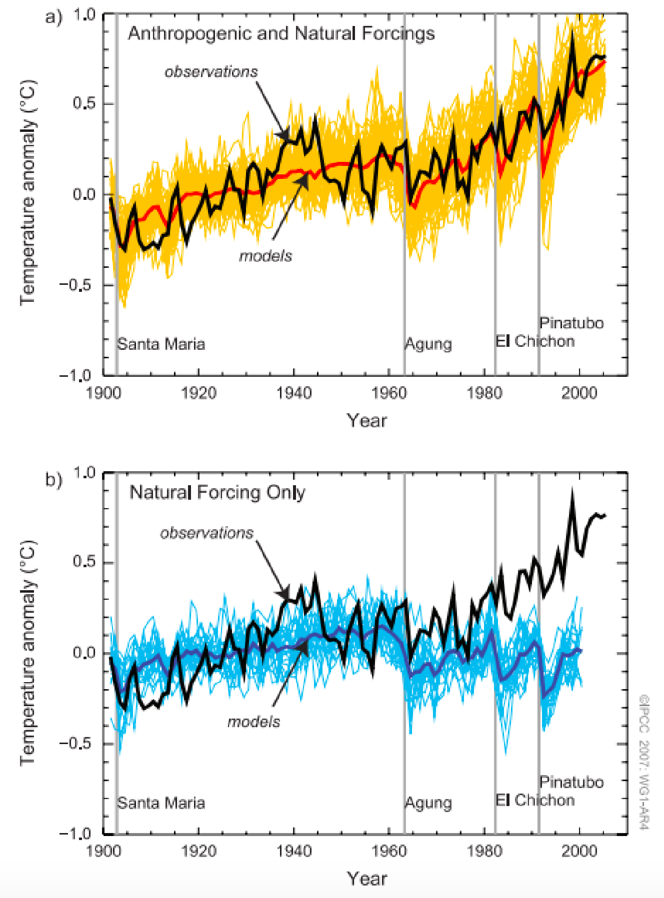

Figure 2.2: **Historical global mean surface temperature anomalies.** Anomalies relative to the period 1901 to 1950, as observed (black line) and as obtained from simulations with both **(a)** anthropogenic and **(b)** natural forcings. **(a)** The thick red curve shows the multi-model ensemble mean and the thin yellow curves show the individual simulations. Vertical grey lines indicate the timing of major volcanic events. **(b)** As in **(a)**, except that the simulated global mean temperature anomalies are for natural forcings only. The thick blue curve shows the multi-model ensemble mean and the thin lighter blue curves show individual simulations. Reprinted from Randall et al.[128].

2100 relative to pre-industrial conditions in 1750 (Fig. 2.3b)[169]. This scenario assumes that GHG emissions will continue increasing until the end of the century (Fig. 2.3a), and atmospheric CO_2 concentrations will more than triple by 2100 relative to 1750. In 2011 the radiative forcing was already about 2.29 ([1.13-3.33]) W/m^2 larger than in 1750 (ref.[164]). In chapter 5, we use the RCP8.5 when estimating future changes in the probability of potential compound flooding in Europe.

2.2 Climate models, downscaling, and impact models

While considerations about certain climate phenomena can be deduced by purely theoretical arguments, climate simulations are relevant both to get a confirmation of the

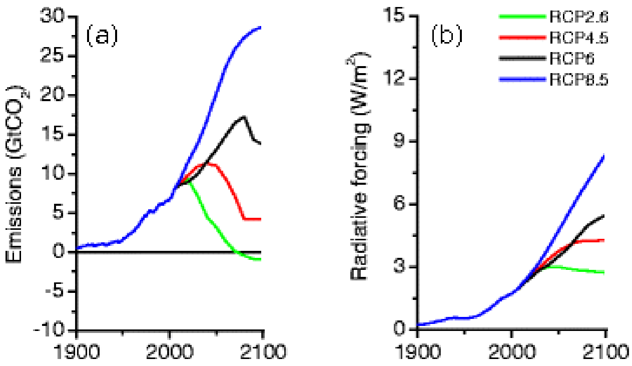

Figure 2.3: **Representative Concentration Pathways (RCPs).** **(a)** Annual total CO_2 emissions in Gigatons of Carbon (GtC) associated with the four RCPs (CO_2 is not the only greenhouse gas, however its emission is the main driver of anthropogenic global warming). The corrsponding radiative forcing is in **(b)**. For example, the RCP2.6 could be reached only through aggressive greenhouse gas reduction. Negative emissions implies that special technologies would be used to remove CO_2 from the atmosphere. Image adapted from Van Vuuren et al.[184].

underlined assumptions and to get a more in-depth understanding of the phenomena themselves. For example, the current intensification of precipitation extremes under global warming is based on a simple physical relation from Clausius-Clapeyron, stated between 1834 and 1850 from the two scientists giving the name to the relation. Then, around 1960-1980, changes in precipitation extremes have been projected for the future based on climate model simulations[44], i.e., models have confirmed the theoretical expectation. Furthermore, high-resolution climate models are still employed to better understand complex physical mechanisms behind the amplification of precipitation extremes, such as the super Clausius-Clapeyron precipitation scaling[83], and cloud-cloud interactions[111]. Thus, climate models are a fundamental tool for better understanding the climate system.

Climate models are especially important to obtain projections of the future climate. Observations of geophysical variables, such as temperature, precipitation, and river discharge, are suitable for monitoring the current state of the climate. However, observations are often too short in time and too sparse in space to assess the current risk associated with extreme events. Furthermore, the climate is changing, and thus climate model simulations, although affected both by biases and uncertainties[98,153], are necessary to provide stakeholders interested in the local climate with future climate projections.

As GCMs have a coarse resolution, they do not explicitly resolve the regional scale topography and physical processes leading to many extreme events, such as precipitation extremes. Therefore, downscaling attempts to bridge the gap between the GCM coarse resolution, and the smaller scale required for assessing local impacts[98]. Downscaling is based on the assumption that the GCM represents well the large-scale atmospheric circulation driving the local variable of interest. Two major downscaling approaches exist. *Dynamical downscaling*, where the output of the GCM is used to drive a higher resolution, dynamical, regional climate model (RCM), to derive the local weather in greater detail. *Statistical downsclaing*, where a statistical relationship is established between large-scale conditions (such as the sea level pressure and wind fields) and the local meteorological variable of interest (such as precipitation); the statistical relationship is then applied to the GCM output to derive the local variable of interest.

To quantify climate-related impacts, such as storm surges, an additional model, which here is referred to as *impact-model*, is required. In fact, many impacts of interest are not simulated by GCMs or RCMs, as it is the case, e.g., for storm surges. In other cases, the impact of interest may not be realistically simulated by GCMs or RCMs. For instance, standard GCMs do not simulate realistic runoff[47,102,172] and soil moisture (if it is simulated), such that additional hydrological modelling is required to estimate the flooding and soil moisture drought, respectively. The additional impact-model can be driven by GCM or downscaled GCM products, and can be of different nature, e.g., statistical or hydrodynamical.

2.3 Compound events

CEs are multivariate extreme events in which the individual contributing events (represented by *contributing variables*) may not be extreme themselves, but their joint occurrence causes an extreme *(CE) impact*[19,84,93,215]. The CE impact may be an hydrological variable such as a gauge level for compound floods, or other relevant variables such as fatalities or economic losses. CEs have received little attention so far, as underlined in the report of the Intergovernmental Panel on Climate Change on extreme events[147].

CEs are responsible for a very broad class of impacts on society. For example, heatwaves amplified by the lack of soil moisture, which reduces the latent cooling, may be classified as CEs[45,143]. The impact of drought cannot be fully described by a single variable[107,156]: analyses have been carried out which consider drought severity, duration[156], maximum deficit[133], as well as the affected area[149]. Another example of CE includes fluvial floods resulting from extreme rainfall occurring on a wet catchment[120,215]. In this thesis, we will focus on compound flooding and soil moisture drought, which will be discussed more in detail in the next sections.

Modelling CE impacts is more difficult than modelling impacts driven by a single variable. Modelling an impact driven by a single variable is complex as a chain of several models may be required (e.g., modelling a storm surge may require to employ: a GCM, an RCM, and a storm surge model). But modelling CEs is more difficult as it requires to consider several variables (e.g., the compound flooding level is estimated based on the storm surge, the river discharge, and the interaction of these two components). Therefore, CE modelling can be computationally very expensive. Furthermore, modelling CE impacts might require - with respect to modelling single-variable driven impacts - a further step for evaluating (and eventually selecting) the climate models used to assess the CE impact. In fact, climate models need to be evaluated before being used for impact assessments. But while the limitations of climate models in representing single variables have been widely investigated, it is not clear how well climate models can capture the multivariate nature of many CEs[30,43].

2.3.1 Compound flooding (CF)

Compound flooding (CF) is an extreme event taking place in low-lying coastal areas as a result of co-occurring high sea level and large amounts of runoff, caused by precipitation. The impact from the two hazards occurring individually can be significantly lower than the result of their interaction[19,84,147,198]. Prominent examples of CF from Europe, the area analysed in this thesis, are the Thames flood in London, 1928; the flash flood in Lisbon[177], 1967; the Avon flood in Bristol, 2014; and the Ravenna flood[19] in 2015. In 2012, the Netherlands almost experienced a flooding of the water board Noorderzijlvest, which led to precautionary evacuation[60,182]. The recently released pan-European (though not fully comprehensive) HANZE database[118] lists 24 co-occurrences of storm surges and river floods along the Irish, UK, Belgian and Polish coasts, the French Atlantic and Mediterranean coast, and the Italian Adriatic coast.

Co-occurring storm surge and heavy precipitation are driven by deep low-pressure systems[198]. Whereas precipitation extremes alone can be caused by convection without intense cyclonic activity[124], the latter is a precondition for extreme surges (Fig. 2.4). Intense cyclones drive storm surges through strong winds pushing water towards the coast, and the barometric pressure effect[19,165]. CF can be caused by several mechanisms[198]. (1) A storm surge can block or slow down the precipitation drainage into the sea[19], causing flooding along the coast[182,198]. Runoff from a river may require a certain time to drain into the sea such that precipitation may have to occur well before the storm surge. Similarly, (2) flood levels of a storm surge may be amplified by any significant amount of precipitation[198]. Finally, (3) a flood may occur when precipitation falls on wet soil that is saturated by a preceding storm surge. The relative importance of these mechanisms in a particular location depends both on the local climate and topography[198].

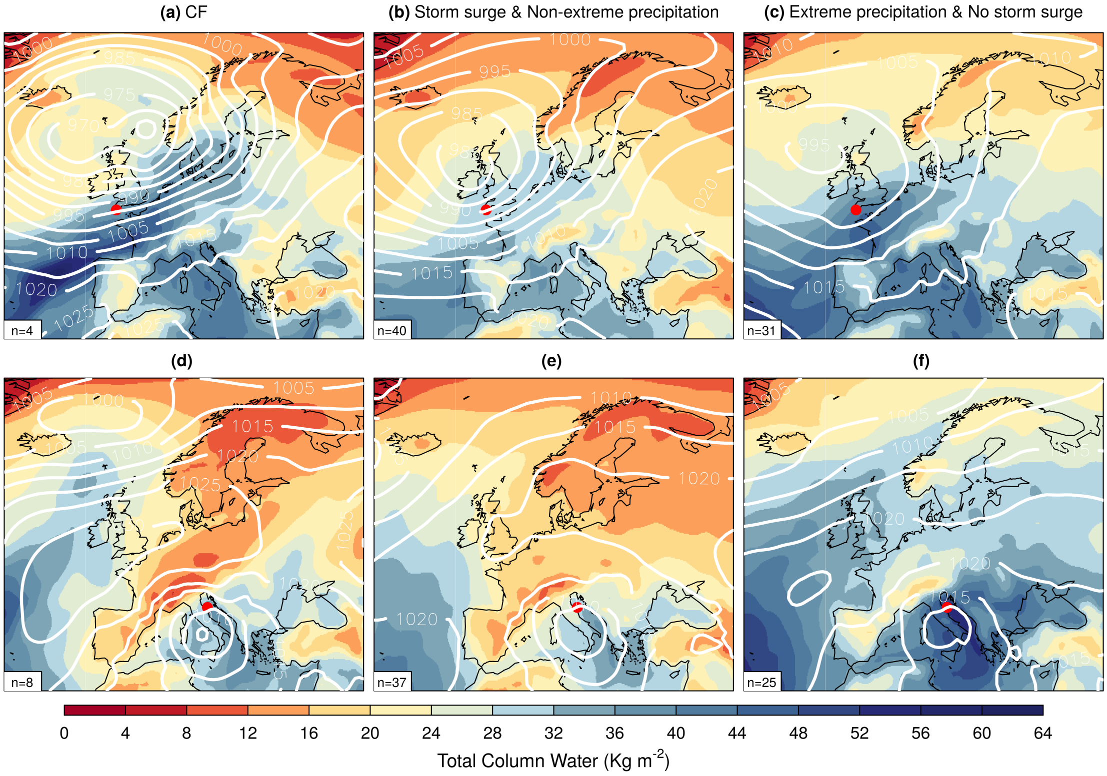

Figure 2.4: **Synoptic weather conditions driving extreme events on coastal locations.** Composite maps of sea level pressure (hPa, in white) and total column water fields computed over days where extreme events ($> 99.5^{th}$ percentile) occurred in Plymouth (UK, top) and Ancona (Italy, bottom) indicated by the red dots (based on ERA-Interim data, 1980-2014). Here, the astronomical tide component of the sea level is not considered to focus only on the meteorological driven part. Extreme events type: (**a**,**d**) compound flooding (CF), (**b**,**e**) storm surge but not extreme precipitation, (**c**,**f**) extreme precipitation but not storm surge. The total number of extreme events considered for computing the composite maps is shown at the bottom-left corner of the panels. Storm surges include the wave setup contribution[195].

2.3.1.1 Modelling CF

A complete CF assessment requires the quantification of the water level of the flooding. Despite CF may happen following the three different mechanisms listed above[20,198], so far studies that have quantified the CF water level have focussed on CF in estuarine regions only (the first mechanism of the list). In these studies, the CF water level is measured through a river gauge which is influenced both by the sea level and the river discharge upstream. Furthermore, several studies have analysed the potential CF probability (along the UK[165], Australia[210], and US[198] coasts), based on the probability of co-occurring precipitation and sea level extremes. The limitation to these two approaches only is explained by (i) the novelty of the CF topic, and by (ii) the availability of only sparse data of the CF water level. The latter makes the modelling of CF challenging, as observations are necessary to calibrate and/or validate models. Indeed, we[19] and other recent literature[119] have suggested to increase the number of water level gauges in locations facing CF risk. Therefore, more research is still needed to understand the dynamics of CF, e.g., to understand how relevant is the third CF mechanism listed above.

Studies that have explicitly quantified the CF probability based on the CF water level have focussed on specific locations, and have employed statistical modelling [180,182,209]. However, no statistical models have been developed that can both account for the temporal variability of the CF (based on the temporal variability of large-scale predictors) and explicitly represent the dependence of the CF variables. Kumbier et al. [80] employed hydrodynamic modelling to highlight, for a single flooding event, the contribution of the storm surge to the total flooding water level.

Recently, Ikeuchi et al. [74] modified a global river routing model to handle both the dynamically changing sea level and the river discharge, in river mouths. In some cases, this modified model can add value to purely river discharge modelling. However, such modelling approach focuses on the water level at mouths of large-scale rivers which are mostly influenced by upstream river discharge, i.e. where the compound effect is relatively small [74]. Nonetheless, in some locations, according to simulations from this model, the compound effect is relevant.

Both statistical and dynamical CF modelling can contribute to the CF research, with different targets. Potentially, hydrodynamic modelling is a great tool, but it is usually computationally very expensive. As Ikeuchi et al. [74] states, "statistical methods might be more suitable for long-term projections than hydrodynamic modelling in terms of computational loads", although their dynamical approach may serve as a starting point for improvements of CF modelling in large rivers [74]. Furthermore, information on the channel bathymetric depths is often missing and this is an issue in river hydrodynamic modelling because accurate bathymetric depth information is required for simulating the river water levels [74]. When there is no information about the channel bathymetric depth, statistical modelling might be helpful if a large enough sample of data is available for the calibration of the statistical model. As observational data are limited in estuarine regions, the exact dynamic of the interaction between river discharge, storm surge, and waves during a CF has not been fully studied yet. Thus, hydrodynamic modelling is a promising tool for improving the understanding of such interaction.

Sea level physical drivers and modelling The total sea water level is given by the superposition of a slow-varying mean sea level, storm surges, wind-driven waves, and astronomical tides [26,104,195]. Total sea level changes are driven by changes of these components and of their interactions. Regional mean sea level rise is driven by several components that cause departures from the global mean sea level rise (SLR). CMIP5 models account only for changes in water density called steric changes, i.e. thermosteric (temperature driven) and halosteric (salinity driven) density changes. These changes are associated with (1) ocean circulation changes due to local variations in salinity and temperature, and (2) water thermal expansion or contraction[3,21]. The melting of continental glaciers and polar ices sheets is an additional relevant source of global SLR[3,195]; such melting is not considered by CMIP5 models, and therefore it is modelled separately[64]. Changes in the geoid associated with the post-glacial isostatic adjustment rebound cause variations of (1) the relative sea level (which has a direct effect on coastal sea level impacts), and the ocean floor height (causing changes in sea level)[26]. Relatively small local sea level changes are also driven by ocean circulation changes due to influx of freshwater from polar ice sheets[3]. Furthermore, wind-driven surface wave changes (caused by atmospheric long-term variability) contribute to interannual-to-multidecadal water level variations[104].

Wind-driven waves are also crucial for short-term extreme sea levels[104,105,195]; other relevant drivers of short-term sea level extremes are storm surges (driven by wind and local sea level pressure) and astronomical tides. Furthermore, non-linear interactions between the sea level components can locally affect the total water level and thus can drive changes in sea level extremes. Surge-tide interactions can be important in shallow waters with large tidal range[17,71,211]. Waves are important for storm surge generation because they change the roughness of the ocean surface. The water depth modulates the bottom friction and the water extent, and thus SLR can affect nearshore wave processes[7,194], storm surges[8,38], and astronomical tide amplitudes[7,8,195]. However, predicting the effect of SLR at continental scale remains a challenge, mostly because the SLR-driven shoreline retreat and the change in nearshore bathymetry (which will modulate changes in surges, tides, and waves) are very difficult to be predicted.

The main methods employed in this thesis are described in the next chapter, however, here I briefly describe some general aspects of the models employed to simulate astronomical tides, storm surges, and waves for the analysis of CF along the European coast (chapter 5). Astronomical tides are simulated via the FES2012 model[25,112,161], which is a fully revised version of a model initiated in the early nineties[82]. The model employs global hydrodynamic tidal solutions (Finite Element Solutions, FESs) of the hydrodynamic equations of the tidal system (including ocean bathymetry); such solutions are improved by assimilating long-term ocean altimetry data and tidal gauges[82]. In total, 32 tidal constituents are provided, and the model runs over a 1/16 degrees resolution grid[25]. Storm surges are simulated via the DFLOW FM open source model[195,197]. This model solves the Navier-Stokes equations for an incompressible fluid under the shallow-water assumption[73], taking into account atmospheric wind and pressure fields as external drivers of the storm surge dynamics. Waves are simulated using the spectral wave model Wavewatch III (version 4.18) forced by the wind-field[105,173]. The model decomposes the irregular wind-driven wave into wave modes; thus, the model solves the balance equation for the wave spectrum. This spectrum gives information on the energy associated with a wave having a fixed direction and frequency, for a fixed location and time step. The balance equation describes the wave propagation, which is influenced by several source terms. In deep water, the main source terms are the wind-wave interaction, the non-linear wave-wave interaction, and the "white-capping" dissipation (see footnote[1]). In shallow water, also other sources are relevant, most notably wave-bottom interactions[173].

2.3.2 Soil moisture droughts

Soil moisture plays a critical role in agriculture and the variability of temperature in Europe[146,213]. Many studies have highlighted the importance of incorporating temperature in drought analysis[6,145,171]. Soil moisture drought refers to moisture deficits in the upper layer of soil known as the root zone. Soil moisture in the root zone is primarily controlled by antecedent precipitation while excesses in evapotranspiration (ET), related to high temperatures, are required to explain the severity of a negative soil moisture anomaly[145,171]. Potential evapotranspiration (PET) measures the evaporative demand of the atmosphere and indicates the amount of ET that would occur given an unlimited water supply. The contribution of PET to soil moisture drought depends on the availability of moisture in the soil for ET to take place[144]. Under moisture-limited conditions, values of PET and ET can diverge where ET may verge to zero while PET can continue to rise with an increase in temperature[144].

The individual roles of precipitation and PET, and that of their dependence driven through land-atmosphere interactions, highlights the compound nature of soil moisture drought. As the CE risk is influenced by the dependence between their drivers[19,63,99,198], understanding the dependence between hot and dry conditions and their impacts is of great importance. For example, overlooking non-linear dependence between hot and dry conditions and crop yields leads to an underestimation of risk in reduced crop yields[213], while the probability of hot and dry summers is underestimated when treating them independently[214]. Underlining this importance are findings of an increase in the concurrence of drought and heat wave events[103].

[1]The "white-capping" dissipation phenomenon is visible as white foam on the sea. It occurs when the speed of the wave crest exceed the phase speed of the wave, causing the front face of the wave to become too steep and "break".

2.3.2.1 Modelling of soil moisture

Despite the importance of soil moisture drought, soil moisture observations are very poor, in contrast to, e.g., temperature or precipitation observations[116]. *Physically-based land surface models* and *drought indices* are employed to estimate soil moisture both in present and future climate. Here, I provide some information on these two modelling approaches; this information is important to put the results of chapter 6 in context.

Representing soil moisture explicitly via *physically-based land surface models* is a complex task, particularly because the lack of homogeneous and long soil moisture data renders difficult the model calibration and validation. Different type of soil moisture models have been developed[151], which can be helpful to compensate for the lack of observations, but only in terms of soil moisture changes over time[116]. Simple models are based on the water balance equation (e.g., refs.[89,116,171]). These models often need to be calibrated to account, e.g., for different soil types, rendering the model performances uncertain under climate change conditions[116], where there are uncertainties about changes in the soil characteristics. The most sophisticated models depend also on information about vegetation, and there is relevant disagreement among available soil moisture model outputs[116].

Drought indices incorporating precipitation and temperature through PET are often employed as proxies of soil moisture[35,187], to analyse both present and future climate. For example, through the inclusion of temperature through PET in indices such as the Standardised Precipitation Evapotranspiration Index (SPEI)[188], the Palmer Drought Severity Index[117], and the Reconnaissance Drought Index (RDI)[178], studies have analysed how drought conditions may change in a warming climate at regional and global scales[33–35,152,160,174,175,189,206]. Based on indices incorporating PET, soil moisture drought events are expected to become more severe in a warming climate[174,189,206]. However, the meaning of this increase in severity can be quite unclear due to the differing contribution of PET to soil moisture drought in different climate conditions[144]. In fact, in dry conditions, PET can have little contribution to the soil moisture[89] and lead to drying biases in drought indices assumed to represent soil moisture[142,152].

Describing soil moisture with drought indices requires one to account for antecedent meteorological conditions that soil moisture holds the memory of. This is done using integrations of a climatic water balance (defined as *precipitation-PET*) varying in length from 1 to 24 months (e.g., SPEI), or through the use of recursive models (e.g., PDSI). The selection of this integration length for indices such as the SPEI is important; a length that is too short will not capture drought persistence while longer periods can include redundant information[174]. Studies using the SPEI or RDI to represent soil moisture generally use integration periods between 3 and 6 months[66,174]. The PDSI is calculated with monthly integrations and it can hold the memory of the previous winter and spring in summer months[35].

The incorporation of a climatic water balance in the drought indices implies that PET influences soil moisture over the same timescale as precipitation. Drying, however, occurs on a daily timescale where excesses in ET can be driven by days of extreme temperature that are filtered out through the use of longer integration periods. Such a feature of long integrations of the climatic water balance can lead to an inability to capture both future changes in drying that may cause droughts to set in quicker in a warmer climate and the occurrence of flash droughts associated with short periods of warm temperature and rapidly decreasing soil moisture[108].

Employing drought indices is much easier than using complex explicitly physically-based approaches. However, the question remains whether such indices can provide an adequate representation of soil moisture drought, or whether more explicitly physically-based approaches are required[58]. We contribute to answering this question in chapter 6, where we assess how the variables employed in common drought indices, namely precipitation and PET, actually contribute to soil moisture.

2.4 Advantages and limitations of statistical modelling of compound events

In this thesis, we develop a conceptual model, implemented via statistical methods, which allows for studying CEs. In the recent literature, more attention has been given to the study of CEs through multivariate statistical methods[147]. Conventional univariate statistical analysis cannot give accurate information regarding the multivariate nature of these events. In principle, combining univariate analyses for studying CEs is appropriate only in the few cases where no dependencies exist between the CE drivers.

Statistical modelling of CEs is useful for several reasons, although - depending on the problem at hand - it can be more or less efficient than dynamical modelling. (1) Statistical modelling can be employed for downscaling the drivers and/or the impact of CEs, which is crucial for risk assessment. For downscaling, the main advantage of statistical models is that they often offer a valid and computationally cheaper alternative to dynamical models. However, also the effort required for building the statistical model should be considered, as statistical models often need to be specifically built for the problem under consideration. Also, a long enough data sample is necessary for the calibration of a statistical model. And even if the data sample is long, the model might not work in a future climate[98]. In fact, the empirical relationships represented by the statistical model may not be valid in a potentially very different future climate. Therefore, when employing statistical downscaling for the future, the statistical model should be able to capture the physical processes that will be influenced by future climate change. Validating the statistical model for the past based on cross-validation might be helpful, however, this validation will likely not be sufficient if the climate characteristics of interest will substantially change in the future. Therefore, based on physical understanding, the user should ensure that the statistical model can properly represent changes in the future climate[98].

Employing dynamical modelling for downscaling has advantages and limitations as well. For instance, dynamical models usually allow for obtaining a variable of interest easily on a continuous spatial domain. For example, in chapter 5, using storm surge and wave data derived from a hydrodynamic models, allows us to study CF along the complete European coast. But while some dynamical models may in principle be very accurate, they may require input data that may be not available, e.g., the channel bathymetric depths for hydrodynamical river level modelling[74], as discussed in section 2.3.1.1 . As for statistical models, limited observations can be an issue also for dynamical models, e.g., limited observations make difficult the model validation.

However, statistical and dynamical modelling of CE are exchangeable only to some extent. Statistical models are useful for: (2) validating the output of the dynamical models themselves[70], e.g., for validating the co-variability of the CE contributing variables[20]; (3) extrapolating return periods of extreme events, where purely empirical estimates are likely biased due to the rarity of the extreme events (as we do, e.g., when studying the CF potential in Europe in chapter 5). Furthermore, (4) uncertainty estimates can be easily obtained via statistical modelling; in general, as observed data are often limited, uncertainties might be substantial and should thus be quantified[19,148].

Furthermore, multivariate statistical modelling of CEs allows for (5) understanding the physical drivers of CEs and their changes via, e.g., conditional sensitivity analysis[19,20,93,106]. To this end, depending on the target, both or either statistical and dynamical models can perform well. For example, to quantify the sensitivity of convective precipitation extremes to changes in sea surface temperature (SST), it is likely that dynamical modelling offers better performances. Indeed, in this case, explicitly representing small-scale physical phenomena should provide better results. Instead, calibrating a statistical model would require long data, and a statistical model would anyway not guarantee to capture the relevant physical processes for the sensitivity study, especially if the target of the study would be to extrapolate the sensitivity of precipitation far beyond the observed SST. In other cases, as some studied in this thesis, e.g., when analysing the influence of precipitation, PET, and of their dependence to soil moisture, it is much easier to implement a statistical model which enables great flexibility to analyse many possible features.

3. Methods

In this chapter, I present the conceptual model that was developed and employed in this thesis for studying compound events (CEs). Then, I introduce the main statistical methods used in the thesis, i.e. copulas and pair-copula constructions. Part of the content of this chapter can be found in Bevacqua et al.[19,20].

3.1 Conceptual conditional model for compound events

Leonard et al.[84] define a CE as "an extreme impact that depends on multiple statistically dependent variables or events". This definition stresses the extremeness of the CE impact rather than that of the individual contributing variables, which may not be extreme themselves, and the importance of the dependence between these contributing variables (see footnote[1]). The physical reasons for the dependence among the contributing variables can be different. There can be a mutual reinforcement of one variable by the other and vice versa due to system feedbacks, e.g., the mutual enhancement of droughts and heat waves in transitional regions between dry and wet climates[147]. Or the probability of occurrence of the contributing variables can be influenced from a large-scale weather condition, as it has occurred in Ravenna (Fig. 1.1), where the low-pressure system caused coinciding extremes of river runoff and sea level. It is clear then, that the dependence among the contributing variables represents a fundamental aspect of CEs, and so this dependence must be properly modelled to represent these extreme events well.

Our statistical *conditional model* consists of: the contributing variables Y_i, the impact h, and the predictors X_j of the contributing variables; the model represents the relationships between these three components. The contributing variables Y_i and their multivariate dependence structure directly drive the CE impact. For instance, in case

[1]According to a recent and more general definition[215], uncorrelated events or variables contributing to extreme impacts, e.g. co-occurring high astronomical tide and storm surge contributing to extreme sea level, are also classified as CEs. However, the dependence is a relevant driver of most of CEs and it makes CE modelling particularly challenging.

of compound floods (CFs), the contributing variables are the runoff and the sea level. The impact h of a CE can be formalized via an *impact-function* $h = h(Y_1, ..., Y_n)$. For example, in the case of CF in Ravenna (chapter 4), we define the river gauge level as the CE impact, but in principle it can be any measurable variable such as agricultural yield or economic loss. The predictors X_j provide insight into the physical processes underlying CEs, including the temporal variability of CEs, and can be used to statistically downscale CEs when the variables Y and the impact h are available for calibrating the model[97].

The downscaling feature is particularly useful for CEs, which are not realistically simulated or may not even be simulated at all by available climate models. For instance, standard global and regional climate models do not simulate realistic runoff[47,102,172], and do not simulate sea surges. Here, our model can be used to downscale these contributing variables, e.g., from simulated large-scale meteorological predictors from past or future climate. In particular, the model provides a simultaneous, i.e. multivariate, downscaling of the contributing variables Y_i, which allows for a realistic representation both of the dependencies between the Y_i, and of their marginal distributions. This is relevant because a separate downscaling of the contributing variables Y_i may lead to unrealistic representations of the dependencies between the Y_i, which in turn would cause a poor estimation of the impact h. The downscaling feature can be useful to extend the hazard probability or risk analysis into the past, where observations of the predictors, but not of the contributing variables and impacts are available.

More specifically, the conceptual conditional model consists of:

1. An impact function to quantify the impact h:

$$h = h(Y_1, ..., Y_n). \tag{3.1}$$

2. Predictors X for the contributing variables Y.

3. A conditional joint probability density function (pdf) $f_{\vec{Y}|\vec{X}}(\vec{Y}|\vec{X})$ of the contributing variables Y, given the predictors X (which we describe through a parametric model, via pair-copula constructions). In particular, both the contributing variables Y and predictors X are time dependent, i.e. $\vec{Y} = \vec{Y}(t)$ and $\vec{X} = \vec{X}(t)$.

A particular type of the model is obtained when the predictors are not considered in the joint pdf, i.e., when considering $f_{\vec{Y}}(\vec{Y})$. This *unconditional model* does not allow for changes of the contributing variables Y and of the impact due to variations of the predictors X. We use these two model types in chapter 4 for studying CF in Ravenna[19].

In general, formalizing the impact h of a CE as in step 1 - to then asses the probability or risk of CE based on values of h - corresponds to the *Structural Approach*[138,148,193], which has recently been formalized by Salvadori et al.[137]. Here, the advantage of the general model we propose is that it allows for taking into account variations of the impact h driven by temporal changes of the predictors X. Through the conditional pdf, the model allows for a realistic representation both of the dependencies between the Y_i, and of their marginal distributions.

A generalization of the model is schematically represented in Fig. 3.1 where, as explained in the following, only some of the represented components are necessary to build different possible model versions. When the variables Y are available (for model calibration) but not the impact h, the model can be used to only estimate the variables Y given the predictors X. This may be useful when assessing the potential CE hazard through, e.g., multivariate return periods of the contributing variables Y[6,53,54,133,136,137,155,156,198]. Moreover, it may happen that the impact h is available, but the variables Y are not. In this case, the model may still be used in the form $f_{h|\vec{X}}(h|\vec{X})$ to directly estimate the impact h, based on the conditional joint pdf of the impact h, given the predictors X. In this case, depending on the physical system, it may be more or less complicated to define the predictors. Also, we observe that eq. (3.1) is general and a possibility for estimating the impact would be to use the conditional joint pdf $f_{h|\vec{Y}}(h|\vec{Y})$. Such an approach may be useful for cases where complex relations exist between the impact h and the variables Y, and therefore it may be difficult to implement, e.g., a proper regression model to describe the impact h. We use this version of the model in chapter 6 for studying soil moisture drought (the impact h) as a CE of precipitation and PET (the contributing variables Y)[93]. Finally, also an impact h caused by only one contributing variable Y driven by several predictors ($\vec{X}$) can be considered as a CE impact[215]; our model can be easily employed to study this type of CEs as well.

3.2 Statistical methods

Modelling CEs is a complex undertaking[84], and due to the complex dependence structure between the contributing variables, advanced multivariate statistical models are necessary to model CEs: here, to implement the conceptual model we use copula-based methods[1,19]. For example, modelling the multivariate probability distribution of the contributing variables with multivariate Gaussian distributions would usually not produce satisfactory results. A multivariate Gaussian distribution would assume that the dependencies between all the pairs are of the same type (*homogeneity of the pair-dependencies*), and without any dependence of the extreme events, also called *tail*

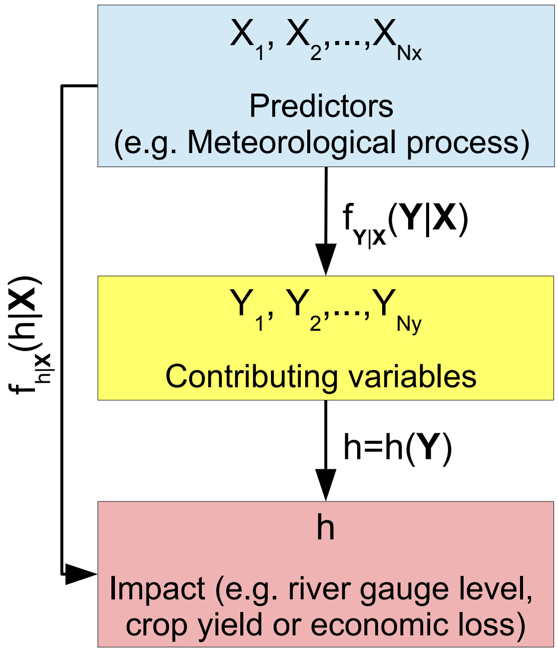

Figure 3.1: **Conceptual model.** Schematic representation of the developed conceptual model (see text).

dependence. Furthermore, a multivariate Gaussian distribution would assume that all of the marginal distributions would be Gaussian. To solve the latter problems, the use of copulas has been introduced in geophysics and climate science[135,141]. Through copulas, it is possible to model the dependence structure of variables separately from their marginal distributions. However, multivariate parametric copulas lack flexibility when modelling systems with dimension greater than two, where heterogeneous dependencies exist among the different pairs[1]. Therefore, this lack of flexibility of copulas would be a limitation when modelling CEs involving more than two variables, or when introducing predictors into the system. Pair-copula constructions (PCCs), proposed by Joe[75], decompose the dependence structure into bivariate copulas and give greater flexibility in modelling generic high-dimensional systems compared to multivariate parametric copulas[1,2,15,67].

An advantage of using a parametric statistical model is that this constrains the dependencies between the contributing variables, as well as their marginal distributions[6,70,133 148,149,155,156]. The parametric structure reduces the uncertainties of the statistical properties estimated from the data, compared to empirical estimates[70]. However, such a reduction of the uncertainties actually depends on the choice of a proper parametric model, in particular when modelling the tail of a univariate or multivariate distribution.

3.2.1 Copulas

Consider a vector $\vec{Y} = (Y_1, ..., Y_n)$ of random variables, with marginal pdfs $f_1(y_1), ..., f_n(y_n)$, and cumulative marginal distribution functions (CDFs) $F_1(y_1), ..., F_n(y_n)$, defined on $\mathbb{R} \cup \{-\infty, \infty\}$. We use the recurring definition $u_i := F_i(y_i)$, where the name u indicates that these variables are uniformly distributed by construction. According to Sklar's theorem[157] the joint CDF $F(y_1, ..., y_n)$, can be written as:

$$F(y_1, ..., y_n) = C(u_1, ..., u_n) \tag{3.2}$$

where C is an n-dimensional Copula[114]. C is a copula if $C : [0,1]^n \to [0,1]$ is a joint CDF of an n-dimensional random vector on the unit cube $[0,1]^n$ with uniform marginals[49,76,134,135].

Under the assumption that the marginal distributions F_i are continuous, the copula C is unique and the multivariate pdf can be decomposed as:

$$f(y_1, ..., y_n) = f_1(y_1) \cdot ... \cdot f_n(y_n) \cdot c(u_1, ..., u_n) \tag{3.3}$$

where c is the copula density. Eq. (3.3) explicitly represents the decomposition of the pdf as a product of the marginal distributions and the copula density, which describes the dependence among the variables independently of their marginals. Eq. (3.3) has some important practical consequences: it allows us to generate a large number of joint pdfs. In fact, inserting any existing family for the marginal pdfs and copula density into eq. (3.3), it is possible to construct a valid joint pdf, provided that suitable constraints are satisfied. The group of the existing parametric families of multivariate distributions (e.g., the multivariate normal distribution, which has normal marginals and copula) is only a part of the realizations which are possible via eq. (3.3). Copulas, therefore, make it easy to construct a wide range of multivariate parametric distributions.

3.2.2 Tail dependence

The dependence of extreme events cannot be measured by overall correlation coefficients such as the Pearson, Spearman or Kendall. Given two random variables which are uncorrelated according to such overall dependence coefficients, there can be a significant probability to get concurrent extremes of both variables; such probability is well represented by the tail dependence[19,70,93]. On the contrary, two random variables which are correlated according to an overall dependence coefficient may not necessarily be tail dependent.

Mathematically, given two random variables Y_1 and Y_2 with marginal CDFs F_1 and F_2 respectively, they are *upper tail dependent* if the following limit exists and is non-zero:

$$\lambda_U(Y_1, Y_2) = \lim_{u \to 1} P(Y_2 > F_2^{-1}(u) | Y_1 > F_1^{-1}(u)) \tag{3.4}$$

where $P(A|B)$ indicates the generic conditional probability of occurrence of the event A given the event B. Similarly, the two variables are *lower tail dependent* if the following limit exists and is non-zero:

$$\lambda_L(Y_1, Y_2) = \lim_{u \to 0} P(Y_2 < F_2^{-1}(u) | Y_1 < F_1^{-1}(u)). \tag{3.5}$$

3.2.3 Pair-Copula Constructions (PCCs)

While the number of bivariate copula families is very large[76,114], building higher dimensional copulas is generally recognised as a difficult problem[1]. As a consequence, the set of copula families having a dimension greater than or equal to 3 is rather limited, and they lack flexibility in modelling multivariate pdfs where heterogeneous dependencies exist among different pairs. For instance, they usually prescribe that all the pairs have the same type of dependence, e.g., they are either all tail dependent or all not tail dependent. Under the assumption that the joint CDF is absolutely continuous, with strictly increasing marginal CDFs, PCCs allow to mathematically decompose an n-dimensional copula density into the product of $n(n-1)/2$ bivariate copulas, some of which are conditional. In practice, this provides high flexibility in building high-dimensional copulas. PCCs allow for the independent selection of the pair-copulas among the large set of families, providing higher flexibility in building high dimensional joint pdfs with respect to using the existing multivariate parametric copulas[1].

When the dimension of the pdf is large, there can be many possible, mathematically equally valid decompositions of the copula density into a PCC. For example, for a 5-dimensional system there are 480 possible different decompositions. For this reason, Bedford and Cooke[14],[15] have introduced *the regular vine*, a graphical model which helps to organize the possible decompositions. This is helpful to choose which PCC to use to decompose the multivariate copula. In this thesis, we concentrate on the widely-used subcategories *canonical* (also known as *C-vine*) and *D-vine* of regular vines. Out of the 480 possible decompositions for a 5-dimensional copula density, 240 are regular vines (60 C-vines, 60 D-vines and 120 other types of vines)[1]. An example of a 5-dimensional

D-vine decomposition follows:

$$
\begin{aligned}
f_{12345}(y_1, y_2, y_3, y_4, y_5) = & f_4(y_4) \cdot f_5(y_5) \cdot f_3(y_3) \cdot f_1(y_1) \cdot f_2(y_2) \\
& \cdot c_{45}(u_4, u_5) \cdot c_{53}(u_5, u_3) \cdot c_{31}(u_3, u_1) \cdot c_{12}(u_1, u_2) \\
& \cdot c_{43|5}(u_{4|5}, u_{3|5}) \cdot c_{51|3}(u_{5|3}, u_{1|3}) \cdot c_{32|1}(u_{3|1}, u_{2|1}) \\
& \cdot c_{41|35}(u_{4|53}, u_{1|53}) \cdot c_{52|13}(u_{5|31}, u_{2|31}) \\
& \cdot c_{42|135}(u_{4|513}, u_{2|513}).
\end{aligned} \tag{3.6}
$$

More details about vines are given in appendix A.3.1, where also the graphical representation of the vine in eq. (3.6) is shown in Fig. A.1a. Details about the statistical inference of the joint pdf (including the selection procedure of vines) can be found in appendix A.4.

As described in section 3.1, the conditional model is based on a conditional joint pdf, e.g., $f_{\vec{Y}|\vec{X}}(\vec{Y}|\vec{X})$, which is decomposed via PCC. Information on conditional joint pdfs decomposed through vines, and on how to sample from such vines, are given in the next section.

3.2.3.1 Sampling and conditional sampling from vines

To simulate a vector $\vec{Y} = (Y_1, ..., Y_n)$ of random variables, with marginal CDFs $F_1(y_1), ..., F_n(y_n)$, whose joint pdf is modelled via a copula, we first simulate from the copula the uniform variables U_i for $i = 1, ..., n$ ($u_i := F_i(y_i)$), and then transform them into Y_i for $i = 1, ..., n$ (via $y_i := F_i^{-1}(u_i)$).

The simulation of the uniform variables from vines is discussed in refs. [13,14,81]. Aas et al. [1] show the algorithms to sample uniform variables from C- and D-vines. Due to the nature of PCCs, the sampling procedure works as a cascade. Once the first variable is simulated from a uniform distribution, each following variable is simulated as conditioned on the previous group of simulated variables.

It is clear then, that to sample from the conditional distribution of $U_{N_{\text{cond}}+1}, ..., U_n$ given values for $U_1, ..., U_{N_{\text{cond}}}$ (i.e. from $f_{U_{N_{\text{cond}}+1},...,U_n|U_1,...,U_{N_{\text{cond}}}}$), it is possible to follow this procedure by simply fixing the first N_{cond} variables at the conditioning values. The approach used here to execute such a procedure, is to select vines from which the conditioning variables would be sampled as first when following the sampling algorithms from Aas et al. [1]. For example, using the D-vine represented in Fig. A.1a of appendix A (eq. (3.6)), we could simulate by fixing the pairs (U_4, U_5) or (U_2, U_1) in case we are interested in conditioning the simulation on two variables.

Following this approach, for D-vines the number of n-dimensional decompositions which allow for conditioning on N_{cond} variables is $N_{\text{cond}}! \cdot (n - N_{\text{cond}})!$. For C-vines the number of the decompositions which allow for such a conditioning is $N_{\text{cond}}! \cdot (n - N_{\text{cond}})!/2$ for $n - N_{\text{cond}} > 1$, and $N_{\text{cond}}!$ for $n - N_{\text{cond}} = 1$. For example, in the case of CF in Ravenna (chapter 4), we model a 5-dimensional system with two conditioning variables (the meteorological predictors), that is $n = 5$ and $N_{\text{cond}} = 2$. Considering that there are not 5-dimensional vines which belong to both the C-vine and D-vine categories[1], the choice of the vine used for the model is done among $(2!/2 \cdot (5-2)!) + (2! \cdot (5-2)!) = 18$ vines. As we need to condition on values (y_4, y_5), we simulate from the copula through conditioning on $(u_4 = F_4(y_4), u_5 = F_5(y_5))$, where F_4 and F_5 are the fitted marginals in the calibration period, while (y_4, y_5) could in principle be any value.

To apply such a sampling procedure, I developed the Algorithms 1 and 2 (appendix A.2), which are a modified version of Algorithms 1 and 2 shown in Aas et al.[1]. As a part of the PhD, these algorithms were made publicly available via the R-package *CDVineCopulaConditional*[18]. Further information about the R-package and the algorithms can be found in appendix A.2.

3.3 Multivariate return periods

In chapter 5, the CF hazard along the European coast is analysed[20]. Data of the local impact of the CF, i.e. the water level driven both by precipitation and sea level, would only be available for a very few locations along the coast. Therefore, we assess the hazard probability via return periods of *potential CF*, i.e. a combination of precipitation and sea level values that is considered *dangerous* (in this study, co-occurring precipitation and sea level extremes). In this study, we employ precipitation and sea level data from dynamical models, without requiring statistical downscaling of these quantities.

This approach corresponds to apply an extremely simplified version of the conceptual model of section 3.1, where the predictors and the impact are not included in the model, and the contributing variables are defined as the sea level (S) and the precipitation (P). Alternatively, such an approach can also be seen as applying the same model as before, but including the impact as the binary variable:

$$h = \begin{cases} 1, & \text{if } (s,p) \text{ is dangerous} \\ 0, & \text{otherwise} \end{cases} \tag{3.7}$$

where dangerous (s,p) are potential CF; then, the return period of $h = 1$ is defined as the return period of potential CF. In this context, the advantage of using the conceptual model is the application of a parametric bivariate pdf on the pairs (S, P) (this pdf is required for computing the return period). Indeed, the parametric distribution allows for obtaining a more robust estimation of large return periods, compared to those obtained via an empirical estimation.

In general, the return period is defined as the average waiting time between dangerous events, i.e. events belonging to a *dangerous region*. The choice of the dangerous region should be based on expert knowledge of the impact behaviour. In the 1-dimensional case, the dangerous region is naturally defined as that of extreme values, e.g., values exceeding a fixed threshold. In the 2-dimensional case, the definition of extreme events is not straightforward and several different definitions are possible for the dangerous region. Thus, several possible return period definitions exist, each of them associated with a different definition of the dangerous region. Among the most common return periods, there are the AND and the OR[54,138,185]. In the context of CF, these are defined as: AND, the average waiting time between events where both sea level *and* precipitation are extreme; OR, the average waiting time between events where either sea level *or* precipitation is extreme.

When studying CF along the European coast (chapter 5), we choose to employ AND return periods as the most extreme CF tends to happen for co-occurring extremes. Specifically, we define the bivariate CF return periods[54,138,185] as the average waiting time between events where sea level and precipitation simultaneously exceed the individual 1-year return levels (i.e. the $\sim 99.7^{th}$ percentiles $s_{99.7}$ and $p_{99.7}$).

To define this AND return period, the probability of co-occurring sea level and precipitation extremes is needed. To allow for a robust estimation, we apply a parametric copula-based bivariate probability distribution. Applying a parametric model for the full range of sea level and precipitation values, one would run the risk of biasing the representation of the extreme tail by the bulk of the bivariate distribution where most data occur. Therefore we apply the model only to pairs of high values. We select pairs where, simultaneously, sea level and precipitation values exceed the individual 95^{th} percentiles (s_{sel} and p_{sel}, respectively) (see footnote[2]). In a very few locations, one might end up with selecting few pairs only. Here we reduce the selection threshold 0.95 to ensure that at least 20 pairs of values are selected (never below 0.9). Clusters of selected event pairs

[2] The pairs of high values where to fit the pdf can actually be defined in different ways. For example, Wahl et al.[198] employed annual maxima for the fit of the pdf. Specifically, their choice leads to two cases: in case I the pairs are defined searching for the annual precipitation maxima and taking the associated sea level values, and vice versa in case II. As a consequence, this lead to two different AND return periods. With respect to the method employed by Wahl et al.[198], our method allows for (1) defining a unique AND return period, and (2) allows for fitting the pdf on a relatively large number of pairs, which should lead to high confidence in the estimated parameter of the pdf.

separated by less than three days are replaced by a unique event which assumes the maximum sea level S and precipitation P observed in the cluster (see Fig. 3.2).

Thus, the bivariate return period is:

$$\begin{aligned} T(s_{99.7}, p_{99.7}) &= \frac{\mu}{P((s > s_{99.7}\ and\ p > p_{99.7}) \mid (s > s_{sel}\ and\ p > p_{sel}))} = \\ &= \frac{\mu}{1 - u_{S99.7} - u_{P99.7} + C_{SP}(u_{S99.7}, u_{P99.7})} \end{aligned} \tag{3.8}$$

where μ is the average time elapsing between the selected pairs, $u_{S99.7} = F_S(s_{99.7})$, F_S is the marginal cumulative distribution of the excesses over the selection threshold (accordingly for precipitation), and C_{SP} is the copula modelling the dependence between the selected pairs.

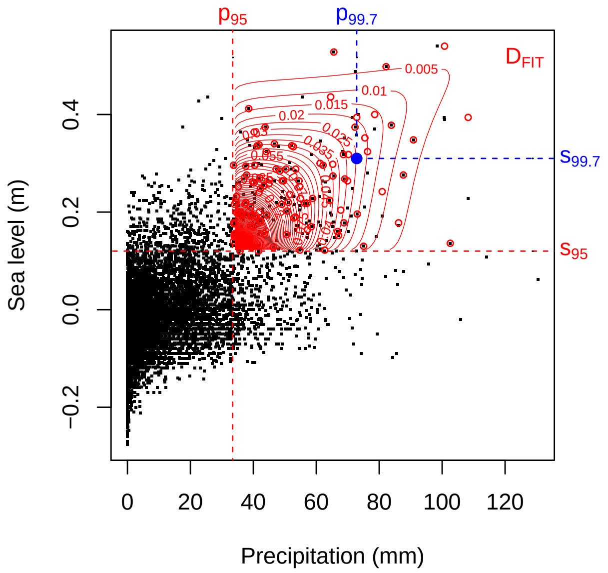

Figure 3.2: **Procedure for computing compound flood (CF) bivariate (*AND*) return periods.** Scatterplot of ERA-Interim simulated pairs (s, p) of sea level and precipitation accumulated within ± 1 days (black points) in Venice (here, sea level is given by the daily maxima of the surge and wave time series superposition; see section 5.2). The 1-year return levels ($\sim 99.7^{th}$ percentiles) of sea level ($s_{99.7}$) and precipitation ($p_{99.7}$) are the thresholds selected for computing the CF return period. The parametric extreme value probability density function (pdf) (red contour lines) is fitted only to pairs in D_{FIT}, i.e. pairs whose individual components are simultaneously larger than the individual 95^{th} percentiles of sea level (s_{95}) and precipitation (p_{95}). In particular, the extreme value pdf was fitted to the red pairs (s, p); the red pairs are different from the original simulated black pairs belonging to D_{FIT}, as the latter were pre-processed when they were separated by less than three days (see section 5.2).The extreme value pdf is obtained via copula theory as $f_{SP}(s, p) = f_S(s) \cdot f_P(p) \cdot c_{SP}(u_s, u_p)$, where f_i are the marginal distributions of sea and precipitation values in D_{FIT}, and c_{SP} is the copula modelling the dependence between sea level and precipitation in D_{FIT}. Here, c_{SP} is a Gumbel copula ($\theta = 1.4$), associated with a Kendall correlation equal to 0.29, and an upper tail dependence equal to 0.36.

4. Multivariate statistical modelling of CF in Ravenna (Italy)

In this chapter, based on the conceptual model presented in chapter 3, we study compound flooding (CF) in Ravenna (Italy). Here, we explicitly quantify the flooding water level as a function of sea and river levels, thus we estimate the CF return periods and the associated uncertainties. The content of this chapter was published as a part of Bevacqua et al.[19].

4.1 Introduction

We focus on the Ravenna case study because of the extreme event that happened on the 6^{th} of February 2015, as presented in the introduction. On the day prior to the event, values of up to approximately 80 mm of rain were recorded in the surrounding area of Ravenna, and around 90 mm on the day of the event itself. The sea level recorded was the highest observed in the last 18 years[9]. The high risk of flooding to population in the Ravenna region has been underlined by the *LIFE PRIMES* project[5], recently financed by the European Commission, whose target is "to reduce the damages caused to the territory and population by events such as floods and storm surges"[4] in Ravenna and its surrounding areas. As pointed out by Masina et al.[101], natural and anthropogenic subsidences represent a threat for the coastal area of Ravenna, characterized by land elevation which is in many places below 2 m above mean sea level[48]. The sea level inundation hazard along the coast of Ravenna has been recently studied by Masina et al.[101], who considered the joint effect of sea water level and significant wave height.

A schematic representation of the catchment on which we focus is shown in the black rectangle of Fig. 4.1. The Y variables, river and sea levels, represent the contributing

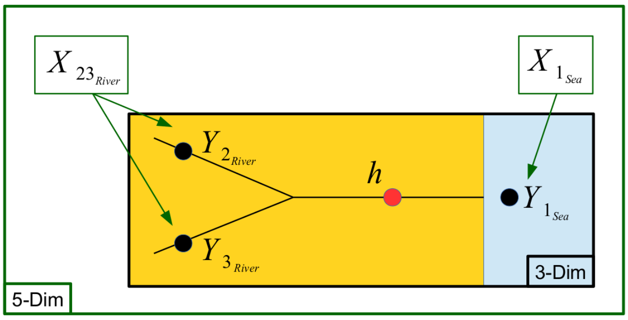

Figure 4.1: **Representation of the hydraulic system of the Ravenna catchment.** The area affected by CF is marked by the red point. The impact is the water level h, which is influenced by the contributing variables Y, i.e. sea and river levels. The variables inside the black rectangle are used to develop the 3-dimensional (*unconditional*) model. The X are the meteorological predictors driving the contributing variables Y, which are incorporated into the 5-dimensional (*conditional*) model.

variables, and the water level h is the impact of the CF. The X variables are meteorological predictors of the contributing variables Y, which will be discussed in more detail later.

Based on the conceptual model presented in chapter 3, here we assess the CF probability in Ravenna. Here, we explicitly define the impact of CF as a function of sea and river levels in order to quantify the flood probability and its related uncertainties. Moreover, we quantify the CF probability underestimation that occurs when the dependence among sea and river levels is not considered. We identify the meteorological predictors driving the river and sea levels. By incorporating such predictors into the statistical model, we extend the analysis of CF into the past, where data are available for predictors, but not for the river and sea level stations. Our research objectives are the following:

1. Implement and test the conceptual model (chapter 3) which allows for representing the dependencies between the contributing variables of the CF.
2. Explicitly define the impact of CF as a function of the contributing variables. This allows us to estimate the CF probability and the related uncertainty.
3. Identify the meteorological predictors for the contributing variables Y. Incorporate the meteorological predictors in the model to gain insight into the physical mechanisms driving the CF and into their temporal variability.
4. Extend the analysis into the past (where data are available for the predictors, but not for the contributing variables Y).

4.2 Data

The data used here for the contributing variables Y and the impact h are water levels at a daily resolution (daily averages of hourly measurements). We use data for the extended winter season (November-March) of the period 2009-2015. Data sources are the *Italian National Institute for Environmental Protection and Research (ISPRA)* for the sea (`www.mareografico.it`), and *Arpae Emilia-Romagna* for rivers and impact. River data were processed in order to mask periods of low quality, i.e. those suspected to be influenced by human activities such as the use of a dam. Moreover, we applied a procedure to homogenise the data of the rivers; details are given in appendix A.1. We do not filter out the astronomical tide component of the sea level, considering that the range of variation of the daily average of sea level is about 1 meter, while that of the astronomical tide is about 9 cm. To check the above, we used astronomical tide obtained through FES2012, which is a software produced by *Noveltis, Legos and CLS Space Oceanography Division* and distributed by *Aviso*, with support from *Cnes* (http://www.aviso.altimetry.fr/). Meteorological predictors were obtained from the *ECMWF ERA-Interim* reanalysis dataset (covering the period 1979-2015, with 0.75×0.75 degrees of resolution[37]). Specifically, for the river predictors, we use daily data (sum of 12-hourly values) of total precipitation, evaporation, snowmelt and snowfall, while for the sea level predictor we use daily data (average of 6-hourly values) of sea level pressure. Further information on the data sources can be found in the *Data availability* section of Bevacqua et al.[19].

4.3 Model development

The extreme impact of compound events (CEs) may be driven from the joint occurrence of non-extreme contributing variables[84,147]. This is the case for CF in Ravenna, where not all extreme values of the impact would be considered if selecting only extreme values of the contributing variables. Therefore we model the contributing variables, without focusing only on their extreme values. Below we show the steps we follow to study CF in Ravenna, based on the conceptual model described in section 3.1. We will go through these steps in detail in the next sections.

1. Define the impact function:

$$h = h(Y_{1_{\text{Sea}}}, Y_{2_{\text{River}}}, Y_{3_{\text{River}}}). \tag{4.1}$$

   The contributing variables Y (sea and river levels) and the impact are shown in the black rectangle of Fig. 4.1).

2. Find the meteorological predictors of the contributing variables Y. For each variable Y_i we found more than one meteorological predictor, which we aggregated into a single variable X_i. We refer to this variable as the predictor X_i of the variable Y_i from now on. Moreover we use the same predictor for the two river levels because they are driven by a similar meteorological influence. The predictors are graphically shown in Fig. 4.1, where we introduce $X1_{\mathrm{Sea}}$ (the predictor of $Y1_{\mathrm{Sea}}$) and $X23_{\mathrm{Rivers}}$ (the predictor of $Y2_{\mathrm{River}}$ and $Y3_{\mathrm{River}}$).

3. Fit the 5-dimensional conditional joint pdf $f_{\vec{Y}|\vec{X}}(Y1_{\mathrm{Sea}}, Y2_{\mathrm{River}}, Y3_{\mathrm{River}}|X1_{\mathrm{Sea}}, X23_{\mathrm{Rivers}})$ of the conditional model (modelled via PCC). To develop the unconditional model, we fit the 3-dimensional pdf $f_{\vec{Y}}(Y1_{\mathrm{Sea}}, Y2_{\mathrm{River}}, Y3_{\mathrm{River}})$, which includes only the contributing variables Y inside the black rectangle of Fig. 4.1. The time series of the contributing variables have significant serial correlations, and this should be considered in order to avoid underestimating the CF probability uncertainties (see appendix A.6 and Fig. A.3 there). Only for the unconditional model, we explicitly modelled such serial correlations through combining PCCs with autoregressive $AR(1)$ models (see appendix A.6).

4. Given the complexity of the problem, an analytical derivation of the statistical proprieties of the impact is impracticable. Therefore, we apply a Monte Carlo procedure. Specifically we simulate the contributing variables Y from the fitted models, and then we define the simulated values of h via eq. (4.1) as:

$$h^{\mathrm{sim}} := h(Y^{\mathrm{sim}}_{1_{\mathrm{Sea}}}, Y^{\mathrm{sim}}_{2_{\mathrm{River}}}, Y^{\mathrm{sim}}_{3_{\mathrm{River}}}) \tag{4.2}$$

   where $\vec{Y}^{\mathrm{sim}}$ are the simulated values of $\vec{Y}$.

5. Perform a statistical analysis of the values h^{sim}. To asses the probability associated with the events, we compute the return levels of h through fitting a Generalized Extreme Value (GEV) distribution to annual maximum values (defined over the period November-March). We quantify the *model uncertainties* (i.e. uncertainties associated with model parameters and structure), which is straightforward through such models. Practically, such uncertainties propagate through to the hazard assessment, and so they must be considered (details about model based return level uncertainty are given in appendix A.5).

To neglect the Monte Carlo uncertainties, i.e., the sampling uncertainties due to the model simulations, we produce long simulations. For example, to obtain the model based return level curve, we simulate a time series $h^{\mathrm{sim}}(t)$ of length equal to 200 times the length of the observed data (6 years). From this, we get a time series of 1200 annual maximum values, to whom we fit the GEV distribution to get the return level. Observation-based return levels are obtained through fitting a GEV to annual maximum values of h^{obs}. The relative uncertainties are computed through propagating the parameter uncertainties of the fitted GEV distribution (more details are given at the end of appendix A.5).

4.3.1 Impact function

The water level h is influenced by river ($Y2_{\mathrm{River}}$ and $Y3_{\mathrm{River}}$) and sea ($Y1_{\mathrm{Sea}}$) levels (Fig. 4.1). We describe this influence through the following multiple regression model:

$$h = a_1 Y1_{\mathrm{Sea}} + a_{21} Y2_{\mathrm{River}} + a_{22} Y2^2_{\mathrm{River}} + a_{31} Y3_{\mathrm{River}} + a_{32} Y3^2_{\mathrm{River}} + c + \eta_{\mathrm{h}}(0, \sigma_h) \qquad (4.3)$$

where $\eta_{\mathrm{h}}(0, \sigma_h)$ is a Gaussian distributed noise having standard deviation equal to σ_h. The contribution of the rivers to the impact h is expressed via quadratic polynomials, which guarantees a better fit of the model according to the Akaike Information Criterion (AIC). In particular, we defined the regression model as the best output of both a forward and a backward selection procedure, considering linear and quadratic terms for all of the Y as candidate variables. The Q-Q plot of the model, i.e. the plot of the quantiles of observed values against those of the mean predicted values from the model, is shown in Fig. 4.2. The points are located along the line $y = x$, which indicates that the model is satisfactory. Omitting one of the variables as predictor reduces model performance, underlining the compound nature of the impact h. The sum of the relative contributions of the rivers is very similar to that of the sea. The parameters of this model (and of those in section 4.3.2) were estimated according to the maximum likelihood approach, solved through QR decomposition (via the *lm* function of the R package *stats*[170]).

4.3.2 Meteorological Predictor Selection

Fig. 4.3 shows the resulting scatter plots of observed predictands (Y^{obs}) and selected observed predictors (X^{obs}). To fit the joint pdf of the conditional model, we use all time steps where data for all of the X and Y variables have been recorded. However, we calibrate the predictors of rivers and sea separately, so we use all available data for each Y variable (during the period November-March). The procedure we use to identify the meteorological predictors is shown below.

4.3.2.1 River levels

The meteorological influence on the two rivers $Y2_{\mathrm{River}}$ and $Y3_{\mathrm{River}}$ is very similar: their catchments are small and close by (as a consequence the Spearman correlation between

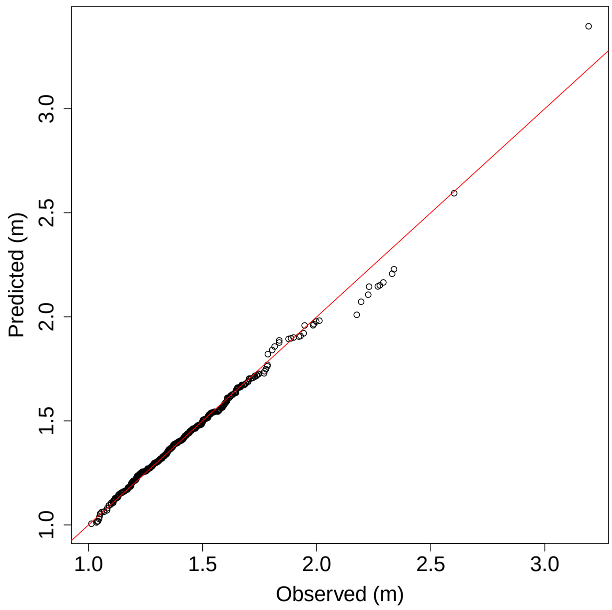

Figure 4.2: **Impact-model validation based on Q-Q plot.** Q-Q plot between the observed impact (X-axis) and the modelled impact (Y-axis) from the regression model (eq. (4.3)).

the rivers is high, i.e. 0.79). In particular, the distance between the two rivers is typically smaller than the grid-resolution of the predictor fields. Therefore we use the same predictor for the two river levels.

The river levels are influenced by the total input of water over the catchments, which is given by the positive contribution of liquid precipitation and snow melt, and by evaporation which results in a reduction of the river runoff. Specifically, we compute the input of water w on the day t^* over the river catchments (one grid point) as:

$$w(t^*) = P_{\text{total}}(t^*) - E(t^*) + S_{\text{melt}}(t^*) - S_{\text{fall}}(t^*) \tag{4.4}$$

where P_{total} is the total precipitation, E is the evaporation, S_{melt} is the snow melt and S_{fall} is the snow fall. The snow fall accounts for the fraction of precipitation which does not immediately contribute to the input of water over the catchments because of its solid state. While a fraction of the water input over the catchment rapidly reaches the rivers as surface runoff, another fraction infiltrates the ground and contributes only later to the river discharge. Compared with the first fraction, the second has a slower response to precipitation and changes more gradually over time. This double effect underlines the compound nature of river runoff whose response to precipitation falling at given time is higher if in the previous period additional precipitation fell in the river catchment. To

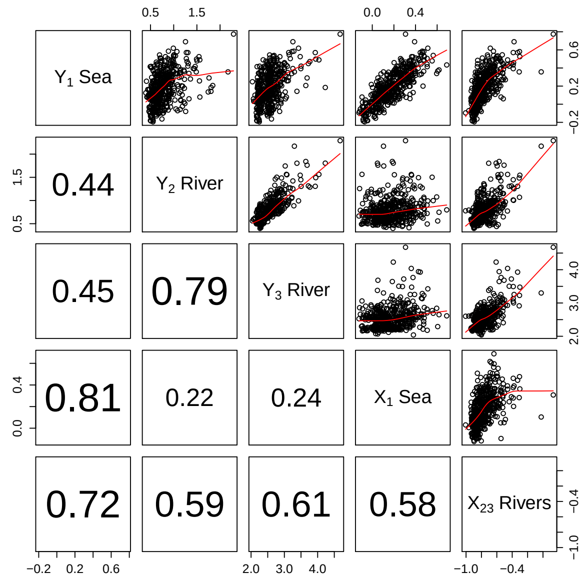

Figure 4.3: **Scatter plots of predictands $Y^{\mathbf{obs}}$ and predictors $X^{\mathbf{obs}}$**. The numbers are Spearman coefficient correlations. The red lines (computed via LOWESS, i.e. *Locally Weighted Scatterplot Smoothing*) is shown to better visualize the relationship between pairs[170].

consider both of these effects we define the river predictor as:

$$X_{23_{\text{Rivers}}}(t) = a_{\text{R}} \sum_{t^*=t-1}^{t} w(t^*) + b_{\text{R}} \sum_{t^*=t-10}^{t} w(t^*) + c_{\text{R}} \tag{4.5}$$

where c_{R} is a constant. We choose the parameters of eq. (4.5) through fitting the right hand side of this equation to the river contributions to the impact, i.e. $Y_{23_{\text{Rivers}}} := a_{21}Y_{2_{\text{River}}} + a_{22}Y^2_{2_{\text{River}}} + a_{31}Y_{3_{\text{River}}} + a_{32}Y^2_{3_{\text{River}}}$ (see eq. (4.3)). The lags $n = 1$ and $n = 10$ days are those which maximise respectively the upper tail dependence and the Spearman correlation between $Y_{23_{\text{Rivers}}}(t)$ and the cumulated w over the previous n days, i.e., $\sum_{t^*=t-n}^{t} w(t^*)$. Here, we use the upper tail dependence to get the typical river response time to the fraction of water which directly flows into the rivers as surface runoff. Similarly, the Spearman correlation is used to get the typical time required for the infiltrated water in the ground to flow into the rivers.

By defining the river predictor as in eq. (4.5), we aggregate the different meteorological drivers of the rivers in the single predictor $X_{23_{\text{Rivers}}}(t)$. Such aggregation allows for a simplification of the system describing the CF, due to a reduction of the involved variables. Furthermore this reduces the variables described by the joint pdf $f_{\vec{Y},\vec{X}}(\vec{Y},\vec{X})$, whose numerical implementation errors can potentially increase with higher dimensionality[67].

All of the terms involved in the multiple regression model (eq. (4.5)) are statistically significant at level $\alpha = 2 \cdot 10^{-16}$. Moreover, the quality of the river predictor $X_{23_{\text{Rivers}}}$

improves (according to the likelihood and to Spearman correlation between $X23_{\text{Rivers}}$ and $Y23_{\text{Rivers}}$) when we use all of the terms in eq. (4.4), instead of only $P_{\text{total}}(t^*)$. The presence of more terms in eq. (4.4) does not increase the number of model parameters.

4.3.2.2 Sea level

Sea level can be modelled as the superposition of the barometric pressure effect, i.e., the pressure exerted by the atmospheric weight on the water, the wind-induced surge, and an overall annual cycle. As for the river predictor, we aggregate the different physical contributions in a single predictor. We define the sea level predictor on day t as:

$$X1_{\text{Sea}}(t) = a_{\text{S}}\, SLP_{Ravenna}(t) + b_{\text{S}}\ \vec{SLP}(t) \cdot \vec{R_{\text{MAP}}} + c_{\text{S}}\, sin(\omega_{1\text{Year}} t + \phi) + d_{\text{S}} \qquad (4.6)$$

where $SLP_{Ravenna}$ is the sea level pressure in Ravenna, $\vec{SLP} \cdot \vec{R_{\text{MAP}}}$ is the wind contribution due to the sea level pressure field SLP, the harmonic term is the annual cycle and d_{S} is a constant term. In eq. (4.6), the SLP field and the regression map are represented as column vectors. We choose the parameters of eq. (4.6) through regressing the sea level $Y1_{\text{Sea}}(t)$ on the right hand side of this equation. A more detailed physical interpretation of the terms is given in the following.

1. $a_{\text{S}} SLP_{Ravenna}$ accounts for the barometric pressure effect [181]. The regression map $\vec{R_{\text{MAP}}}$ indicates which anomalies of the SLP field are associated with high values of the residual of the barometric pressure effect (see Fig. 4.4, where also more details are given). Particularly, according to the geostrophic equation for wind, these pressure anomalies induce wind in the Adriatic Sea towards Ravenna's coast. Therefore, the projection of the SLP field onto this regression map, i.e, the term $\vec{SLP}(t) \cdot \vec{R_{\text{MAP}}}$, describes the wind-induced change in sea level at time t.

2. $c_{\text{S}}\ \ sin(\omega_{1\text{Year}} t + \phi)$ describes the remaining annual cycle of the sea level which is not described by barometric pressure effect and wind contribution. This harmonic term could be driven by the annual hydrological cycle [179], i.e., due to cyclic runoff of rivers which flow into the Adriatic sea, or due to density variations of the sea water (caused by the annual cycle of water temperatures). The astronomical tide may explain a minor fraction of this term. The range of variation of $c_{\text{S}}\ \ sin(\omega_{1\text{Year}} t + \phi)$ is about 10% of that of the sea level. When we use the predictor to extend the analysis to the period 1979-2015 this term will be kept constant assuming that the annual cycle has not drastically changed in past years. Moreover, we will not consider long-term sea level rise because its influence on both sea and impact h level variations is negligible over the considered period (the observed rate of sea

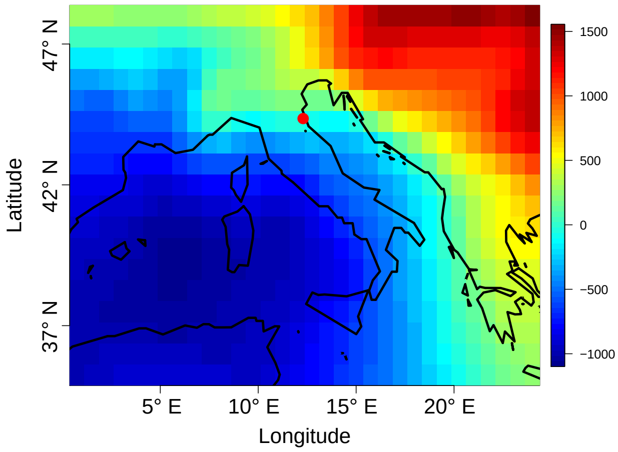

Figure 4.4: **Regression map employed to develop the sea level predictor.** The regression map $\vec{R_{\mathrm{MAP}}}$ is used in eq. (4.6). The value of the regression map in the location (i, j) is given by $R_{\mathrm{MAP}}(i, j) = var(R_0)^{-1} \cdot cov(R_0, SLP_{i,j})$, where $R_0(t)$ is the residual of the barometric pressure effect obtained from the fit of the linear model $a_0\, SLP_{Ravenna}(t) + d_0$ to $Y_{1_{\mathrm{Sea}}}(t)$. The Regression map is equivalent to a 1-dimensional maximum covariance analysis[203]. The red dot indicates Ravenna.

level rise in the North Adriatic Sea has been $\sim 0.8mm/year$[115]). Also, the relative sea level rise has been negligible over the considered period[24].

All the terms involved in the multiple regression model are statistically significant at level $\alpha = 2 \cdot 10^{-16}$.

4.4 Results

The results of the unconditional and conditional models are presented in the following sections. Details regarding the statistical inference of the joint pdfs (the selected pair-copula constructions and fitted pair-copula families) can be found in appendices A.3.1 and A.4.

4.4.1 Unconditional (3-dimensional) model

The unconditional model reproduces the joint pdf of the contributing variables $(Y_{1_{\mathrm{Sea}}}, Y_{2_{\mathrm{River}}}, Y_{3_{\mathrm{River}}})$, and, in conjunction with the autoregressive models, also the serial correlations. The model is used to simulate values of the impact h and assess the CF return periods, with related uncertainties.

Fig. 4.5 shows, qualitatively, a good agreement between simulated and observed contributing variables Y. In Fig. 4.6 we show the return levels of the impact h. There is

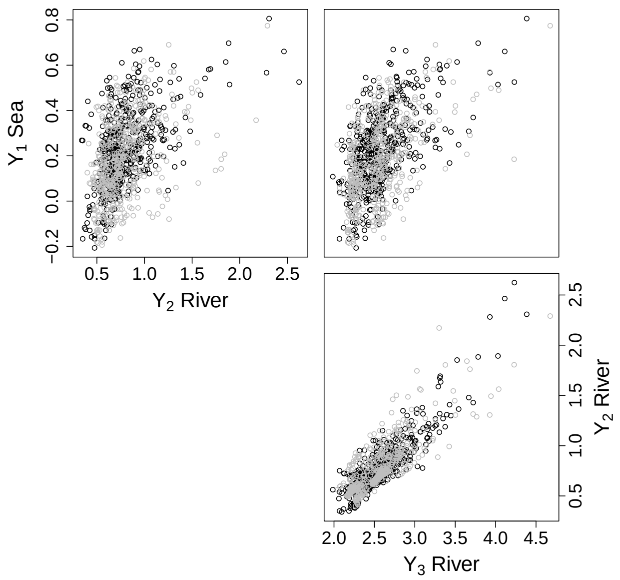

Figure 4.5: **Comparison of observed and simulated CF contributing variables.** Scatter plots of observed (grey) against simulated (black) contributing variables Y. The simulated series are obtained via the 3-dimensional model (including the serial correlation), and have same length as the observed.

good agreement between the model and observation based expected return levels, even for return periods larger than six years (the length of the observed data). For return periods larger than shown in Fig. 4.6, the agreement slowly decreases. The model based expected return period of the highest CF observed (3.19 m) is 18 years (the 95% confidence interval is $[2.5, \infty]$ years, where ∞ indicates a value larger than 10^{50} in this context from now on). The reason for such large uncertainty in the return period is the shortness of available data. However, the model based uncertainties are large but still smaller, up to return periods of about 60 years, than those obtained when computing the return level directly (based on the GEV) on the observed data of the impact (Fig. 4.6). Moreover, when considering a model which does not take the serial correlation of the contributing variables Y into account, we get an underestimation of the return period uncertainties. For example, the amplitude of the 95% confidence interval of the 20-years return level is underestimated by about 50% (not shown).

4.4.2 Conditional (5-dimensional) model

This model allows for assessing the change in the CF probability due to temporal variations of the meteorological predictors of the contributing variables Y. We calibrate the model to the period 2009-2015. After validating the model for the period 2009-2015, we use predictors of the period 1979-2015 to extend the analysis of CF probability to the past. We assess the quality of the model by comparing predictions with observations.

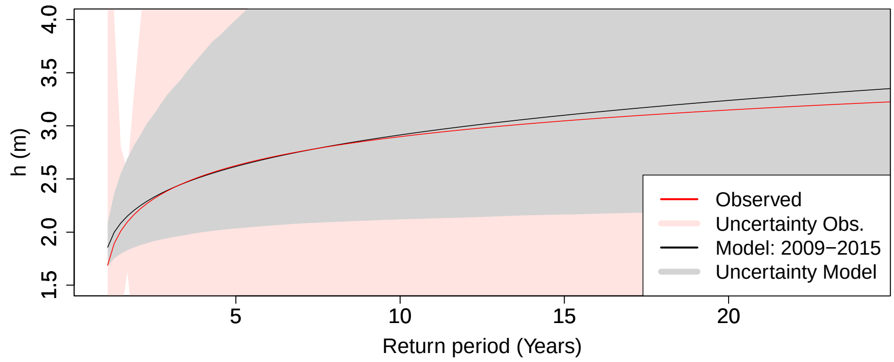

Figure 4.6: **Return levels of compound flooding based on the unconditional model.** Return levels of the impact h with associated 95% uncertainty intervals. The return level computed on h^{obs} is shown in red (uncertainty shown in light red). The model based return level is shown in black (uncertainty is in grey).

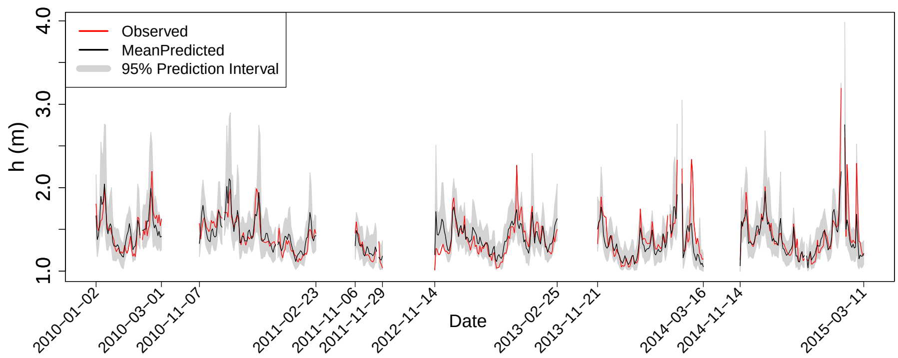

Figure 4.7: **Validation of the conditional model time series.** The validation is obtained through a 6-fold cross-validation. h^{obs} is shown in red. The average and 95% prediction interval of 10^4 simulated time series are respectively shown in black and grey.

Specifically, we look at its overall accuracy by considering the root-mean-square error between model predictions and observed data. Moreover, we look at the accuracy of the model when predicting extreme values of the impact h (defined as values of h larger than the 95-percentile of h^{obs}), using the Brier score (see appendix A.7). To assess the quality of the model, avoiding overfitting, we perform a 6-fold cross-validation (see appendix A.8).

The cross-validation time series of the impact h is visually compared with h^{obs} in Fig. 4.7. The average of the simulated cross-validation time series in general follows the temporal progression of h^{obs} (Fig. 4.7), and about 94% of the observed impact values lie within the 95% prediction interval. In particular, the highest flood observed is well predicted and lies inside the prediction interval. The Brier score based on the cross-validation time series is $BS_{CV} = 0.029$, while that relative to the reference model, i.e. the climatology (see appendix A.7), is $BS_{CL} = 0.046$. The resulting Brier skill score is $BSS = 1 - BS_{CV}/BS_{CL} = 0.38$, which indicates that the model is more accurate than the reference model in predicting extreme values of the impact h. In general, the skill of the model, both in terms of root-mean-square error and Brier score, does not change much when the cross-validation is not performed. This underlines that no artificial skill is present in the model. These positive results provide good confidence for extending the impact time series to the period 1979-2015. It also makes the model potentially interesting for flood forecasting and warning.

In Fig. 4.8A we show the return levels of the impact h. As in the unconditional model, return levels are stationary, i.e., estimated through fitting a stationary GEV distribution to annual maximum values. The discrepancy between model and observation based return levels for the conditional model is smaller than for the unconditional, in particular for high return periods. It may happen that the dependencies between river and sea levels are not considered in some analyses when assessing the flooding probability. Kew et al. [77] show in Rotterdam, which is affected by floods driven both from surge and river discharges, that the boundary conditions used to build the protection barrier were determined assuming independence between sea level and river discharge. Here we observe that ignoring such a dependence may result in an underestimation of the estimated flooding probability. The expected return period of the highest CF observed (3.19 m), computed over the period 2009-2015, is 20 years (the 95% confidence interval is $[4.9, \infty]$ years). When not considering the dependencies between river and sea levels, the expected return period of the highest CF observed increases to 32 years (the 95% confidence interval is $[6.7, \infty]$ years). Fig. 4.8B shows that the return level estimates are reduced by about 0.2 m when not considering such dependencies between sea and river levels. In particular, at the 95% confidence level, the return levels are underestimated when not considering these dependencies for return periods smaller than about 40 years. The same, however, cannot be clearly concluded for return periods larger than 40 years because of the large uncertainties (Fig. 4.8B). A similar result is obtained from the unconditional model (not shown). Therefore, although there is not a large difference in the return levels when treating sea and rivers independently or not, in Ravenna it should be relevant to consider their dependencies for flood risk estimation. An imprecise risk assessment may bring negative societal consequences due to inadequate information provided for infrastructural adaptation.

To estimate the CF return periods based on predicted values of the impact during the past, we run the simulations through conditioning on predictors of the period 1979-2015. This allows us to get a more robust estimation of the CF probability compared to that obtained considering only the period 2009-2015. The return levels in Fig. 4.8A (dashed line), are similar to that estimated when analysing the period 2009-2015. Although this result suggests a stationarity of the return levels during the period 1979-2015, we investigate if there has been any trend in the CF return levels during the recent past. To do this, we computed time-dependent return levels. Specifically, we computed stationary return levels on moving temporal windows of six years during the period 1979-2015, based on h^{sim} values obtained through conditioning on predictors belonging to these windows. However, we did not observe any long-term trend in the CF return levels. Moreover, analysing the return levels computed on moving temporal windows during the period 1979-2015, we did not observe any long-term trend neither in the return levels of storm surge nor in that of river floods (not shown).

During the period 1979-2015, there has not been a long-term trend in the CF return levels due to a variation of the marginal distributions of the predictors, or in their dependence. To study this, we computed the return levels on moving temporal windows in the cases described below. First, we simulated the impact through conditioning the Y^{sim} variables on predictors having the observed marginal distributions of the period 1979-2015, but fixing the dependence to that observed during 2009-2015. Secondly, we simulated the impact through conditioning on predictors having the observed dependence of the period 1979-2015, and fixed marginal distributions to the ones observed during 2009-2015. In both cases, we did not find any long-term trend in the return levels (not shown).

4.5 Discussion and conclusions

Based on the conceptual model presented in section 3.1, we have studied compound flooding (CF) in Ravenna. Here, the contributing variables of the CF are the river and sea levels, whose combination drives the impact, i.e., the water level in between the river and the sea.

We used a specific adaptation of the model to statistically downscale the river and sea level from meteorological predictors, and therefore estimate the impact of the CF as a function of the downscaled sea and river levels. The accuracy of the estimated impact appears satisfactory, such that the model is potentially interesting for use in both flood forecasting and warning. Also, the model based expected return levels of the impact are about the same as those directly computed on observed data of the impact. Although the model based uncertainty on these return levels is very large (due to the shortness of the available data), for return periods smaller than about 60 years it is smaller than that obtained computing the return periods directly on the observed data of the impact. In general, uncertainties can often be substantial because data for model calibration are often limited, thus uncertainties should be quantified to avoid drawing conclusions that may be misleading.

We calibrate the model over the period 2009-2015, and by including meteorological predictors obtained from the *ECMWF ERA-Interim* reanalysis dataset, we extend the

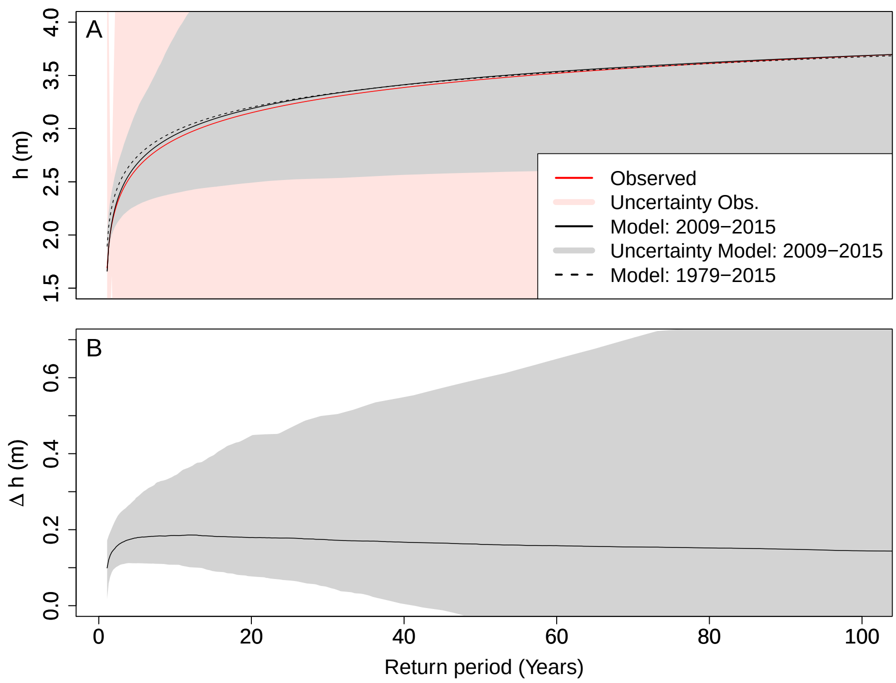

Figure 4.8: **Return levels of compound flooding based on the conditional model.** A: return levels of the impact h with associated 95% uncertainty intervals. The return level computed on h^{obs} is shown in red (uncertainty shown in light red). The model based return level computed for the period 2009-2015 (black) is based on h^{sim} values simulated for days where the observed data were available (uncertainty is shown in grey). The model based return level computed for the period 1979-2015 (black dashed) has uncertainty of similar amplitude to that of period 2009-2015 (not shown). B: difference between model based return level obtained when considering the realistic dependence between sea and river levels, and when assuming that they are independent. To make the dependencies between the sea and the river levels independent but keep the dependence between the two rivers, we shuffled the sea level data after each simulation, that guarantees random association between sea data and each of the rivers [182]. The black line represents the median of the bootstrap samples.

CF analysis to the full period of 1979-2015, to obtain a more robust estimation of the return periods. The expected return period of the highest CF observed, computed over the period 1979-2015, is 19 years (the 95% confidence interval is $[3.7, \infty]$ years). Moreover, we did not observe any long-term trend in CF return levels during the period 1979-2015.

Ignoring the estimated dependence between sea and river levels may lead to an underestimation of the CF probability. Specifically, assuming independence between sea and river levels, the expected return period of the highest CF observed - computed over the period 2009-2015 - is 32 years (the 95% confidence interval is $[6.7, \infty]$ years). When assuming the estimated dependence between sea and river levels, it decreases to 20 years (the 95% confidence interval is $[4.9, \infty]$ years). In other cities affected by sea surges and river flooding, e.g., in Rotterdam, protection barriers were designed assuming independence between sea level and river discharge [77], a decision which is still debated about[77,78,180]. In Ravenna, it should be relevant to consider these dependencies for the flood risk estimation. An imprecise risk assessment may harm the population at risk due to inadequate information provided for infrastructural adaptation. In general, when considering generic CEs, their associated risk may be substantially influenced by the dependence between the contributing variables, and so this dependence should be considered.

In the context of CF, only a few studies have explicitly quantified the CF impact[182,208,209], probably because of practical difficulties in quantifying the impact. For example, to quantify the impact of CF in the river mouth, it is necessary to have water level data at a station where both the influence of sea and river are seen. However, we have found few locations where these stations exist as, maybe in part, stakeholders are usually interested in data where only the influence of the river or the sea is seen. Also, for places where data show both the influence of sea and river, the measurements can be affected by human influences such as pumping stations between river and sea stations. Therefore, we argue that to obtain a more in-depth knowledge of these events, it may be very useful to create an archive containing data for locations where CF have been recorded, and eventually increase the effective number of measurements in places which are supposed to be under risk of CF.

5. Higher CF probability in Europe under anthropogenic climate change

In this chapter, based on the multivariate return periods described in section 3.3, we estimate the probability of potential compound flooding (CF) along the European coasts both under present and future climate conditions. The content of this chapter is part of Bevacqua et al.[20], which is currently under revision for publication.

5.1 Introduction

Several studies have demonstrated the importance and damaging nature of CF for selected locations[19,60,80,109,182]. Comprehensive studies, however, exist only for the UK[165], Australia[204,210] and the US coast[198]. The latter study detected an increasing probability of CF during the past decades, although it was not possible to attribute this increase to anthropogenic climate change. But given that extreme precipitation[123], river flooding[65], and extreme sea levels[57,64,195] are expected to increase under future climate change, it is likely that also the CF probability will increase along with these driving processes. Furthermore, coastal cities are expected to further grow in the coming decades[57] and more and more people will be exposed to CF, rendering an analysis of CF in the future urgent. So far, only the effect of mean SLR on the changing CF hazard has been analysed, and only for selected locations in the US[109]. The future CF probability, taking into account future changes of precipitation, storm surges, waves, and astronomical tides, has not been assessed yet.

Our study aims to close this research gap. We analyse the present and future CF hazard along the European coasts. A precise CF hazard probability assessment can in practice only be site-specific because the actual CF hazard depends strongly on local conditions such as the shape of the coastline, the orography and land surface of the surrounding land area where precipitation is collected. Furthermore, the final CF risk estimate depends also on the existing flood protection, and the exposed population and assets. Modelling such local details would, however, preclude a continental-scale analysis. Thus we limit ourselves to modelling the *probability of potential CF*: we follow the approach of previous studies[64,198] and model the probability of co-occurring extreme sea levels and heavy precipitation. For the sake of brevity, however, we will write *CF probability* only. At the end of the 21st century, SLR will be the primary threat for coastal areas (appendix B, Fig. B.1), Societies are aware that they will need to adapt to this impact of climate change by raising dikes, constructing new flood protection, or abandoning coastal areas[57,64]. However, CF may pose an additional hazard that has to be considered. Therefore, for the projections, we focus on the additional CF hazard caused by the meteorological CF drivers, without considering mean SLR.

5.2 Data and Methods

To characterise extreme sea level, we consider daily maximum values of the superposition of storm surges (including waves) and astronomical tides. In the following, we will refer to these maxima simply as sea level. Storm surges and waves are simulated with the hydrodynamic DFLOW FM[195–197] and Wavewatch III[105,195,196] models respectively, driven with ERA-Interim reanalysis data[37] for present climate (1979-2014), and with six selected CMIP5 models[168] for present (1970-2004) and future climate (2070-2099); astronomical tides are simulated separately (see Methods for more details about the sea level modelling). Precipitation is directly taken from the reanalysis and the climate models. On each day, we consider accumulated precipitation within a time range of ± 1 days, which allows us to account for the mentioned mechanisms responsible for CF (see section 2.3.1), and precipitation occurring just before and after midnight of the storm surge day[99]. We define univariate extremes of the individual hazards as events occurring on average every 1 year for sea level and precipitation. (The results are qualitatively similar when employing 200-days and 5-years as thresholds.) CF return periods are defined as the average waiting time between the co-occurrence of these extreme events[185] (appendix B, Fig. B.5). We model the dependence of sea level and precipitation extremes by a copula-based multivariate probability model. For an evaluation of the simulated CF probability see appendix B (Fig. B.2, B.3, and B.4). Further information about data and methods follow.

5.2.1 Data

Storm surges are simulated with the DFLOW FM model using a flexible mesh setup (forced with 6-hourly wind and atmospheric pressure fields)[112,195–197]. Waves are simulated with the model Wavewatch III[105,195,196] (forced with 6-hourly wind field). Astronomical tides are simulated every six hours using the FES2012 model[25,112,161], which makes use of satellite altimetry data. The resulting sea level data are available every ∼25 km along the coastline. Comprehensive validation and detailed information of the models can be found in refs.[105,112,195–197] (general information on the models can be found also at the end of section 2.3.1.1). Our analysis is based on quantile values, therefore we do not bias correct simulated data. Sea level and precipitation data are based on ERA-Interim and six selected models from the CMIP5 multi-model ensemble (appendix B, Table B.1). Precipitation is taken from the grid point nearest to each coastal location. CMIP5 models are selected based on the skill in representing the synoptic climatologies and inter-annual variations across the north-east Atlantic region[105,122,195–197]. The GFDL-ESM2G model is not considered along the Black Sea coast because of instabilities of the surge model. Choosing well performing CMIP5 models reduces the risk of artefacts caused by the delta change approach[96] (see below).

The effect of SLR on the astronomical tide is quantified through dynamic tidal ocean simulations (using the DFLOW FM model). The simulations consider SLR scenarios resulting from the combination of steric changes with three land-ice scenarios of water contributions from ice sheets and glaciers[64]. The analysis is described in detail in Vousdoukas et al.[195] with the only difference that we consider changes in the complete time series, rather than in the daily maxima only. Since the sensitivity of the final tide amplitude to the land-ice scenarios is very small[195], we consider the median of the three scenarios only. The actual observed time-lag between the surge and astronomical tide sequences is random. The estimated CF return periods are thus just one random realisation of all possible time-lags between surges and astronomical tides. To get an estimate of a more likely CF return period we compute the median of all possible estimates. We observe that this procedure does not allow to take into account the variability of the return periods due to the natural variability of the meteorological conditions. For the ERA-Interim driven data, we obtain this estimate by calculating 240 individual estimates based on the superposition of (i) the simulated surge time series (including waves), and (ii) the randomly shifted tide time series. The part of the tide series beyond the length of the surge series was moved to the start date. From this ensemble we compute the median of the CF return periods (Fig. 5.1). It turned out that the difference between the standard estimate and the bootstrap-based estimate was small. As this procedure is computationally expensive, we therefore refrained from applying it to the CMIP5-based data. More in-depth information about data sources can be found in the *Data availability* section of Bevacqua et al.[20].

Assessing the effect of all the non-linear interactions between the sea level components (i.e. SLR, astronomical tides, waves, and storm surges), would render a continental study of present and future climate unfeasible because of the high computational costs. Therefore, in this study, we do not account for these non-linear interactions, except for the influence of SLR on astronomical tides. As discussed in chapter 2, in principle, treating these components as independent variables can affect the accuracy of the sea level extremes, especially in shallow water bodies. However, previous studies have demonstrated the validity of the approach of treating the sea components as independent for climate change projections[72,88,162,202], and this approach is common in similar large-scale studies[87,196]. These non-linear interactions would not qualitatively change the conclusion of our large-scale study.

5.2.2 Return periods

As explained in section 3.3, we define the bivariate CF return periods[54,138,185] as the mean waiting time between events where sea level and precipitation simultaneously exceed the individual 1-year return levels (i.e. the $\sim 99.7^{th}$ percentiles $s_{99.7}$ and $p_{99.7}$). The marginal distributions of sea level and precipitation beyond the selection thresholds are modelled by a Generalised Pareto Distribution (GPD). Copulas were fitted to (u_S, u_P) (obtained via empirical marginal cumulative distribution function (CDF)[185]), and selected via Akaike information criterion from the families: Gaussian, t, Clayton, Gumbel, Frank, Joe, BB1, BB6, BB7, BB8. Marginal distributions and copulas were fitted through a maximum likelihood estimator (via the *ismev*[61] and *VineCopula*[140] R-packages). Goodness of fit of marginals and copulas was tested based on the Cramer-von-Mises criterion[51] (one-tailed; $N_{boot} = 100$ for copulas) (via the *eva*[10] and *VineCopula*[140] R-packages respectively). The projected change (%) of the return period T (Fig. 5.2a) is estimated as $\Delta T(\%) = 100 \cdot (T^{2070\text{-}2099} - T^{1970\text{-}2004})/T^{1970\text{-}2004}$ for the individual CMIP5 models.

5.2.3 Sampling uncertainty of ERA-Interim based CF return periods

To obtain the 95% sampling uncertainty range of the ERA-Interim based CF return periods in Fig. 5.2c, we apply a resampling procedure. The uncertainty is computed in the eleven representative locations whose return periods are shown in black in Fig. 5.2c. We base our estimate of sampling uncertainty on the previously generated 240 bivariate sea level/precipitation time series (where surge and precipitation is identical, only astronomical tides have been resampled). Each of these 240 bivariate time series are used for a further resampling procedure by combining bootstrapped numerator and denominator values of the return period expression (eq. (3.8)). The numerator bootstrapped μ values are obtained based on resampling of the observed times elapsing between the selected pairs (s_i, p_i) employed for fitting the parametric probability density function (pdf); the denominator bootstrapped values are obtained based on resampling of the observed pairs (s_i, p_i) used for the fit of the pdf. The final return period sampling uncertainty range is defined as the 2.5^{th} - 97.5^{th} percentile interval of the 240·240 return period estimates. This procedure is preferred to a classic resampling of all of the pairs, which - here - would overestimate the obtained median return period due to the serial correlation of the sea level time series. Based on a large sample of data without any serial correlation, we estimated that our procedure overestimates by 30% the 95% sampling uncertainty range (with respect to a classic resampling procedure). Thus, conclusions about the detection of a climate change signal in the future (Fig. 5.2c) are conservative.

5.2.4 Delta change approach

We compute CF return period for future via the delta change approach[98], i.e. multiplying the ERA-Interim based historical return period $T_{Era}^{1980-2004}$ by the individual CMIP5 model i variation of the probability $T_{Model\ i}^{2070-2099}/T_{Model\ i}^{1980-2004}$. The present day reference period is the intersection of the ERA-Interim and the historical CMIP5 data, for which sea level simulations are available. See appendix B: (Fig. B.4) for comparing return periods based on ERA-Interim and individual CMIP5 models, and (Fig. B.9) for CMPI5 model-mean return periods in present and future.

5.2.5 Return period for independent drivers

We estimate the CF return period assuming independence between precipitation and sea level via shuffling (500 times) the cumulated precipitation time series (during 1980-2014), and plugging an independent copula in eq. (3.8). Then, we extract the median of the 500 return periods associated with the shuffled time series. The shuffling is required because the average time elapsing between the events μ in eq. (3.8), and the marginals F_S and F_P, are also affected by the dependence between precipitation and sea level.

5.2.6 Attribution of return period variation

We carry out three experiments[19] to assess how the CF probability would change in future when only considering variation - with respect to the present - of: (a) the dependence between sea level and precipitation, (b) the sea level and (c) precipitation overall marginal distributions (i.e. the distribution of the sea level without reference to precipitation, and vice versa). We estimate the relative change of the probability that would have occurred for experiment (i) as $\Delta_{\mathrm{exp\ i}} = 100 \cdot (T^{\mathrm{fut}}_{\mathrm{exp\ i}} - T^{\mathrm{pres}})/T^{\mathrm{pres}}$ (Fig. 5.3), where T^{pres} is the return period for the present period and $T^{\mathrm{fut}}_{\mathrm{exp\ i}}$ is computed as follows. Experiment (a): given the variables $(S_{\mathrm{fut}}, P_{\mathrm{fut}})$, we get the associated empirical cumulative distribution $(U_{S_{\mathrm{fut}}}, U_{P_{\mathrm{fut}}})$. From the variables S_{pres} and P_{pres} we define the empirical CDFs $F_{S_{\mathrm{pres}}}$ and $F_{P_{\mathrm{pres}}}$, through which we define $S_{\mathrm{a}} = F^{-1}_{S_{\mathrm{pres}}}(U_{S_{\mathrm{fut}}})$ and $P_{\mathrm{a}} = F^{-1}_{P_{\mathrm{pres}}}(U_{P_{\mathrm{fut}}})$. The variables $(S_{\mathrm{a}}, P_{\mathrm{a}})$ have the same Spearman correlation and tail dependence[19] as $(S_{\mathrm{fut}}, P_{\mathrm{fut}})$, but marginal distributions as in the present period. We compute the return period $T^{\mathrm{fut}}_{\mathrm{exp\ a}}$ based on $(S_{\mathrm{a}}, P_{\mathrm{a}})$. Experiment (b): given the variable S_{pres}, we get the associated empirical cumulative distribution $U_{S_{\mathrm{pres}}}$. From the variable S_{fut} we define the empirical CDFs $F_{S_{\mathrm{fut}}}$, through which we define $S_{\mathrm{b}} = F^{-1}_{S_{\mathrm{fut}}}(U_{S_{\mathrm{pres}}})$. The variables $(S_{\mathrm{b}}, P_{\mathrm{pres}})$ have the same Spearman correlation and tail dependence as during the present, but the marginal distribution of S_{b} is that of the future. We compute the return period $T^{\mathrm{fut}}_{\mathrm{exp\ b}}$ based on $(S_{\mathrm{b}}, P_{\mathrm{pres}})$. Experiment (c): as experiment (b), exchanging precipitation and sea level variables.

5.3 Results

The highest CF probability in present climate is experienced mostly along the Mediterranean Sea (Fig. 5.1). The Atlantic coast appears to be particularly exposed to co-occurring storm surges and extreme precipitation (appendix B, Fig. B.6). But here the effective probability is slightly reduced because of the high tidal range (appendix B, Fig. B.6): no CF occurs when the peak of the storm surge occurs during low astronomical tide[56]. In present climate, about 3% of the coastline experience return periods of compound flooding shorter than 6 years. These regions are the Gulf of Valencia (Spain), the north-western Algeria, the Gulf of Lion (France), south-eastern Italy, the northwest Aegean coast, southern Turkey, and the Levante region (Fig. 5.1). The statistical dependence between sea level and precipitation greatly enhances the probability of CF along the European coasts: when ignoring the dependence, the CF return period increases by up to two orders of magnitude (365 years is the expected return period in the independent case).

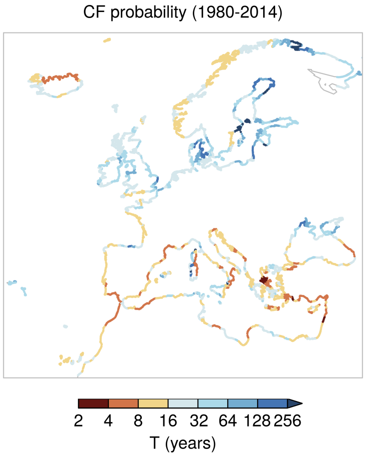

Figure 5.1: **Present probability of potential compound flood (CF).** Return periods of CF (co-occurring sea level and precipitation extremes, i.e. larger than the individual 1-year return levels) based on ERA-Interim data.

In a warmer future climate, the probability of CF is projected to robustly increase particularly along the west coast of Great Britain, northern France, the east and south coast of the North Sea, and the eastern half of the Black Sea (Fig. 5.2a and Fig. B.7 in appendix B). The fraction of coastlines experiencing return periods lower than 6 years is projected to increase from 3% in present climate to 11% at the end of the 21st century. Hotspot regions where return periods will fall below this value are the Bristol Channel and the Devon and Cornwall coast in the UK, as well as the Dutch and German North Sea coast (Fig. 5.2b).

The forced climate change signal appears to emerge from the uncertainty about present probability mostly along the Western British Isles, the North and Baltic Sea (regions 3, 4, and 5 in Fig. 5.2c). Along the Noorderzijlvest water board, which also faces the greatest SLR, the model-mean probability of potential CF occurrence will triple. The Norwegian West coast around Bergen will see a fivefold increase in potential CF frequency. Along much of the Mediterranean coast, climate models do not agree about the direction of future changes in CF probability, along the Strait of Gibraltar CF probability is even expected to decrease (Fig. 5.2a and Fig. B.7 in appendix B).

Changes in CF probability can in principle be caused by changes in the probability of extreme sea levels, in the probability of extreme precipitation, or in the dependence between both hazards[19,109,182,198]. For Europe and the Mediterranean, the main driver of future changes in CF probability appears to be changes in precipitation (Fig. 5.3). A warmer atmosphere will allow storms to carry more moisture resulting in heavier precipitation. This thermodynamic effect dominates along the North Atlantic storm track in Northern Europe, and the Mediterranean storm track[123]. But weaker upward winds will reduce or balance the thermodynamic increases of extreme precipitation along

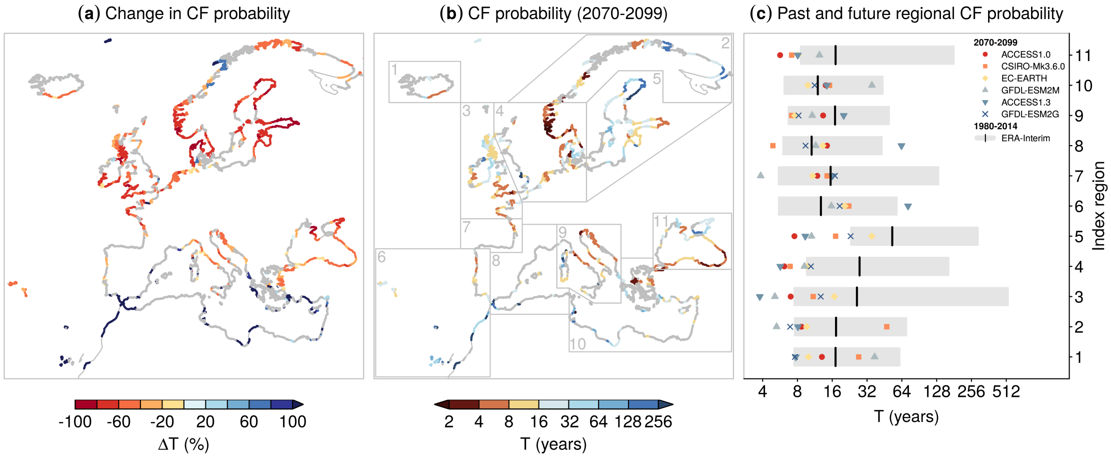

Figure 5.2: **Future probability of potential compound flood (CF).** (**a**) Multi-model mean of projected change (%) of CF return periods, between future (2070-2099) and present (1970-2004) climate. (**b**) Return periods for the future (2070-2099). Grey points indicate locations where only 4 or fewer out of 6 models agree on the sign of the return period change (3 or less out of 5 models in the Black Sea). Areas of grey points in (**a**) and (**b**) are slightly different, as the former are computed taking into account the past period (1970-2004) and the latter the period (1980-2004) (see delta change approach in Methods). (**c**) Median value of CF return periods over regions defined in (**b**) for past (1980-2014, based on ERA-Interim (Fig. 5.1)) and future (2070-2099) climate, separately for individual models. For ERA-Interim, grey shading illustrates the sampling uncertainty 95% range.

the North African coast[123], and will even reverse the full precipitation response over north-western Africa[123] (panel c, also Fig. B.8 in appendix B). For most regions, the considered models do not agree on the sign of changes in CF probability due to changes in the dependence between precipitation and extreme sea levels (panel a, see also Methods). Changes in the occurrence of extreme sea levels cause a CF probability decrease along the Mediterranean coast, and an increase along the the west coast of Great Britain and North Sea, and eastern cost of the Baltic Sea (panel b, also Fig. B.8 and B.7 in appendix B).

5.4 Discussion and conclusions

Rising mean sea levels will pose the main threat along coastal areas in a warmer climate, and changes in storm surges and precipitation will additionally alter the coastal flood hazard. Coastal planning agencies in Europe are aware of these changing hazards and will likely develop adaptation strategies[57,64,201]. Here we have demonstrated that CF may pose a severe additional flood hazard that has to be taken into account for a full risk assessment. In particular Northern Europe will experience an increasing CF hazard beyond the effects of mean sea level rise, caused mainly by more intense precipitation in a warmer climate.

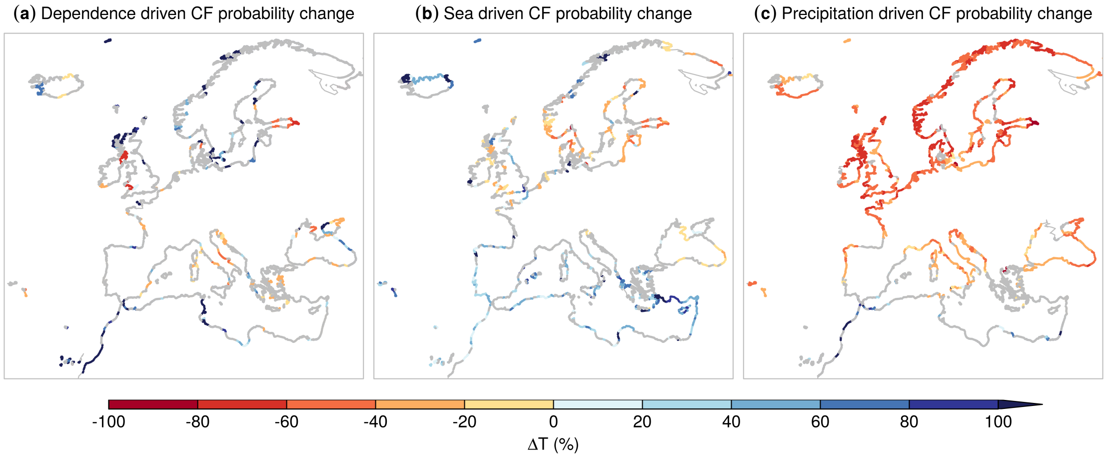

Figure 5.3: **Attribution of probability change in potential compound flood (CF) to changes in dependence and marginal distribution.** Multi-model mean of projected change (%) of CF return periods between future (2070-2099) and present (1970-2004) when only taking into account future changes of: the overall (**a**) dependence (Spearman and tail dependence[19]) between sea level and precipitation, (**b**) sea level distribution, and (**c**) precipitation distribution (Methods). The total projected probability variation (Fig. 5.2a) is not given by the sum of these three cases (**a**, **b**, **c**), as the overall dependencies and marginal distributions do not contribute linearly to the CF return periods. SLR is not considered in the definition of future sea levels (see text). Grey points indicate locations where only 4 or fewer out of 6 models agree on the sign of the return period change (3 or less out of 5 models in the Black Sea).

Ignoring the dependency in the occurrence of heavy precipitation and storm surges may severely underestimate the CF impact in a warming climate[198,215]. Thus, in CF prone areas, especially in areas experiencing an increasing CF hazard, additional coastal protection measures may be required. As such interventions are a costly challenge with potentially adverse effects on coastal societies and ecosystems, they need to be carefully planned. Here, detailed local assessments are required integrating information about precipitation, discharge, surges, topography and land-use, relative sea level rise and existing and planned protection measures[198]. Our study identifies European regions potentially facing CF in a warmer future climate and thereby provides a continental-scale basis for such planning activities.

6. Soil moisture drought in Europe: a compound event of precipitation and potential evapotranspiration on multiple timescales

In this chapter, we employ the conceptual model (presented in chapter 3) to assess how variables employed in common drought indices, namely precipitation and potential evapotranspiration (PET), contribute to soil moisture drought. The content of this chapter was published in Manning et al.[93].

6.1 Introduction

Drought indices incorporating precipitation and temperature through PET are often employed as proxies of soil moisture[35,187]. As evapotranspiration (ET) is moisture limited in dry climates, the use of such drought indices has often been criticised. Thus, the question remains whether such indices can provide an adequate representation of soil moisture drought[58]. We, therefore, assess the contributions of both precipitation, PET, and their dependence (on multiple timescales related to both meteorological drought and heat waves) to soil moisture drought. Understanding the contribution of PET and precipitation to soil moisture in different climates can help in the interpretation of future changes depicted by drought indices.

Based on the conceptual model presented in section 3.1, we describe soil moisture as a function of precipitation integrated over preceding months, and PET integrated over

Table 6.1: **Information about the FLUXNET sites used throughout this study.**

Site	Site Name	Lat.	Long.	Site Type
(a)	Dripsey, Ireland	51.99^o N	8.75^o W	Grassland
(b)	Hainich, Germany	51.08^o N	10.45^o E	Forest
(c)	Klingenberg, Germany	50.89^o N	13.52^o E	Grassland
(d)	Oensingen, Switzerland	47.28^o N	7.73^o E	Grassland
(e)	Pang/Lambourne, UK	51.45^o N	1.27^o W	Forest
(f)	Le Bray, France	44.72^o N	0.77^o W	Forest
(g)	Amplero, Italy	41.9^o N	13.6^o W	Grassland
(h)	Las Majadas del Tietar, Spain	39.94^o N	5.77^o W	Savanna/Grassland
(i)	Bugacpuszta, Hungary	46.69^o N	19.6^o E	Grassland
(j)	Mitra IV Tojal, Portugal	38.48^o N	8.02^o W	Grassland
(k)	Vall d'Alinya, Spain	42.15^o N	1.45^o E	Grassland

recent days. This conceptual framework allows us to capture days of extreme temperature within the PET variable and its dependence on antecedent conditions. We aim to demonstrate the individual contributions of precipitation and PET to the estimation of soil moisture drought and highlight where, when and over what integration period lengths PET and its dependence with precipitation are important for the estimation of soil moisture.

6.2 Data

We employed the Fluxnet dataset [11] for this study using 11 stations situated across Europe. The sites were selected based on the data quality and length, and also following the recommendations of Rebel et al. [129]. Table 6.1 provides a summary of the site characteristics. To aid the interpretation of the results, we classify the sites as wet or dry based on values of soil moisture. Locations are provided in Fig. 6.1. At each site, soil moisture measurements from the top 30cm of soil are provided along with precipitation data as well as the variables required for the calculation of PET via the reference crop Penman-Monteith equation, as described in ref. [212]. These variables include incoming solar radiation, temperature, wind speed and relative humidity. Among the selected sites, two general land cover types are available; grassland and forest. The data used here are at a daily resolution. We use soil moisture values for the summer months of June, July and August (JJA). For the contributing meteorological variables, we used observations that extend back into previous months in order to calculate integration periods prior to a given soil moisture observation.

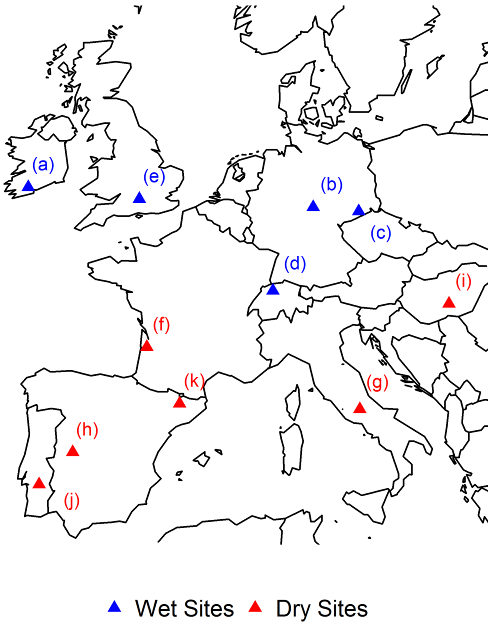

Figure 6.1: **Fluxnet sites.** Locations of Fluxnet sites employed for this study.

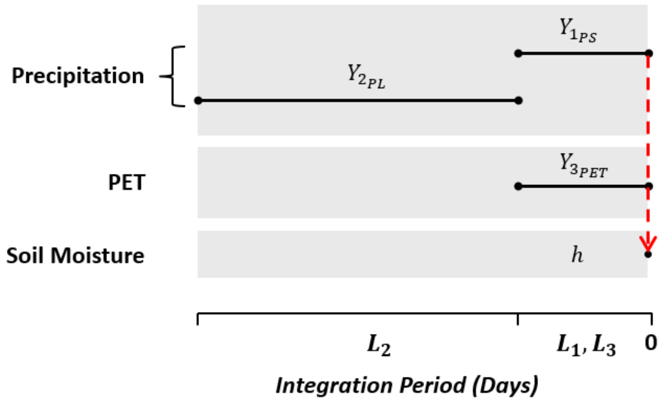

Figure 6.2: **Soil moisture drivers.** Schematic of the variables used in this study to construct the soil moisture model.

6.3 Model development

We use the conceptual model presented in section 3.1 in the version $f_{h|\tilde{Y}}(h|\tilde{Y})$, which allows us to describe soil moisture h as an impact of contributing meteorological variables Y. Details about the statistical inference of the multivariate pdf $f_{h|\tilde{Y}}(h|\tilde{Y})$, including the selection of the PCC, are given in appendix C. The contributing meteorological variables include a short-term precipitation variable ($Y_{1_{PS}}$), a long-term precipitation variable ($Y_{2_{PL}}$) and a PET variable ($Y_{3_{PET}}$) that are integrated over periods L_1, L_2 and L_3 respectively. A schematic representation of the variables modelled is given in Fig. 6.2.

$Y1_{PS}$ and $Y2_{PL}$ respectively represent the most recent and antecedent precipitation that influence the short and long-term variability of soil moisture. Their respective integration periods L_1 and L_2 are non-overlapping. Two precipitation variables are required to better capture the temporal distribution of precipitation that would otherwise be lost using one long-term integration only.

$Y3_{PET}$ represents PET integrated over the period L_3. PET is often employed as an estimate of ET in drought indices given the lack of ET data. We calculate PET using the reference crop Penman-Monteith equation as defined in ref.[212] where it is derived from incoming solar radiation, temperature, wind and the actual and saturation vapour pressures. $Y3_{PET}$ includes temperature within its calculation and so can capture heat waves that influence the drying of soil moisture. Depending on the question at hand, the integration length L_3 is varied, more details are given in the next sections.

When performing conditional sampling of h, given observed Y, we produce a stochastic time series of h. Repeated simulations conditioning on observed Y will produce multiple time series with varying statistics and agreement with observed h values[125]. Throughout this study, given an observed time series of Y, we produce an ensemble consisting of 1000 members of h time series and obtain a probabilistic forecast of h at each time step.

6.3.1 Meteorological predictor selection

We describe soil moisture h as a function of two precipitation variables, $Y1_{PS}$ and $Y2_{PL}$, integrated over periods L_1 and L_2, and a PET variable, $Y3_{PET}$, integrated over the period L_3. By developing a statistical model with these variables and soil moisture, we look to answer the following three questions:

1. What are the individual contributions of the meteorological variables Y_i to the estimation of soil moisture h on timescales related to meteorological drought and heat waves?
2. What relevance does the dependence between antecedent precipitation ($Y2_{PL}$) and recent PET ($Y3_{PET}$) have for the estimation of low soil moisture values?
3. What relevance does PET have for the estimation of soil moisture over varying integration lengths L_3?

To answer these questions, we propose two sets of Y variables, $S1$ and $S2$. Questions 1 and 2 are then approached using variable set $S1$ while Question 3 is approached using variable set $S2$. The difference between $S1$ and $S2$ is the integration L_3 chosen at each site. A short integration period is considered for PET in S1, while a long integration period is considered for PET in S2. For each value of $\mathrm{L_i}$ used, the contributing meteorological variable $\mathrm{Y_i}$ may be defined as:

$$\begin{aligned} Y1_{PS}(t) &= \sum_{t-L_1+1}^{t} p(t) \\ Y2_{PL}(t) &= \sum_{t-(L_1+L_2)+1}^{t-L_1} p(t) \\ y3_{PET}(t) &= \sum_{t-L_3+1}^{t} pet(t), \end{aligned} \tag{6.1}$$

where $p(t)$ and $pet(t)$ are respectively daily precipitation and PET.

We address the first two questions with variable set $S1$. The selected $\mathrm{L_i}$ for $S1$ must result in Y variables that provide satisfactory estimates of soil moisture h, hold physically meaningful dependencies and capture timescales relevant for both meteorological drought and heat waves. Physically meaningful dependencies are obtained by constraining $\mathrm{L_i}$ such that $\mathrm{L_1} = \mathrm{L_3}$ and through ensuring that there is no overlap between $\mathrm{L_2}$ and the short-term integrations.

Based on the analysis described below, we find a difference between grassland sites and forest sites. Forest sites require a longer integration $\mathrm{L_1}$. This is possibly explained by the deeper root systems at forest sites which filter the influence of short-term variability in rainfall on the integrated soil column. We therefore choose two sets of L; LG and LF for grassland and forest sites respectively. At all grassland (forest) sites, the same LG (LF) are used.

We choose integrations of $\mathrm{LG_1} = \mathrm{LG_3} = 7$ and $\mathrm{LG_2} = 63$ for grassland sites. For forest sites, we choose integrations of $\mathrm{LF_1} = \mathrm{LF_3} = 30$ and $\mathrm{LF_2} = 60$. We thus use information of precipitation over the previous 70 and 90 days for each daily soil moisture observation at grassland and forest sites respectively.

To select $\mathrm{LG_i}$ ($\mathrm{LF_i}$) in $S1$, we firstly calculate the Spearman correlation between $\mathrm{Y_i(t)}$ and h(t) for multiple integrations within a window of 120 days prior to day t. We then choose the integration length that maximises the Spearman correlation for each Y_i. Integration periods are then constrained such that $\mathrm{LG_1} = \mathrm{LG_3}$ ($\mathrm{LF_1} = \mathrm{LF_3}$). This ensures physically meaningful dependencies and avoids arbitrary dependencies that would otherwise arise between differing $\mathrm{LG_1}$ ($\mathrm{LF_1}$) and $\mathrm{LG_3}$ ($\mathrm{LF_3}$).

The sensitivity of the conditional model's performance, in representing h conditioning on Y, to changes in LF (LG) is tested by varying the short-term LG (LF) by $+/-4$ days while the long-term integration LG (LF) is varied by $+/-10$ days. Changes in performance are found to be minimal (not shown). Assuming the same LG (LF) at all grassland (forest sites) and constraining the integration periods is therefore expected to have little weight in the outcome of this analysis.

We acknowledge in $S1$ that the influence of most recent daily temperature extremes on soil moisture is potentially filtered out at forest sites by setting $LF_3 = 30$. This is addressed in variable set $S2$ where we assess the relevance of the selection of L_3 to the estimation of h (Question 3). In $S2$, two models are constructed using a short and long-term integration of L_3. The same LG_1, LF_1, LG_2, and LF_2 as $S1$ are used while LG_3 and LF_3 are set to 7 and 70 days, and 7 and 90 days respectively.

6.3.2 Model evaluation metrics

The model simulations are evaluated overall and in their ability to represent low values of soil moisture h. Using the Brier score (BS), we evaluate the accuracy of probabilistic predictions of low h values defined as those below the 15^{th} percentile of observed soil moisture (see appendix A.7). The model is also evaluated in its ability to capture the persistence of drought conditions using an empirical drought persistence probability (PP), defined as:

$$PP = Pr(h_{t+1} < F_h^{-1}(0.15) \quad | \quad h_t < F_h^{-1}(0.15)), \tag{6.2}$$

that is the probability that a drought (soil moisture is below the 15^{th} percentile) at time $t+1$ is observed, given a drought at time t.

6.4 Results

The set of variables $S1$ (described in section 6.3.1) are employed to evaluate the contributions of the individual Y variables and that of their dependence structure to soil moisture. To achieve this we perform a number sensitivity simulations and compare them with a control simulation (CTRL). All simulations carried out are done through a K-fold cross-validation to avoid over-fitting. K here is the number of summers in a time series at a given site. In each simulation, we thus remove one summer at a time when fitting the copula parameters but use the same marginal PDFs for each period. In this way we only cross-validate the PCC rather than the entire multivariate statistical model. For each simulation, we then produce a probabilistic forecast of h consisting of 1000 members through conditioning on specified values of Y.

6.4.1 Model performance

The CTRL simulation is performed through sampling h conditioned on observed values of Y. The performance of CTRL may be qualitatively gauged from Fig. 6.3. Plots shown in panels (a) to (e) are results from wet sites while those from (f) to (k) are results from dry sites. The mean value of h from CTRL at each time step can be seen to follow the temporal evolution of observed soil moisture (h^{obs}) quite well while h^{obs} is generally found within the 95% confidence interval of CTRL. Also shown within each panel in Fig. 6.3 are the persistence probabilities of low h for observed (PP_{obs}) and mean simulated h (PP_{sim}). PP_{sim} and PP_{obs} are found to be very similar at all wet sites and most dry sites although PP_{sim} is generally less than PP_{obs} at dry sites. A comparison of the observed ACF, estimated up to order 10, with the ACF derived from the mean of the simulation also showed close correspondence at each site (not shown). Such results indicate good agreement between the observed h and simulated mean h in terms of temporal evolution and the persistence of low values.

To provide information of the performance of the model in terms of the probabilistic forecast, we calculate Brier scores (BS) and Brier Skill Scores (BSS) for CTRL at each site (Table 6.2). In general we see good BS and positive BSS that range from 0.06 to 0.12 and 0.04 to 0.51 respectively with medians of 0.09 and 0.25. These BSS indicate that the model is better than the climatology at predicting low soil moisture values. Low BSS values are seen at Site (c) where we also see poor correspondence between h^{obs} and the mean of CTRL. Optimising the performance of the model at this site through changing integration periods does not bring a noticeable improvement indicating that the proposed model and variables included do not predict soil moisture correctly at all sites. However, with satisfactory results generally obtained at most sites, we employ the model for use in sensitivity analysis in a number of tests presented below.

6.4.2 Assessment of contributing variables to soil moisture

We test the contribution of $Y1_{\mathrm{PS}}$ (short-term precipitation), $Y2_{\mathrm{PL}}$ (long-term precipitation), and $Y3_{\mathrm{PET}}$ (PET), to the estimation of h in three sensitivity simulations SENS-$Y1_{PS}$, SENS-$Y2_{PL}$, and SENS-$Y3_{PET}$ respectively. For each sensitivity simulation, h is sampled conditioning on the median value of the respective variable to be tested and

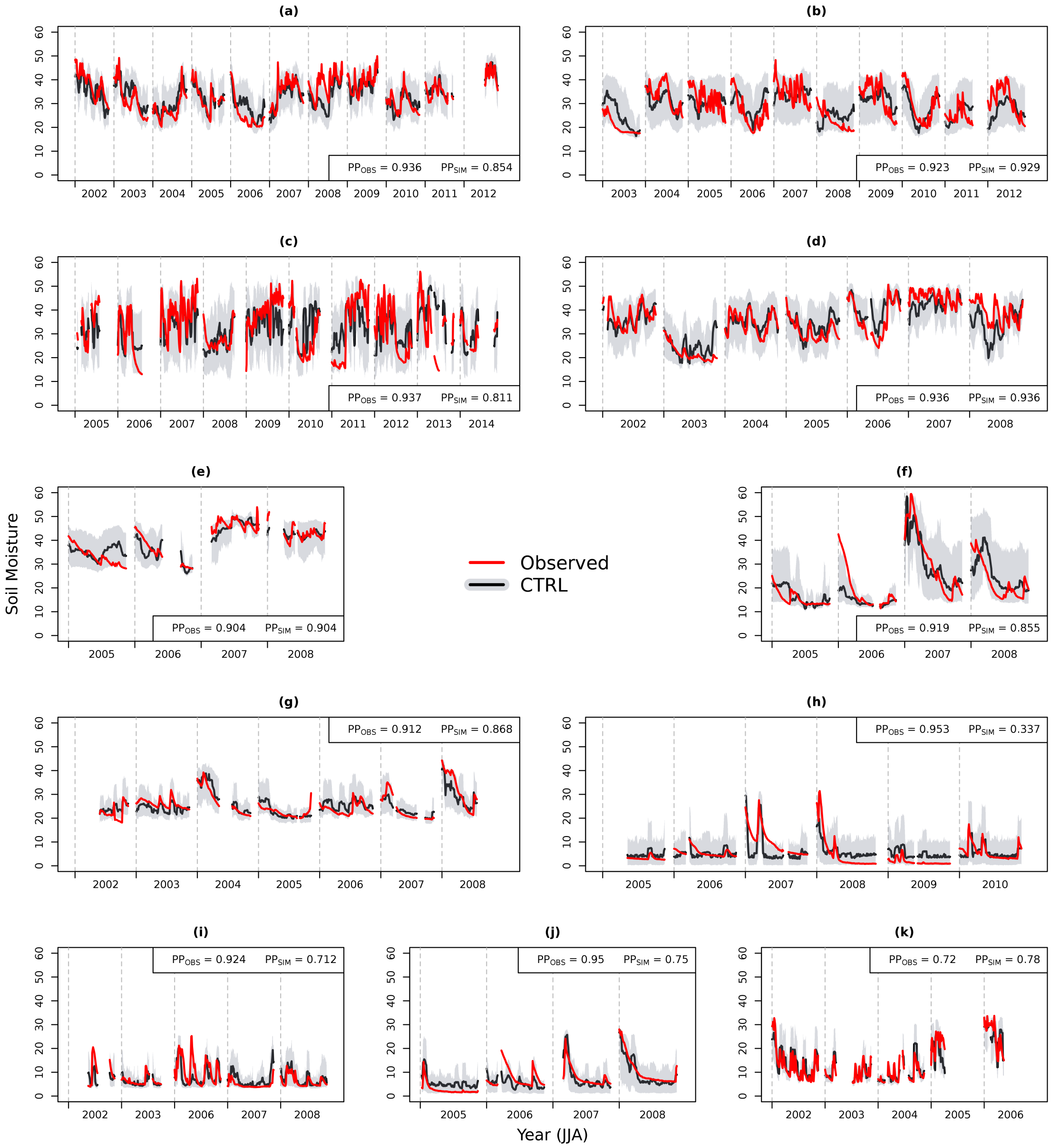

Figure 6.3: **Validation of the modelled soil moisture time series.** Observed time series (red) alongside the cross-validation time series of the CTRL mean (black) and the 95% prediction interval (grey), obtained from 1000 simulations, at wet sites are (a) to (e) and dry sites (f) to (k). Also provided within each panel are the order 1 persistence probabilities calculated from the observed (PP_{obs}) and CTRL mean (PP_{sim}) timeseries.

Table 6.2: **Assessment of contributing variables to soil moisture (statistics).** Brier scores (BS), Brier Skill Scores (BSS) and mean bias for CTRL, SENS-$Y_{1_{PS}}$, SENS-$Y_{2_{PL}}$, and SENS-$Y_{3_{PET}}$ simulations calculated for soil moisture values below the observed 15^{th} percentile. Bias values for SENS-$Y_{1_{PS}}$, SENS-$Y_{2_{PL}}$, and SENS-$Y_{3_{PET}}$ are given as percentage change relative to CTRL

Site	Score	CTRL	SENS-$Y_{1_{PS}}$	SENS-$Y_{2_{PL}}$	SENS-$Y_{3_{PET}}$
(a)	BS	0.09	0.10	0.12	0.10
	BSS	0.25	0.21	0.01	0.18
	Bias	3.89	+5%	+113%	+45%
(b)	BS	0.11	0.13	0.10	0.11
	BSS	0.15	-0.01	0.17	0.15
	Bias	4.33	+107%	-1%	+33%
(c)	BS	0.12	0.14	0.11	0.12
	BSS	0.04	-0.1	0.13	0.06
	Bias	10.66	+51%	-24%	+2%
(d)	BS	0.06	0.06	0.09	0.08
	BSS	0.51	0.49	0.26	0.39
	Bias	3.52	+45%	+149%	+83%
(e)	BS	0.09	0.10	0.09	0.12
	BSS	0.28	0.25	0.27	0.03
	Bias	3.62	-15%	+78%	+81%
(f)	BS	0.08	0.07	0.06	0.13
	BSS	0.36	0.43	0.53	-0.01
	Bias	0.37	-215%	+207%	+720%
(g)	BS	0.09	0.09	0.11	0.09
	BSS	0.31	0.24	0.15	0.30
	Bias	1.48	+43%	+86%	+6%
(h)	BS	0.12	0.13	0.12	0.13
	BSS	0.04	0.00	0.05	0.003
	Bias	3.28	+9%	-3%	+4%
(i)	BS	0.12	0.13	0.12	0.13
	BSS	0.07	0.002	0.04	-0.06
	Bias	1.24	-9%	+5%	+52%
(j)	BS	0.12	0.12	0.12	0.12
	BSS	0.09	0.10	0.05	0.06
	Bias	2.8	-8%	+10%	+16%
(k)	BS	0.08	0.13	0.12	0.08
	BSS	0.36	0.01	0.09	0.37
	Bias	1.05	+205%	+146%	+10%

the observed values of the other two Y variables. To assess the contributions of all variables, we compare the mean of each simulation with the CTRL mean. We also compare the probabilistic forecasts from SENS-Y_i with CTRL using the BS, BSS and the mean ensemble bias computed for values of h below the observed 15^{th} percentile (Table 6.2).

At wet sites, precipitation is generally seen to have the most influence on low soil moisture values while PET can act to amplify the low soil moisture anomaly during drought periods. Comparing the means of the three sensitivity simulations with the mean of CTRL (Fig. 6.4), larger overestimations of low h values with respect to CTRL are generally seen in either of the simulations assessing the influence of a precipitation variable, SENS-$Y_{1_{PS}}$ or SENS-$Y_{2_{PL}}$, than is seen in SENS-$Y_{3_{PET}}$. Underlining this are larger changes in positive bias of low soil moisture values seen from SENS-$Y_{1_{PS}}$ or SENS-$Y_{2_{PL}}$ than from SENS-$Y_{3_{PET}}$ (Table 6.2). A comparison of BSS for each simulation in Table 6.2 also shows a larger reduction in skill of forecasting values below 15^{th} percentile in either SENS-$Y_{1_{PS}}$ or SENS-$Y_{2_{PL}}$ than in SENS-$Y_{3_{PET}}$. Focusing on drought events at wet sites (a), (b) and (d) in 2003 and 2006, years in which heat waves have also occurred[27,130], we see from the mean of the simulations (Fig. 6.5) that removing the influence of precipitation can lead to the misspecification of a drought event with the green line largely above the black line (CTRL). On the other hand, removing the influence of PET can result in the underestimation of the severity of the event with the blue line only just higher than the black during a drought event.

At dry sites, we see that precipitation again holds the main influence over soil moisture while PET generally offers little added benefit to the estimation of soil moisture. The main differences of CTRL with SENS-$Y_{1_{PS}}$ and SENS-$Y_{2_{PL}}$ are found for high values of soil moisture (Fig. 6.4). Low values in these sensitivity simulations are generally equivalent with CTRL as the medians of $Y_{1_{\mathrm{PS}}}$ and $Y_{2_{\mathrm{PL}}}$ are associated with relatively low values due to the positively skewed nature of the variables' distributions. Little or no difference is seen between SENS-$Y_{3_{PET}}$ and CTRL simulations for low values of soil moisture. Large percentage changes in bias for low soil moisture values are seen at sites (f) and (i), though the actual changes in soil moisture are relatively low (Table 6.2). This would be expected at dry sites during summer where soil moisture normally reaches low levels such that ET is moisture-limited and will diverge from PET. Extremes of PET driven by extreme temperatures would then have little added effect to the severity of soil moisture drought in dry locations.

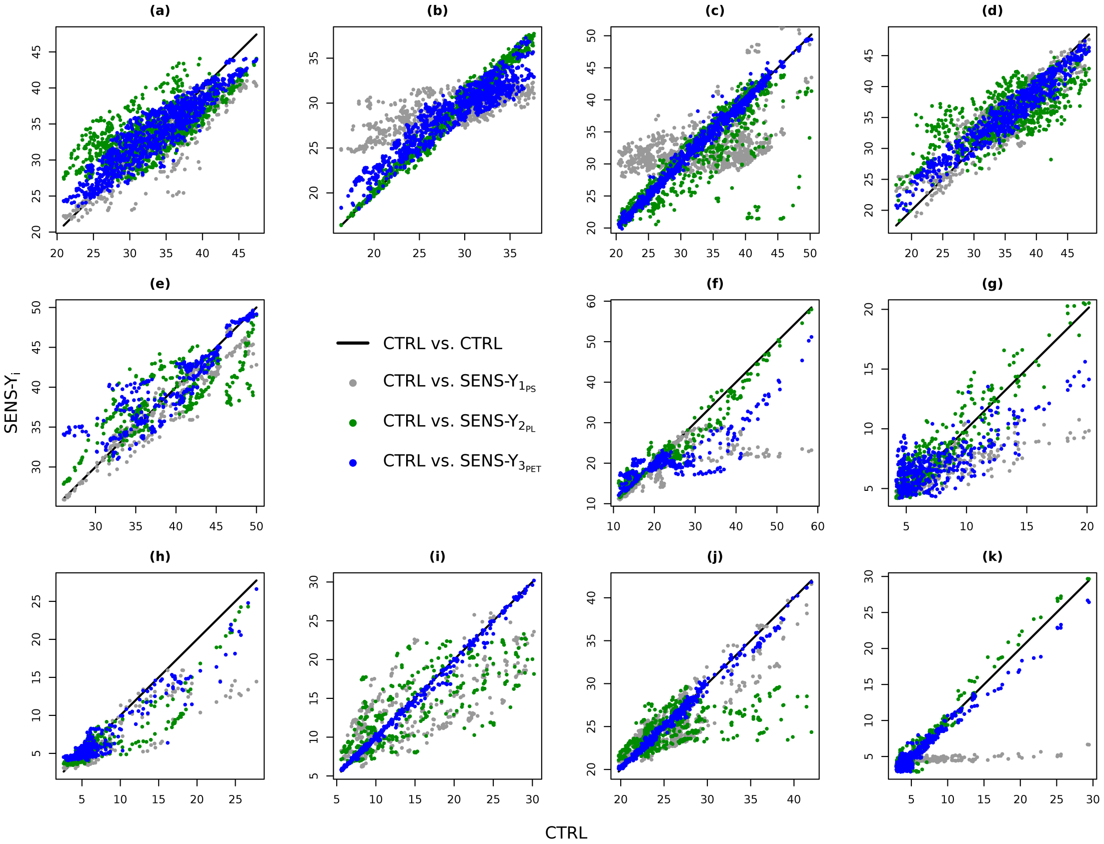

Figure 6.4: **Assessment of contributing variables to soil moisture.** Comparison of the mean of the cross-validaiton simulations of CTRL with SENS-$Y_{1_{PS}}$, SENS-$Y_{2_{PL}}$ and SENS-$Y_{3_{PET}}$ at wet sites (a) to (e) and dry sites (f) to (k). Values are ordered according to CTRL from low to high such that the closer the correspondence of points to the diagonal, the smaller the change in the estimation of soil moisture in the given sensitivity simulation.

6.4.3 Assessing the relevance of the dependence between the contributing variables

The contribution of the dependence between $Y_{2_{\mathrm{PL}}}$ and $Y_{3_{\mathrm{PET}}}$ to the estimation of low h values is assessed using sensitivity simulation IND-$Y_{2_{PL}}$. IND-$Y_{2_{PL}}$ is used to highlight where interactions between drought and heat wave conditions, arising through land-atmosphere interactions, act to amplify drought conditions. To illustrate the dependence between $Y_{2_{\mathrm{PL}}}$ and $Y_{3_{\mathrm{PET}}}$, we calculate Spearman's ρ and a measure of tail dependence, λ_q, calculated as:

$$\lambda_q = Pr(Y_{3_{PET}} > F_3^{-1}(q) \quad | \quad Y_{2_{PL}} < F_2^{-1}(1-q)) \tag{6.3}$$

where $q = 0.9$ in this case. $\lambda_{0.9}$ can be interpreted as the fraction of days when $Y_{3_{\mathrm{PET}}}$ was greater than its observed 90^{th} percentile when $Y_{2_{\mathrm{PL}}}$ was less than its 10^{th} percentile.

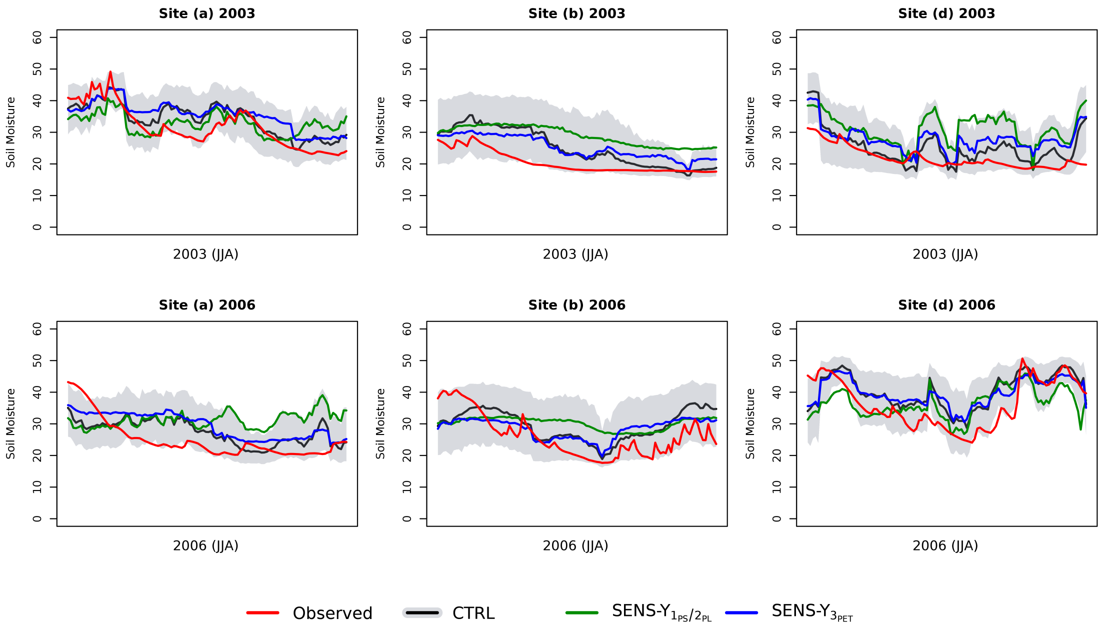

Figure 6.5: **Assessment of contributing variables to soil moisture during 2003 and 2006 heat waves.** Mean cross-validated time series of simulations assessing the contributions of precipitation and PET to the estimation of soil moisture and CTRL (black) for the summers (JJA) of 2003 and 2006 at wet sites (a), (b) and (d). Time series of mean simulated values are presented for SENS-$Y2_{PL}$ (green) and SENS-$Y3_{PET}$ (blue) at wet sites (a) and (d) while time series of SENS-$Y1_{PS}$ (green) and SENS-$Y3_{PET}$ (blue) are presented for site (b).

For two independent variables, the expected value of λ_q is $1 - q$. Values of ρ and λ_q for each site are given in Fig. 6.6. At many sites we observe a negative dependence between $Y2_{\mathrm{PL}}$ and $Y3_{\mathrm{PET}}$, as measured by ρ, and an increased probability of extreme PET ($Y3_{\mathrm{PET}}$) when antecedent precipitation ($Y2_{\mathrm{PL}}$) had been extremely low.

To test the relevance of such dependence in IND-$Y2_{PL}$, we break the dependence between $Y2_{\mathrm{PL}}$ and the short-term variables, $Y1_{\mathrm{PS}}$ and $Y3_{\mathrm{PET}}$. This is achieved by shuffling $Y2_{\mathrm{PL}}$ such that it is randomly associated with them. A probabilistic forecast of h, consisting of 1000 members, is then produced sampling from the multivariate distribution where we condition on the observed values of $Y1_{\mathrm{PS}}$ and $Y3_{\mathrm{PET}}$ and the shuffled $Y2_{\mathrm{PL}}$. To account for sampling variability of the shuffling process, we produce 1000 IND-$Y2_{PL}$ probabilistic forecasts.

We obtain a kernel density estimate of the PDF produced from each of the 1000 IND-$Y2_{PL}$ simulations. The mean density and the 95% confidence interval of IND-$Y2_{PL}$ PDFs are calculated and presented alongside the PDFs of CTRL and h^{obs} (Fig. 6.6). The statistical significance of the difference between the CDFs of CTRL and IND-$Y2_{PL}$ is assessed at the 5^{th}, 10^{th}, and 15^{th} percentiles of observed soil moisture. CTRL is considered significantly different for a given percentile if the associated soil moisture

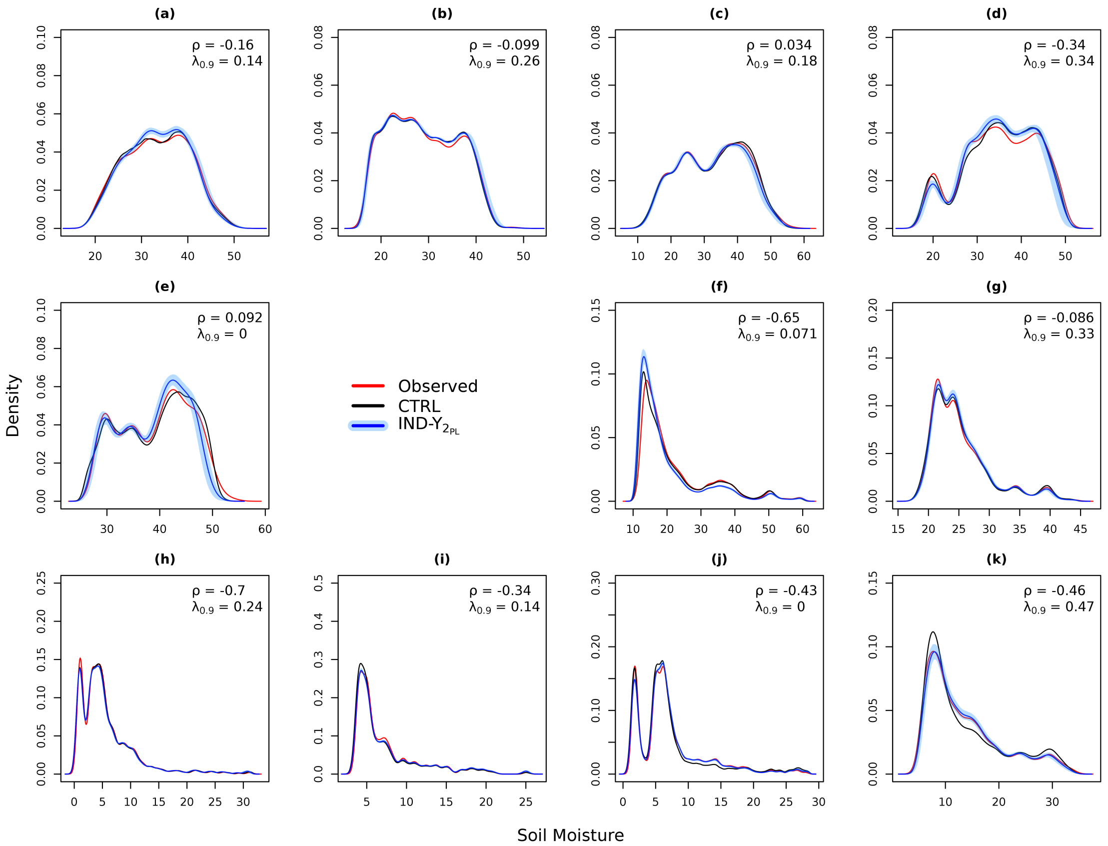

Figure 6.6: **Assessment of the contributing variable dependencies to soil moisture.** Kernel density estimates of observed soil moisture (red) and soil moisture simulated via cross-validation from probabilistic forecasts CTRL (black) IND-$Y_{2_{PL}}$ (blue) simulations. The blue line and shading respectively represent the mean density and 95% confidence interval obtained from the 1000 IND-$Y_{2_{PL}}$ simulations.

value of CTRL is less than the lower bound of 95% confidence interval of that percentile from IND-$Y_{2_{PL}}$. This would signify that the probability of values below that percentile are underestimated when the the dependence between $Y_{2_{\mathrm{PL}}}$ and $Y_{3_{\mathrm{PET}}}$ is broken.

Statistically significant differences are found between all three percentiles at Site (d) where we also see a noticeable difference between PDFs (Fig. 6.6 (d)). A negative dependence as well as a significant dependence in the tails is also observed here. Site (d) lies in a transitional region where land-atmosphere interactions can lead to the mutual reinforcement of drought and heat wave events[144]. This result highlights the importance of the interplay between drought and heat wave conditions, driven by land-atmosphere interactions, to the reinforcement of drought conditions in such locations.

Statistically significant differences between the percentiles tested are also found at wet sites (a), (b) and (e) and dry sites (g) and (j), though relatively little difference is observed between CTRL and IND-$Y_{2_{PL}}$ PDFs at these sites for values below the tested percentiles (Fig. 6.6). We observe negative dependencies (ρ) and tail dependencies (λ_q)

at these sites which highlights that the concurrence of such conditions may be important for the estimation of low values of soil moisture. These dependencies are also observed at other dry sites but no significant differences between assessed percentiles are found. Such dependencies at these sites are perhaps of little relevance for soil moisture during summer as extremes of PET may be energy-limited in wet climates while soil in dry climates may have little available moisture for ET. In dry conditions then, extremes of PET in combination with extremely low antecedent precipitation will have little effect on moisture levels in soil.

6.4.4 Relevance of PET over short and long integration periods

The variable set $S2$, as described in the Meteorological Predictor Selection section, is used to demonstrate the relevance of PET, integrated over various durations LG_3 and LF_3, to the estimation of soil moisture h. We fit two models at wet sites (a), (b) and (d) where we see contributions of PET to the estimation of soil moisture drought in variable set $S1$ (Fig. 6.5). The integration periods used for precipitation variables, $\mathrm{Y}_{1_{\mathrm{PS}}}$ and $\mathrm{Y}_{2_{\mathrm{PL}}}$, in $S1$ remain the same. For the simulation PET-INT$_S$, we set $\mathrm{LG}_3 = \mathrm{LF}_3 = 7$ and for the simulation PET-INT$_L$ we set $\mathrm{LG}_3 = 70$ and $\mathrm{LF}_3 = 90$.

Based on the mean of the simulations (Fig. 6.7), better representation of drought onset can be seen at sites (a) and (d) in the PET-INT$_S$ simulations where the black line generally follows red (observed) at the beginning of an event when initial drying is taking place. On the other hand, drought persistence is generally captured better by the PET-INT$_L$ simulation where the blue line remains low with the red line in comparison to the black. Better BSS are found for simulations using a long-term integration of PET at sites (a) and (b). Increases of BSS, from PET-INT$_S$ to PET-INT$_L$, of 0.24 to 0.36 and 0.18 to 0.25 are found at each site respectively while little difference is seen between simulations at site (d) with BSS equal to 0.51 and 0.52.

Although these results are somewhat qualitative, they highlight that both short- and long-term integrations of PET are important for the estimation of drought events in this framework. Longer integrations are generally better in capturing the persistence of drought conditions as they can account for the memory soil moisture holds of drying during the event. Short-term integrations however, are better in capturing drought onset as they are able to account for short intense periods of drying that can accelerate the propagation of meteorological drought to soil moisture drought. With drought events expected to set in quicker in a warming climate[175], it will be important to detect such changes in the intensity of drying over short periods in spring and summer that are filtered out in longer integrations of PET. This may be of particular relevance in

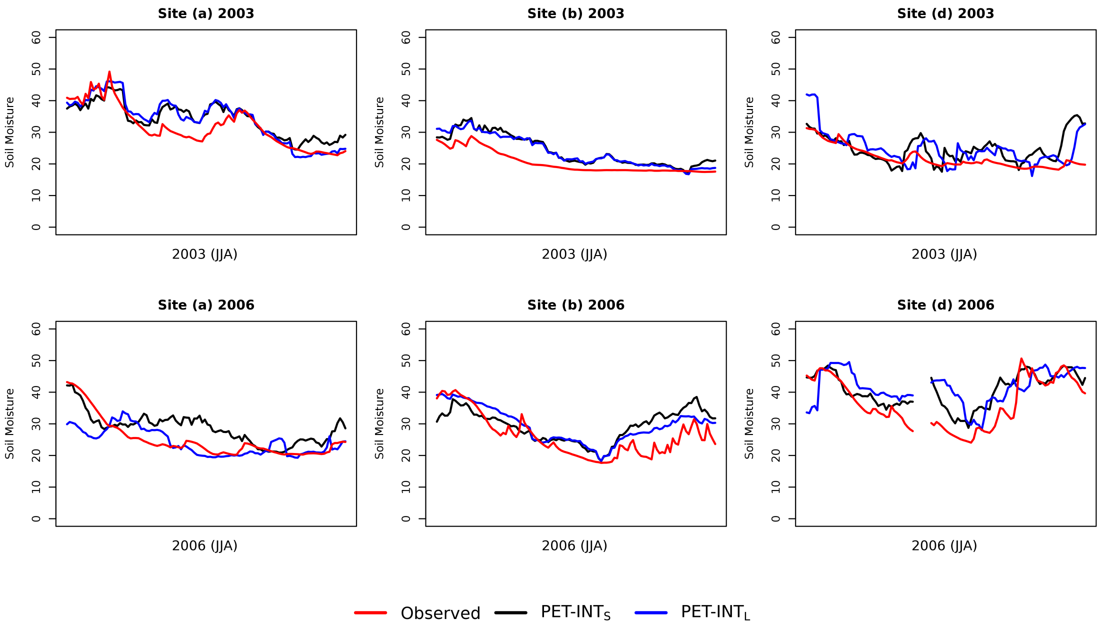

Figure 6.7: **Sensitivity of soil moisture to the integration period of PET.** Mean cross-validation time series of simulations from models PET-INT$_S$ in which PET is considered over a short integration period (black) and PET-INT$_L$ in which PET is considered over a long integration period (blue) along with the observed time series (red) for the 2003 and 2006 drought events at wet sites (a), (b), and (d).

Europe where early onset of drought conditions can have large implications for extreme temperatures in summer[186].

6.5 Discussion and conclusions

In this study, based on the conceptual model presented in section 3.1, we have analysed soil moisture drought over Europe as a compound event of variables employed in common drought indices, namely precipitation and potential evapotranspiration (PET), and assessed the individual roles of these variables and that of their dependence structure to the estimation of soil moisture. The overall aim was to explore the compound nature of soil moisture drought and the differences that exist between wet and dry climates.

Within the model we considered precipitation and PET over timescales related to meteorological drought and heat waves respectively. These timescales were considered to assess the influence of heat wave conditions on soil moisture, as well as dependencies driven by land-atmosphere interactions that can cause a mutual reinforcement between drought and heat wave events in Europe. We applied the model to data from 11 Fluxnet sites situated in wet, transitional and dry climates in Europe and generally found satisfactory performance of the model. We thus employed it in a number of sensitivity experiments to assess the relevance of contributing variables and their dependence structure to the estimation of soil moisture drought.

Results obtained from sensitivity experiments were in line with previous studies. Precipitation was found to hold the main control over soil moisture drought. PET was required only when it departs from normal conditions[188] to partly explain the severity of drought conditions in wet climates[145,171], while little or no contribution was found in dry climates[89] during summer. The concurrence of extremely low antecedent precipitation with extremely high PET was found to be most relevant at a site situated in a transitional climate region between wet and dry climates where land-atmosphere interactions are most relevant for the development of soil moisture drought[146]. The concurrence of these conditions was also seen at many dry sites though were found to have little relevance for soil moisture. This lack of relevance at dry sites is presumably related to the limited availability of moisture in soil for actual evapotranspiration (ET) to occur such that PET and Extremes of PET could have little influence to a low soil moisture anomaly.

The aforementioned contribution of PET is based on a short-term integration period that was used to capture the influence of heat waves on soil moisture. At wet sites, this short integration period is found to be effective in describing the onset of drought events as it can capture initial drying that occurs on a daily basis. It can however be ineffective in capturing the persistence of drought conditions, which longer integrations can better account for, as it neglects the memory soil moisture may hold of PET and the intense drying that may have occurred throughout a drought event. The differences found between short and long integrations of PET may become relevant in the analysis of changes in the onset of drought events using drought indices. A warmer climate may cause droughts to set in quicker[175] and lead to flash droughts[108]. Such drying may be hidden through the use of longer integration periods of PET in an index such as the Standardised Precipitation Evapotranspiration Index (SPEI), or through a recursive model used for the Palmer Drought Severity Index (PDSI) that retains memory of PDSI values from previous time steps.

Advantages of using drought indices include the simplicity they offer, as well as the widespread availability of meteorological datasets compared to those of soil moisture. Although they are not specifically designed to represent soil moisture[144], indices such as the SPEI, PDSI and the Reconaissance Drought Index (RDI) provide a convenient means of combining precipitation and PET into a kind of impact function that may be implicitly linked to soil moisture.

However, soil moisture drought is not a simple phenomenon to characterise with drought indices due to differing contributions and relevant integration periods of meteorological variables in wet and dry climates. The use of a climatic water balance (*Precipitation-PET*) in the SPEI and PDSI assumes over-simplified relationships between precipitation, PET and soil moisture[142], and implies that the statistical relevance of precipitation and PET to the estimation of soil moisture are the same over a given integration period. With such simplifications comes a loss of information such as short intense periods of drying that may be filtered out through the inclusion of redundant information when using a long integration period for PET.

Through the inclusion of PET, these indices are expected to provide a better picture of changes in drought conditions in a warming climate than indices that use precipitation alone such as the Standardised Precipitation Index (SPI). Ubiquitously applying indices, that incorporate PET, across different climates can provide a general overview of the response of drought conditions to global warming. It is however important to note that severe drought, as depicted by these indices, will have a different meaning for soil moisture drought in wet and dry climates. ET is limited by moisture availability and so will diverge from PET in dry conditions leading to an overestimation of the actual drying taking place with respect to soil. In contrast, land surface models account for this moisture limitation by capturing the physical relationship between PET and soil moisture, they can therefore provide a more reliable estimate. Their use within coupled climate models to study changes in soil moisture drought is particularly advocated for by Berg et al.[16], who also demonstrate the added complexity of diverging changes to soil moisture at different soil depths that cannot be disentangled using drought indices.

Despite discrepancies between PET and ET in dry conditions, extremes of PET will still be indicative of the drying potential of the atmosphere. Such atmospheric drying potential may possibly have adverse effects on crop yields and contribute to other environmental hazards such as wildfires that are mediated by the availability of moisture in vegetation[55,132].

Much information of soil moisture and other drought impacts may be deduced from drought indices and their response to a warming climate. To do so requires careful interpretation and detailed knowledge of the involved variables' influence on soil moisture in a given climate. It is therefore important that drought indices incorporating PET are interpreted within the context of the climate in which they are applied, whilst also keeping in mind the applications they are designed for.

In our impact focused approach, we have made use of the little soil moisture data that is available across different locations and climate types in Europe to demonstrate the compound nature of soil moisture drought during summer. These results provide further insight into the relationship between soil moisture and drought indices that incorporate PET. It is hoped that this insight will aid with the interpretation of drought indices in a given climate and season so that as much information as possible may be gained from their application.

7. Conclusions

"We are at the very beginning of time for the human race. It is not unreasonable that we grapple with problems. But there are tens of thousands of years in the future. Our responsibility is to do what we can, learn what we can, improve the solutions, and pass them on."[42]

- Richard Feynman, Engineering and Science (1955)

The main objectives of this thesis were outlined in the Introduction (chapter 1) as: (1) develop a conceptual model for compound events (CEs), implemented via Pair-copula constructions (PCCs). Based on this model, study compound flooding at (2) the local and (3) continental scales, and (4) analyse soil moisture drought. Here, with respect to these four parts, I summarise the main results and discuss their implications. This will be followed by an outlook including future potential research on CEs.

7.1 Summary and implications

Conceptual model development. We developed a conceptual model, implemented via pair-copula constructions (PCCs), which allows for quantifying the CE hazard probability or risk, as well as the associated uncertainty (Bevacqua et al.[19]). In the conditional version, the model includes predictors, which could represent for instance meteorological processes. The inclusion of predictors in the model (1) provides insight into the physical processes underlying CEs, as well as into the temporal variability of CEs, and (2) allows for statistically downscaling CEs and their impacts. The non-conditional version allows for estimating statistical characteristics of rare events, such as large return periods, and the associated uncertainties.

The downscaling feature of the conditional model can be used to extend the risk assessment back in time to periods where observations of the predictors are available, but not of the contributing variables and impacts, or to assess potential future changes in

CEs based on predictors from climate model projections. The conceptual model is particularly useful to downscale large-scale predictors from climate models in cases where the local contributing variables driving the impacts of CEs are either not realistically simulated, or not simulated at all by the available climate models. As such, the model can be used to assess future risk of CEs based on multi-model ensembles as available from the CMIP [168] and CORDEX [52] archives. When using this or other conditional statistical models for downscaling in a climate change context, the user should ensure that the model can properly extrapolate information in a climate that is different from that where the model is calibrated [98].

Here, we successfully employed PCCs for implementing the conceptual model. We suggest considering the use of PCCs for modelling CEs which involve more than two contributing variables, or when predictors are included in the system as additional variables. PCCs are particularly useful to model CEs, when the variables have different dependence structures, e.g., when only some of the variable pairs are characterised by tail dependence. To model such types of structures, even multivariate parametric copulas, which were introduced in climate science to overcome some difficulties in modelling multivariate density distributions [141], lack of flexibility. PCCs are more convenient: by decomposing the dependence structure into bivariate copulas, they give high flexibility in modelling generic high dimensional systems. The implementation of the conditional conceptual model via PCCs requires to employ a conditional pdf decomposed via PCCs; although this implementation is in principle not straightforward, I encourage the interested users in using the R-package *CDVineCopulaConditional* (Bevacqua [18]) which strongly simplify the implementation process.

Uncertainty estimates are essential to avoid drawing misleading conclusions about CE risk estimates. The developed model allows for a straightforward quantification of sampling uncertainties, which we suggest to quantify when assessing the CE hazard or risk. However, uncertainties can be very wide when the sample of data available for the model calibration is relatively small (chapter 4). In general, the amplitude of the uncertainties increases with the ratio between the dimension of the system and the length of available data for model calibration. Furthermore, we showed that uncertainties are even larger when data show serial correlation, indeed it is like the effective sample size of data with serial correlation is smaller than those without [148]. Thus, in practice, uncertainties associated with CE risk estimates can be very large because of the shortness of the available data: reducing these uncertainties is a challenge. To meet this challenge, employing a well performing dynamical model to extend the available data where to calibrate a statistical model might be helpful in some cases [182].

The developed conceptual model can be employed for modelling and understanding other types of CEs. After the successful application of the conceptual conditional model to the studies of compound flooding and soil moisture drought, we have employed the model in Switanek et al.[166] for statistical downscaling of multi-site daily precipitation over river catchments. In this context, the conceptual model allows for representing the spatial inter-dependencies of the precipitation field over the river catchment. A good representation of these dependencies is relevant because they are a crucial driver of the river discharge, as highlighted, e.g, in a recent perspective paper on CEs published in *Nature Climate Change*[215]. Furthermore, Liu et al.[85] employed a very similar conceptual model to ours for understanding the influence of global warming and different ENSO states on floods in Texas. Thus, we encourage to employ the conceptual model for gaining a better physical understanding of other CE types, and for estimating the associated CE risk.

CF in Ravenna (Italy). In chapter 4 (Bevacqua et al.[19]), we adapted the developed conceptual model to study compound flooding (CF) in Ravenna. We explicitly modelled the impact (water level) of the CF in the river mouth as a function of the downscaled sea and river levels. The performance of the model in simulating the impact is very satisfactory, such that the model may be used for flooding forecasting and warning. Here, the model was implemented both in the non-conditional and conditional versions. The former does not include meteorological predictors, and it allows for obtaining flooding return period estimates including uncertainties. Similar return period estimates were obtained via the conditional model, which was calibrated over the period 2009-2015 by including meteorological predictors obtained from the *ECMWF ERA-Interim* reanalysis dataset, and then used to extend the CF analysis to the full period of 1979-2015. This extension allows for getting a more robust estimation of the return periods. During the period 1979-2015, we did not observe any long-term trend in the CF return periods. The expected return period of the highest CF observed is about 20 years; however, the associated 95% confidence interval is very large due to the shortness of the data used for calibrating the model.

Ignoring the dependence between sea and river levels would result in an underestimation of the CF probability: the expected return period of the highest CF observed increases from about 20 to 32 years when switching from the dependent to the independent case. In Ravenna, the dependence between sea and river levels should be considered for flood risk assessment.

Present and future CF probability along the European coast. In chapter 5 (Bevacqua et al.[20]) we assessed the CF hazard along the European coasts both in the present and in future climate according to the business-as-usual (RCP8.5) scenario. To enable a continental scale assessment, we limited the analysis to the *probability of potential CF*, i.e. we modelled the probability of a co-occurrence of extreme sea level and heavy precipitation. Under current climate conditions, the locations experiencing the highest CF probability are mostly located along the Mediterranean Sea. In the future, Northern Europe will experience an increasing probability of CF beyond the effects of mean sea level rise, caused mainly by more intense precipitation in a warmer climate.

Rising mean sea levels will pose the main threat along coastal areas in a warmer climate, and changes in storm surges and precipitation will additionally alter the coastal flood hazard. Coastal planning agencies in Europe are aware of these changing hazards and should develop adaptation strategies[57,64,201]. We demonstrated that CF may pose a severe additional flood hazard that has to be taken into account for a full risk assessment[215]. Thus, in CF prone areas, especially in areas experiencing an increasing CF hazard, additional coastal protection measures may be required. In these areas, detailed local risk assessments are required to plan adaptation strategies. To this end, a complex modelling chain is required[198] which can simultaneously integrate information about precipitation, discharge, surges, topography and land-use, relative sea level rise and available or planned flood protections. Our study identifies European regions potentially facing CF in a warmer future climate and thereby provides a continental-scale basis for adaptation planning activities.

Local risk assessments of CF should consider the dependence between precipitation and storm surge to avoid potential severe risk underestimation. Ignoring this dependence leads to a large increase (up to two orders of magnitude) of the CF return periods in this study[20], while this increase is smaller for CF in Ravenna (from 20 to 32 years) according to Bevacqua et al.[19]. The different methodology used in the two studies explains these differences (and also differences found between other studies in the literature): (1) the contribution of the dependence is typically larger when employing bivariate AND return periods as in the European study, rather than an impact function as in the Ravenna case study (not shown). (2) As the sea level is typically more correlated with precipitation than with river levels, considering precipitation (European study) rather than river levels (Ravenna's study) enhances the relevance of the dependence on the final CF impact. Depending on the employed methodology and on the analysed location, the contribution of the dependence for CF might result more or less large; however, the dependence should be always considered to avoid potential severe risk underestimation[19,20,119,182,198,208,209].

Improving the CF monitoring system would allow for a better understanding of this type of flooding. To monitor CF in a river mouth, it is necessary to have water level data at a station where both the influence of sea and river are seen. We found a few locations where these stations exist[119] as, maybe in part, stakeholders are usually interested in data where only the influence of the river or the sea is seen. Thus, several studies have focused on the estimation of the probability of potential CF, and only a few studies have explicitly quantified the CF impact[19,80,182,208,209]. Improving the CF monitoring system and creating an archive containing data for locations where CF events have been recorded would contribute to obtaining a more in-depth knowledge of CF. Hydrodynamic model experiments at the local scale are another relevant mean for improving the understanding of CF, for example to quantify the contribution of waves to the total CF.

Furthermore, an extension of this European study of the CF hazard at the global scale is hoped to inform coastal adaptation planners. Based on ERA-Interim reanalysis data, preliminary results show that for the past (1979-2014), the highest probability of co-occurring storm surges and extreme precipitation is along the northern Atlantic coast, in Madagascar, India, central Chile, along the US and western Pacific coasts, and in the Hurricane region (not shown). However, in regions where tropical cyclones (TCs) are frequent, employing non-downscaled CMIP5 model data (as in this study) to analyse, e.g., future changes in CF, might be challenging[41]. In fact, while TCs should be the main CF driver in regions where TCs are frequent[20,198], CMIP5 models have limitations in representing TCs[23]. Also, further large-scale CF assessments should consider river discharges[74,119], and a relatively large model ensemble to estimate the natural variability of the CF hazard.

The contribution of potential evapotranspiration (PET) and precipitation to soil moisture drought in Europe. An explicit representation of soil moisture via physically based land surface models is difficult[116], therefore drought indices incorporating precipitation and PET are often employed as proxies of soil moisture[35,187], to analyse both present and future climate. Can these indices provide an adequate representation of soil moisture drought?[58] This study contributed to addressing this question via assessing how the variables employed in common drought indices, namely precipitation and PET, contribute to soil moisture.

As in previous studies, we found that precipitation holds the main control over soil moisture drought. Positive anomalies of PET (integrated over a short-term period to represent heat waves) partially drive the drought severity only in wet climates[188]. In dry climates, PET is less relevant for soil moisture drought, probably because of the limited moisture in the soil for actual evapotranspiration (ET) to occur[89]. At wet sites, PET integrated over short-term period can describe the onset of drought events as it can capture initial drying that occurs on a daily basis, while the persistence of drought conditions is better captured by longer-term integrated PET which takes into account the effect of intense drying, that may have occurred during a drought event, on soil moisture. This differences found between short and long integrations of PET may become relevant in the analysis of changes in the onset of drought events using drought indices. A warmer climate may cause droughts to set in quicker[108,175], but such drying may be hidden through the use of longer integration periods of PET in, e.g., an index such as the Standardised Precipitation Evapotranspiration Index (SPEI).

Indices that incorporate both precipitation and PET, such as the SPEI and the Palmer Drought Severity Index (PDSI), are expected to provide better information of future drought changes than indices that use precipitation alone such as the Standardised Precipitation Index (SPI). However, we showed that soil moisture drought is not a simple phenomenon to characterise due to differing contributions and relevant integration periods of PET and precipitation. Thus, the use of a climatic water balance (i.e., *precipitation-PET*) in the SPEI and PDSI assumes over-simplified relationships between precipitation, PET and soil moisture[142].

With all due caution, information of soil moisture and other drought impacts may be deduced from drought indices. Our study shows that the relevance of PET for soil moisture is not straightforward and depends on the local climate. Therefore, indices incorporating PET to characterise soil moisture should be interpreted very carefully within the context of the climate in which they are applied. Ubiquitously applying indices incorporating PET can provide a general overview of the response of drought conditions to global warming. However, severe drought as depicted by these indices will have a different meaning in wet and dry climates. ET is limited by moisture availability and so will diverge from PET in dry conditions leading to an overestimation of the actual drying taking place with respect to the soil. Despite discrepancies between PET and ET in dry conditions, an extreme PET will still be indicative of the drying potential of the atmosphere[215], which could have adverse effects on crop yields and contribute to, e.g., wildfires that are mediated by the availability of moisture in vegetation[55,132].

7.2 Outlook: future steps in the CE research

Many major natural catastrophes are caused by CEs. So far, for simplification or missing understanding of the physical processes underlining these major events, the risk of extreme weather and climate impacts has been mostly estimated based on individual drivers, or combining multiple drivers assuming they are independent. However, such approaches may cause severe underestimation of the risk, leading to serious mal-adaptation with severe consequences for society. First of all, to provide better risk assessments, it should be recognised both in the climate science and stakeholder communities that many of the major impacts are caused by CEs[215], and thus that addressing extreme impacts as CEs would be very important for society.

A CE oriented climate research is especially relevant in the current climate change context, which might expose the deficit of some of the used impact-models in providing future risk estimates. Many of the existing impact models, e.g. crop yield[213] or heat-stress[43] models, might fail under future climate change conditions. In fact, many impact models are too simple, e.g., as discussed for drought indices in Manning et al.[93]. Some models are based on purely empirical relationships between the occurring impacts and the detected drivers, i.e. they are built to work in the past and present climate, but they might fail in the future because climate change might alter the relationships observed in the past[98]. An impact model driven by a single variable would fail in the future if the multivariate compound nature of the impact will "emerge" due to changes in the multivariate distribution of the actual drivers. For example, a city situated along a river mouth may be exposed only to river flooding in the present, but could see emerging storm surge, and potentially CF, risk in the future due to SLR. Thus, an impact-model accounting only for river flooding would fail in the future. Similarly, temperature and humidity represent well the human heat-stress in the present. But, locally, future global warming might lead to anomalous hot days occurring under windy and/or cloudy conditions that would mitigate the impact of temperature and humidity. Thus, for future projections, it might be relevant to consider also wind and solar radiation in heat-stress models. When necessary, impact models should be (re-)built based on a deep physical understanding of the process leading to the impact, and on expert knowledge of climate change. Such a deep understanding of the physics behind CE impacts represents a crucial step towards more reliable projections of CE risk under climate change.

Focussing on observed extreme events which caused very large impacts is a way forward to gain physical understanding of CEs. Identifying these observed extreme events inevitably requires a collaboration between climate and stakeholder communities. Then, understanding CE requires to identify the processes and variables contributing to the final extreme compound hazard (a *bottom-up approach*[215]), i.e. (1) the local variables driving the impact, which ultimately will feed back into the impact-model development, and (2) the large-scale variables or atmospheric circulations driving the local weather. Identifying the processes leading to CEs provides relevant information for (impact and climate) model validation and improvement, as it indicates which are the processes that require particular attention.

A systematic CE oriented validation of climate models is necessary. While limitations of climate models in representing single variables have been widely investigated, studies are only starting to focus on the projections of multiple variables and events[30,43]. Therefore, it is not clear how well climate models capture the multivariate nature of many CEs, including the physical mechanisms driving them and their changes[30]; existing modelling products used to assess the risk associated with these CEs may therefore lead to serious mal-adaptation. A CE oriented validation of climate models requires to adopt CE impact-related metrics, which need to be built or identified among the existing, possibly through a collaboration between environmental scientists and statisticians. In this direction, it should be better investigated how well, and where, General Circulation Models (GCMs) and Regional Climate Models (RCMs) simulate the dependencies between CE drivers. For example, according to preliminary results of this thesis, it appears that higher-resolution models represent higher dependencies between storm surge and precipitation variables. Thus, for CF and other CEs, it would be relevant to understand the required resolution for a proper representation of such dependencies.

In parallel with the evaluation of statistical characteristics such as the dependencies between local CE drivers, a process-based model evaluation should be carried out focussing both on the local- and large-scale CE drivers. Evaluating how climate models represent the large-scale processes driving CEs is crucial, for example, for understanding whether typical downscaling and bias corrections methods can provide impact modellers with a good representation of the local CE drivers. For instance, data from models which cannot represent the temporal persistence of atmospheric blocking systems, which should be the main driver of the duration of hot and dry conditions, should not be used by impact modellers interested in the duration of these compound extremes. Small-scale processes, which are usually parametrized by climate models, might also strongly affect the CE impact and should be validated. For example, it could be relevant to define whether convection permitting models are required for a proper representation of the covariability between temperature and humidity, which is a driver of heat stress[43] and mortality[110]. Ultimately, model validation will feed back both into the improvement of GCMs and RCMs in representing CEs, and into the model selection which can be a relevant step to obtain robust future projections of the CE impact.

Storyline approaches[106,154], aiming at "telling"[60] how high-impact weather events would look like in the future, are a further way to push the CE research forward. Although a CE oriented model validation of GCMs has started only recently[30], we already know that there are large uncertainties in the future evolution of atmospheric circulations, both because of natural variability and model errors[153]. Therefore, in many cases, attempting to quantitatively describe changes in frequency and magnitude of a certain CE type would lead to very large uncertainty, and thus the storyline approach has been introduced[60,154,176]. The storyline approach aims at investigating how, e.g., a single event observed in the past would look like in a warmer climate. Thus, rather than simulating long-time series of future climate, such an approach requires to simulating only one or a few events; therefore, the approach allows for increasing the model resolution which in turn likely leads to a better representation and understanding of the event itself[60]. This approach is particularly appropriate for CEs as it would push forward the relatively little physical understanding that we have of some CEs and of their changes.

For example, it could be useful to employ a storyline approach to understand how the CF inundation would be affected by a warmer climate. So far, it has been shown that a warmer sea can cause a relevant increase both in extreme precipitation[106,183,192], and in storm surges driven by tropical cyclones[167]. But the sensitivity of CF to a warmer climate has not been studied yet. Such a sensitivity study would require to combine high-resolution climate and inundation models (e.g., Kumbier et al.[80]). Furthermore, Zappa and Shepherd[205] adopted the storyline approach in an innovative way to tell how the future regional climate (in terms of seasonal precipitation and wind extremes) will change depending on plausible future changes of the atmospheric circulations. Such an approach might be employed to investigate changes in (i) the co-occurrence of extremes (e.g., precipitation and wind extremes[99]), including a comparison of the analyses for the individual hazards, and in (ii) cyclone tracks.

As the relevance of CEs has been highlighted only recently, many types of CEs need to be investigated yet. Many devastating CEs are characterised by rapid succession or long-duration of extreme conditions, therefore focussing the research also in their direction would be relevant. For example, flooding can be caused by a series of consecutive intense precipitation events, such as the devastating Pakistan flood in 2010, which resulted from a clustering of extreme precipitation events in July and August[100]. A number of studies have analyzed the clustering of cyclones[40,90,126,191], however, the occurrence of a cyclone does not always coincide with extreme precipitation, and vice-versa[124]. As the clustering of extreme precipitation has been studied only for the past over limited regions[12,190], further studies are necessary to close several research gaps.

Also, an event of persistent precipitation lasting for days over the same region can cause record floods, as occurred in the Balkan region in 2014 due to the stationarity of the cyclone Yvette[159], and similarly in 2017 when Hurricane Harvey[79] and the storm Kai-tak[113] hit Texas and Philippines, respectively. Kossin[79] has recently observed that slow-moving tropical cyclones have increased in number in the last decades. Such behaviour might have been partially driven by high amplitude quasi-stationary Rossby waves caused by hemispheric circumglobal wave resonance[91,92,159]. Recent years have seen a clustering of resonance events in the northern hemisphere[31], and there is some evidence in the literature that hemispheric wave resonance may be influenced by anthropogenic climate change[92]. Thus, it would be important to understand how the frequency of stationary cyclones (considering also long-lasting precipitation events) will change in the future because of human influence and natural variability. This might be challenging, mostly because the large-scale circulations that influence stationary cyclone occurrences might be very uncertain[153]. However, a storyline approach similar to that developed by Zappa and Shepherd[205] might be adopted to better understand the drivers of stationary cyclone occurrences (and of changes in their occurrences).

As the last example of a CE deserving attention, I mention the combination of persistent concurrent drought and heatwave conditions that can increase the likelihood of wildfires, negatively affect the global economy, and threaten vegetation health, e.g., prompting tree mortality[46,103,150,158,207,213]. While co-occurring drought and heatwave conditions have been analysed (e.g., refs.[103,150,213]), there is lack of research about the persistence of this CE, which can strongly exacerbate the risk. Thus, in Manning et al.[94], we are studying this hazard over Europe, based on the methodology developed in Bevacqua et al.[20].

The category of CEs embraces a large number of extreme events in the climate system. As the climate system is composed of several components which continuously interact in space and time, it is natural that an accurate assessment of many extreme impacts requires a CE oriented approach. In particular, it could be acknowledged that the beginning of a CE oriented research might have no precise origin in the past, as we are embedded in a complex climate system that, already in the past, inspired us to approach some problems through *multivariate reasoning*. But while the available computational power increases and/or we get a better understanding of the climate system, explicitly addressing many impacts as CEs becomes unavoidable. Thus, the recent introduction of the CE concept in the scientific community could be seen as a mean for highlighting that a CE oriented research is very relevant to advance the research on extreme events. Also, a CE oriented research might be seen as a useful problem-solving approach for looking at extreme events from a novel perspective, which can lead to new and insightful scientific findings. Overall, a CE oriented research will allow for improving risk estimates of extreme events with invaluable benefits for society. I hope this thesis has contributed to advancing the research on CEs and to highlighting that there are many research gaps to be closed. While climate research advances, the best *modelling approach* to improve future risk estimates is to reduce greenhouse gas emissions.

A. Appendix

A.1 Homogenisation of river level data

The *zero reference level* of river measurements is the water level in the river defined as zero in the measurements. In general, such a zero reference level may change during different periods of observation, due to technical reasons. As the zero reference level of rivers $Y2_{\mathrm{River}}$ and $Y3_{\mathrm{River}}$ varied in the first three years but remained constant in the second three, we homogenised the former with respect to the latter at both rivers. We performed such homogenisation assuming that the precipitation falling into the catchment during one year is responsible for the average river level in the same year. For each river $Y\mathrm{i}_{\mathrm{River}}$, we fitted the linear model $Y\mathrm{i}_{\mathrm{River}}^{\mathrm{annual}} = a_{\mathrm{i}} P_{\mathrm{i}}^{\mathrm{annual}} + b_{\mathrm{i}}$ in the last three years (those having constant zero reference level), where $Y\mathrm{i}_{\mathrm{River}}^{\mathrm{annual}}$ is the annual average of $Y\mathrm{i}_{\mathrm{River}}$ and $P_{\mathrm{i}}^{\mathrm{annual}}$ is the annual cumulated precipitation over the river basin (data from *ECMWF ERA-Interim* reanalysis dataset). Finally, for each river, we translated the zero reference level of the first three years, such that the linear model was valid in these years as well.

A.2 CDVineCopulaConditional: an R-package for sampling from conditional C- and D-vine copulas

The R-package *CDVineCopulaConditional*[18] provides tools for sampling from a conditional copula density decomposed via Pair-Copula Constructions as C- or D- vines. A list of these tools, including a comprehensive description for their use, can be found in the online documentation of the package in the CRAN repository[18].

The package is based on two main new algorithms. These algorithms allow for conditional sampling from a C- or a D-vine from which the conditioning variables would be sampled as first when following the sampling algorithms from Aas et al.[1]. Specifically, given a C- or a D-vine of the variables $(X_1, ..., X_{N_{\mathrm{cond}}}, X_{N_{\mathrm{cond}}+1}, ..., X_n)$, Algorithms 1 and 2 allow for the conditional sampling of $(X_{N_{\mathrm{cond}}+1}, ..., X_n)$ given $(X_1 =$

$x_1^{\text{cond}}, ..., X_{N_{\text{cond}}} = x_{N_{\text{cond}}}^{\text{cond}}$), where N_{cond} is the number of conditioning variables. When the conditioning variables are not given ($N_{\text{cond}} = 0$), Algorithms 1 and 2 reduce to the special cases of Algorithms 1 and 2 shown in Aas et al. [1]. *CDVineCopulaConditional* includes tools for selecting the best pair-copula families and the best vine structure (based on information criteria) among those which allow for such conditional sampling.

The employed approach for the conditional simulation is not the only possible[14], but despite the fact that the best vine is selected among a fraction of all the possible, it can provide very satisfactory results, as we show in this study. Also, we refer to refs. [22,86] as other works where conditional joint pdfs decomposed as C-vines were used for statistical modelling.

Algorithm 1 Algorithm to simulate uniform variables $\vec{X} = (X_1, ..., X_{N_{\text{cond}}}, X_{N_{\text{cond}}+1}, ..., X_n)$ from a C-vine. Generates one sample $x_{N_{\text{cond}}+1}, ..., x_n$ conditioned on given values $x_1^{\text{cond}}, ..., x_{N_{\text{cond}}}^{\text{cond}}$. The h-function is defined as in Aas et al. [1]. $\Theta_{j,i}$ is the set of parameters of the copula density $c_{j,j+1|1,...,j-1}$.

```
Sample w_{N_cond+1}, ..., w_n independent uniform on [0,1].
if N_cond ≠ 0 then
   for i in (1, ..., N_cond) do
      w_i = x_i^cond
   end for
end if
x_1 = v_{1,1} = w_1
for i in (2, ..., n) do
   v_{i,1} = w_i
   if i > N_cond then
      for k in (i − 1, i − 2, ..., 1) do
         v_{i,1} = h^{−1}(v_{i,1}, v_{k,k}, Θ_{k,i−k})
      end for
   end if
   x_i = v_{i,1}
   if i == n then
      Stop
   end if
   for j in (1, ..., i − 1) do
      v_{i,j+1} = h(v_{i,j}, v_{j,j}, Θ_{j,i−j})
   end for
end for
```

A.3 Vines and sampling procedure

In this appendix, more details about vines are given, focusing on C- and D-vines.

Algorithm 2 Algorithm to simulate uniform variables $\vec{X} = (X_1, ..., X_{N_{\text{cond}}}, X_{N_{\text{cond}}+1}, ..., X_n)$ from a D-vine. Generates one sample $x_{N_{\text{cond}}+1}, ..., x_n$ conditioned on given values $x_1^{\text{cond}}, ..., x_{N_{\text{cond}}}^{\text{cond}}$. The h-function is defined as in Aas et al. [1]. $\Theta_{j,i}$ is the set of parameters of the copula density $c_{i,i+j|i+1,...,i+j-1}$.

Sample $w_{N_{\text{cond}}+1}, ..., w_n$ independent uniform on [0,1].
if $N_{\text{cond}} \neq 0$ **then**
  for i *in* $(1, ..., N_{\text{cond}})$ **do**
    $w_i = x_i^{\text{cond}}$
  end for
end if
$x_1 = v_{1,1} = w_1$
if $N_{\text{cond}} < 2$ **then**
  $x_2 = v_{2,1} = h^{-1}(w_2, v_{1,1}, \Theta_{1,1})$
else
  $x_2 = v_{2,1} = w_2$
end if
$v_{2,2} = h(v_{1,1}, v_{2,1}, \Theta_{1,1})$
for i *in* $(3, ..., n)$ **do**
  $v_{i,1} = w_i$
  if $i > N_{\text{cond}}$ **then**
    for k *in* $(i-1, i-2, ..., 2)$ **do**
      $v_{i,1} = h^{-1}(v_{i,1}, v_{i-1,2k-2}, \Theta_{k,i-k})$
    end for
    $v_{i,1} = h^{-1}(v_{i,1}, v_{i-1,1}, \Theta_{1,i-1})$
  end if
  $x_i = v_{i,1}$
  if $i == n$ **then**
    Stop
  end if
  $v_{i,2} = h(v_{i-1,1}, v_{i,1}, \Theta_{1,i-1})$
  $v_{i,3} = h(v_{i,1}, v_{i-1,1}, \Theta_{1,i-1})$
  if $i > 3$ **then**
    for j *in* $(2, ..., i-2)$ **do**
      $v_{i,2j} = h(v_{i-1,2j-2}, v_{i,2j-1}, \Theta_{j,i-j})$
      $v_{i,2j+1} = h(v_{i,2j-1}, v_{i-1,2j-2}, \Theta_{j,i-j})$
    end for
  end if
  $v_{i,2i-2} = h(v_{i-1,2i-4}, v_{i,2i-3}, \Theta_{i-1,1})$
end for

A.3.1 Vines

Shown below are the general expressions to decompose an n-dimensional pdf via PCCs as C-vines (eq. (A.2)) or D-vines (eq. (A.1))[1]:

$$f_{Y_1,...,Y_n}(y_1,..,y_n) = \prod_{k=1}^{n} f(y_k) \prod_{j=1}^{n-1} \cdot \\ \cdot \prod_{i=1}^{n-j} c_{i,i+j|i+1,...,i+j-1}\{F(y_i|y_{i+1},...,y_{i+j-1}), F(y_{i+j}|y_{i+1},...,y_{i+j-1})\} \tag{A.1}$$

$$f_{Y_1,...,Y_n}(y_1,..,y_n) = \prod_{k=1}^{n} f(y_k) \prod_{j=1}^{n-1} \prod_{i=1}^{n-j} c_{j,j+i|1,...,j-1}\{F(y_j|y_1,...,y_{j-1}), F(y_{j+i}|y_1,...,y_{j-1})\}. \tag{A.2}$$

The 5-dimensional vine that we use for the conditional model is shown in eq. (3.6), where (Y_1, Y_2, Y_3) are the variables $(Y1_{\text{Sea}}, Y2_{\text{River}}, Y3_{\text{River}})$, and (Y_4, Y_5) are the predictors $(X1_{\text{Sea}}, X23_{\text{Rivers}})$. The graphical representation of that decomposition is shown in Fig. A.1A, where the concept of *tree* is introduced.

A.3.1.1 3-Dimensional vine

In total, a 3-dimensional copula density can be decomposed in three different ways, and each of these vines is both a D-vine and a C-vine. For this application we use the following vine.

$$\begin{aligned} f_{123}(y_1, y_2, y_3) = & f_1(y_1) \cdot f_2(y_2) \cdot f_3(y_3) \\ & \cdot c_{12}(u_1, u_2) \cdot c_{23}(u_2, u_3) \\ & \cdot c_{13|2}(u_{1|2}, u_{3|2}). \end{aligned} \tag{A.3}$$

This decomposition is represented graphically in Fig. A.1B. We underline that, in eq. (A.3), the rigorous expression of the conditional copula density $c_{13|2}$, of the pair (U_1,U_3) given $U_2 = u_2$, would be $c_{13|2}(u_{1|2}, u_{3|2}; u_2)$. In eq. (A.3), $c_{13|2}$ is written under the assumption of a *simplified PCC*, i.e. the parameters of $c_{13|2}$ are the same for all values of $u_2 \in (0, 1)$. The simplified PCC may be a rather good approximation, even when the simplifying assumption is far from being fulfilled by the actual model[68,163]. Copula parameters that are functions of the conditioning variables, and thus violate the

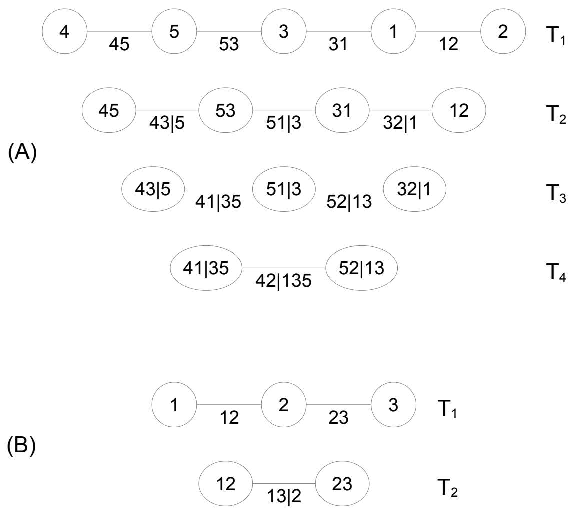

Figure A.1: **Graphical representation of D-vines.** (A): representation of the 5-dimensional D-vine in eq. (3.6). There are 4 trees (T_1, T_2, T_3, T_4), and 10 edges. Each edge represents a pair-copula density, and the label indicates the subscript of the corresponding copula. For example, the edge 43|5 represents the copula density $c_{43|5}$. The decomposition of the joint pdf related to the represented vine is obtained by multiplying all the represented pair-copula densities (10 in this case) and the marginal pdfs of each variable. For more details see Aas et al. [1]. (B): representation of the 3-dimensional vine in eq. (A.3). There are 2 trees (T_1 and T_2), and 3 edges.

simplifying assumption, are approximated by the average over all values of the conditioning variables. The effect of this approximation on the estimated impact is likely to be small[68,163] (a discussion on the effect of the approximation is available in the online documentation of the review process of Bevacqua et al. [19]).

In this study of compound floods (CFs), the variables (Y_1, Y_2, Y_3) of eq. (A.3) are the $(\varepsilon 1_{\text{Sea}}, \varepsilon 2_{\text{River}}, \varepsilon 3_{\text{River}})$ introduced in appendix A.6. Specifically, the vine of eq. (A.3) represents that used at the first step of the procedure in appendix A.5. The vine that we use at the third step of the procedure in appendix A.5 is:

$$\begin{aligned} f_{123}(y_1, y_2, y_3) = {} & f_3(y_3) \cdot f_1(y_1) \cdot f_2(y_2) \\ & \cdot c_{31}(u_3, u_1) \cdot c_{12}(u_1, u_2) \\ & \cdot c_{32|1}(u_{3|1}, u_{2|1}) \end{aligned} \tag{A.4}$$

where $(Y_1, Y_2, Y_3) = (Y1_{\text{Sea}}, Y2_{\text{River}}, Y3_{\text{River}})$.

A.4 Statistical inference of the joint pdf

Statistical inference on a pdf decomposed via a PCC is in principle very computationally demanding. As can be seen from eq. (A.3), the arguments of the copulas are influenced from the choice of the marginals (because of $u_i = F_i(x_i)$), and the argument of the copula in each level, is influenced from the fit of the copulas in the previous levels too. Thus, the estimation of the parameters of the full pdf (marginals and pair-copulas) should be performed together. Moreover the structure of the vine has to be chosen, increasing the demands of computational resources.

To overcome these obstacles, some techniques have been developed. The complications regarding the dependence of the copula parameters from the marginals estimation can be overcome using empirical marginals[50]. This allows for the estimation of copula parameters without the need of considering the marginals. However, to take into account that the estimation of the parameters of each pair copula depends on those of the upper levels, the estimation of the parameters of all the pairs should be performed at the same time. This way of estimating the parameters is called semiparametric (SP). The estimator we use here is the stepwise semiparametric (SSP). It was proposed by Aas et al.[1] and then Hobæk Haff et al.[69], and despite being asymptotically less efficient than the SP[69], it produces very satisfactory results and speeds up the procedure considerably[67]. As in SP, the PCC parameters are estimated independently of the marginals, but the estimation of the PCC parameters is performed level by level, plugging in the parameters from previous levels at each step[67].

Here, for each marginal pdf we use a mixture distribution composed of the empirical and the Generalized Pareto Distribution (GPD) for the extreme. For each predictor X, the GPD is fitted to data above a threshold defined here as their respective 95-percentile. For each of the contributing variables Y, this threshold was chosen requiring that the mean of the simulated extreme values from the joint pdf, was as near as possible to the maximum observed value of the variable Y we were fitting. Adding the GPD to the empirical marginal for the extremes is necessary so to not constrain the model to simulate values of the variables Y with maximum values that never exceed those observed during the calibration period.

We use the AIC to select the best vine structure among C- and D-vines (those selected are shown in sections A.3.1.1 and 3.2.3). In particular, for every possible C- and D-vine, we fit all possible families through the maximum likelihood estimation, and then we select the best family according to the AIC. Then, we select the best vine according to the AIC for the full model. The pair-copula families are chosen among those available in the R package *VineCopula*[140]. In particular, for the unconditional model all of the available families are considered during the selection, while for the conditional model we restricted the choice to the first 31 families listed in the documentation file of the package. This is because of technical issues regarding the simulation of data from the conditional pdf of the conditional model. Once the vine is selected, to better assess the

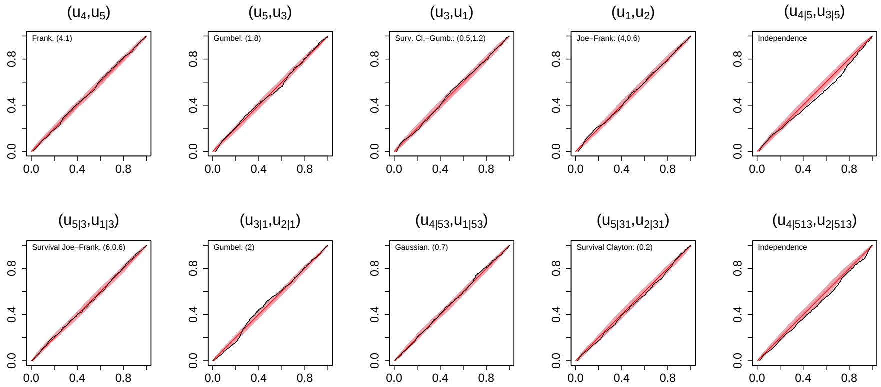

Figure A.2: **K-plots of the pair-copula families selected for the 5-dimensional model.** The name of the families and parameters are shown on the top-left of each plot. In abscissa the empirical K-function and in ordinate the K-function based on fitted copula. The 95% confidence interval (shown in light red) is obtained from 10^4 K-plots computed on simulated pairs (with same length as the observed data) from the selected pair-copula families.

quality of the fit of each pair-copula, we employ both the Cramer-von Mises test (results are not shown here) and the K-plot (Fig. A.2). This is a plot of the Kendall-function $K(w) = P(C_{i,j}(U_i, U, j) \leq w)$ computed with the fitted copula, against $K(w)$ computed with the empirical copula obtained from the observed uniform data. This diagnostic plot indicates a good quality of the fit when the points follow the diagonal[49,70]. We note that the $K(w)$ of the fitted copula is computed using Monte Carlo methods (long simulations allow for neglecting the associated sampling error). In Fig. A.2 we show the resulting K-plots and the selected copulas with their respective parameters for the 5-dimensional PCC (K-plots for the 3-dimensional are not shown). The families chosen for copulas $c_{43|5}(u_{4|5}, u_{3|5})$ and $c_{42|135}(u_{4|513}, u_{2|513})$ according to the AIC were describing slightly negative dependencies (< 0.1), but for physical reasons we expect these copulas to describe slightly positive dependencies. We argue that this result is due to uncertainties of the model. Therefore we choose independent copulas for these pairs, which is a compromise between the expert knowledge we have about the data and the result of the fit. When assuming independent copulas for these two pairs, the corresponding K-plots show only a small deviation from the diagonal (right side of Fig. A.2). Moreover these K-plots are mostly inside the 95% confidence interval of the K-plots, which confirms the reasonability of choosing these two independent copulas.

The R packages *CDVineCopulaConditional*[18] and *VineCopula*[140] were used to work with copulas. The GPDs for the marginal distributions were fitted through the function *gpd.fit* of the R package *ismev*[61].

A.4.1 Selected pair-copula families

In the case of the unconditional model, the fitted pair-copula families to the observed contributing variables Y - relative to the vine of eq. (A.4) - are: *Survival BB1* (parameters: 0.49, 1.15) for $c_{31}(u_3, u_1)$, *BB8* (parameters: 4.01, 0.6) for $c_{12}(u_1, u_2)$, *Tawn type 1* (parameters: 2.59, 0.73) for $c_{32|1}(u_{3|1}, u_{2|1})$. The selected families relative to the vine of eq. (A.3), i.e. the one fitted to $(\varepsilon 1_{\mathrm{Sea}}, \varepsilon 2_{\mathrm{River}}, \varepsilon 3_{\mathrm{River}})$ introduced in appendix A.6, are: *t-copula* (parameters: 0.15, 3.44) for $c_{12}(u_1, u_2)$, *Tawn type 2* (parameters: 2.85, 0.71) for $c_{23}(u_2, u_3)$, *Survival Gumbel* (parameter: 1.13) for $c_{13|2}(u_{1|2}, u_{3|2})$. In the case of the conditional model, the selected pair-copula families with relative parameters, fitted to the observed data of contributing variables Y and predictors X, are shown in Fig. A.2.

A.5 Model and return periods uncertainty estimation via parametric bootstrap

The flexibility of copula theory to model multivariate distributions has determined its spread in literature, and more recently in climate science. However, we stress that the uncertainties associated with the fitted model (both in the parameter estimates and the choice of the model) should be considered. This is particularly important, as it often happens that because of the limited sample size of the available data, these uncertainties are large and so cannot be neglected[148]. Practically they have a direct influence on the uncertainties of hazard probability and risk analyses. In particular, we observed that the uncertainties are also controlled by the dependence values between the modelled pairs (not shown).

In this study, we find uncertainties in the joint pdf (*model uncertainties*) which propagate into large uncertainties when assessing the compound flood (CF) return periods. This does not mean that such models are not useful, but instead that the results should be interpreted being aware of these existing uncertainties. Also, even if large, the obtained uncertainties in the CF return periods are smaller than those obtained computing the return periods directly from the observed data of the impact, underlining another advantage of applying such procedures.

Both for the unconditional and conditional model, we use a parametric bootstrap to assess the model and subsequent CF return period uncertainty, as follows:

1. Select and fit a model that can reproduce the statistical characteristics of $\vec{Y}^{\mathrm{obs}}$ ($(\vec{Y}^{\mathrm{obs}}, \vec{X}^{\mathrm{obs}})$ for the conditional model): dependence among the variables and

their marginal distributions. For the unconditional model we include also the serial correlation as described in appendix A.6.

2. Simulate $B = 2.5 \cdot 10^3$ samples of the contributing variables Y (as well as predictors X for the conditional model) with the same length as the observed data.

3. On each of the $B = 2.5 \cdot 10^3$ samples, fit a joint pdf via PCCs (the structure of the PCC is the same as that fitted on the observed data, while the pair-copulas families are re-selected for each sample).

4. From each of these $B = 2.5 \cdot 10^3$ models, simulate a sample of contributing variables Y of length equal to 200 times the observed (for the conditional model the contributing variables Y are simulated as conditioned on the predictors X).

5. For each sample, compute the simulated impact sequence as $h^{\text{sim}} = h(Y^{\text{sim}}_{1_{\text{Sea}}}, Y^{\text{sim}}_{2_{\text{River}}}, Y^{\text{sim}}_{3_{\text{River}}})$ and estimate the corresponding return level curves. Return levels are estimated through fitting the Generalized Extreme Value (GEV) distribution on annual maximum values. We simulated samples of length 200 times the length of the observed data (6 years), to get - for each sample - 1200 annual maximum values on which we fit the GEV distribution. This allows us to neglect the uncertainty of the return levels driven by the sampling because the uncertainties of the GEV distribution parameters are negligible.

6. Estimate the uncertainties on the return levels through identifying the 95% confidence interval (i.e. the range $2.5 - 97.5\%$) of the $B = 2.5 \cdot 10^3$ return level curves.

As underlined in step 1, for the unconditional model, we explicitly model the serial correlations of the contributing variables Y when computing the uncertainties. This was done to avoid an underestimation of the CF return period uncertainties (see appendix A.6). For the conditional model, step 3 is a rigorous bootstrap procedure, while for the unconditional model this step is an approximation. In fact, for the unconditional model, at step 3 we should have fitted the same type of model as fitted in step 1, i.e. that could include the serial correlations. Unfortunately, such a procedure was not feasible because of computational limitations, and we had to proceed by approximation, i.e. fitting a pdf via a PCC without considering the autoregressive processes. In particular, the computational limitations were due to the *tuning procedure* explained in appendix A.6. Therefore we used the best method possible to avoid underestimation of the CF return period uncertainties, but we underline that we used such an approximation.

The uncertainty of the return levels obtained via the observed data h^{obs} are computed through propagating the parameter uncertainties of the GEV distribution fitted to the annual maxima of h^{obs} (Fig. 4.6). In particular, the fitted GEV distribution is a function of the parameters μ (location), σ (scale) and η (shape)[29]. The GEV based return level RL_{t} associated with the return period t is a function of the three parameters (μ, σ, η)[29]. We obtained the standard deviations of the three parameters (μ, σ, η), respectively s_μ, s_σ, s_η, via the *gev.fit* function of the R package *ismev*[61]. To estimate the standard deviation of the return level RL_{t}, we propagated the standard deviations of the three parameters (μ, σ, η) using the formula:

$$s_{\text{RL}_\text{t}} = \sqrt{\left(\frac{\partial RL_t}{\partial \mu}\right)^2 \cdot s_\mu^2 + \left(\frac{\partial RL_t}{\partial \sigma}\right)^2 \cdot s_\sigma^2 + \left(\frac{\partial RL_t}{\partial \eta}\right)^2 \cdot s_\eta^2} \tag{A.5}$$

where s_{RL} is the standard deviation of the return level RL. The final 95% interval of uncertainty of the return level RT_{t} is obtained as $RT_{\text{t}} \pm 2s_{\text{RL}_\text{t}}$.

A.6 Incorporation of the AR(1) in the unconditional model

Given a statistical model describing time series with serial correlations, to avoid an underestimation of the model uncertainties computed via bootstrap procedure, it is necessary to use a model which can reproduce the serial correlation. During the bootstrap procedure, simulating samples without serial correlation, and then re-fitting the model to each of them, would mean to assume that the data carry more information than they actually do. In fact, it is like the effective sample size of data with serial correlation is smaller than those without[148]. Here we introduce the procedure we used to build a multivariate statistical model that can represent the serial correlation and the marginal pdf of the variables, and the statistical dependencies between them. The steps taken follow below.

1. Fit a linear Gaussian autoregressive model of order 1, $AR(1)$:

   $$Y_i(t) = c \ + \ \varphi Y_i(t-1) \ + \ \varepsilon_i(t) \tag{A.6}$$

   on the i^{th} marginal time series ($i = 1, 2, 3$), i.e. $(Y1_{\text{Sea}}, Y2_{\text{River}}, Y3_{\text{River}})$. The chosen $AR(1)$ requires that the modelled variable is Gaussian distributed so, before the fit, we transformed the river variables via the log_e function, which guarantees a more similar behaviour to the Gaussian. The observed sea variable was not transformed because it had already a behaviour similar to Gaussian.

2. Assured via the autcorrelation function (ACF) that $\varepsilon_i(t)$ has no longer a significant serial correlation, fit the joint pdf via PCCs on the residual variables $(\varepsilon_1, \varepsilon_2, \varepsilon_3)$.

We observe that the dependencies of these modelled pairs via PCCs, are not usual physical dependencies between the contributing variables (i.e. sea and river levels), but between their residuals with respect to the $AR(1)$ models.

3. Simulate the residuals $(\varepsilon_1^{\text{sim}}, \varepsilon_2^{\text{sim}}, \varepsilon_3^{\text{sim}})$ and plug into the i^{th} autoregressive model. Finally, to get the simulated contributing variables Y, the river variables were transformed via the exp function.

We observe here that when selecting the fitted pair-copulas and parameters for the residuals via the AIC, the simulated contributing variables Y had a smaller dependence with respect to the observed. We therefore proceeded through a *tuning procedure*, i.e. we built a routine to automatically tune the parameters of the fitted families, requiring that the Kendall rank correlation coefficient among the variables Y were well simulated.

In Fig. A.3, the autocorrelation functions of the Y^{obs} variables are compared with those of Y^{sim} simulated from the fitted model. Because of the gaps in the Y^{obs} time series, not all the observations are usable to compute the ACF (in particular the percentage of usable data decreases when increasing the Lag at which the ACF is computed). We therefore computed the ACF up to a Lag of about 25 days, which guarantees to use at least the 35% of data from the observed time series. Up to a Lag of about 15 days, except for a very few cases with the variable $Y_{3_{\text{River}}}$, the ACFs of the observed data are always inside the 95% interval of the ACFs obtained from the fitted model.

We consider this result as satisfactory because our target is to include the serial correlation of the contributing variables Y into the model, and we can see that even for the variable $Y_{3_{\text{River}}}$, the values of the ACFs have a significant serial correlation. Also, considering that the ACF is only slightly misrepresented for just one of the three time series, we argue that this is likely to have only a small effect on the final assessment of the model uncertainties.

A.7 Brier score for extreme values

We employ the Brier score to assess the accuracy of the probabilistic predictions of the conditional model when predicting extreme values of the impact h. For compound flooding, we defined an extreme of h as a value larger than the 95-percentile of h^{obs}. The Brier score is:

$$BS = \frac{1}{N}\sum_{t=1}^{N}(p_{\text{t}} - o_{\text{t}})^2 \tag{A.7}$$

where p_{t} is the probability of getting an extreme value h from the model at time t, while o_{t} is 1 if $h^{\text{obs}}(t)$ is extreme and 0 otherwise. We get the value of p_{t} through a

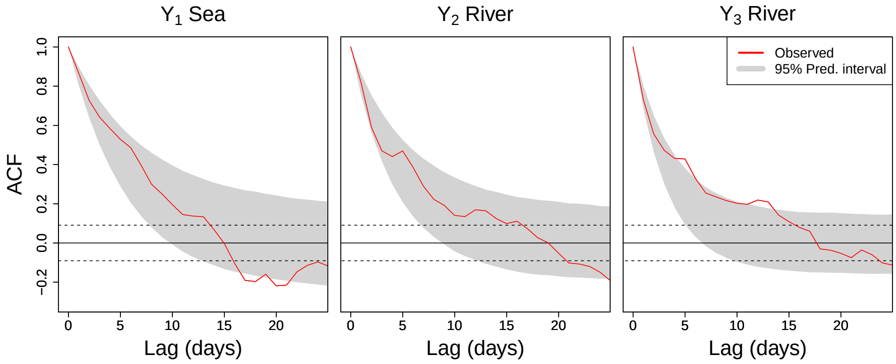

Figure A.3: **Validation of the unconditional model based on the autcorrelation function (ACF).** ACF of the observed time series (shown in red) against the ACF 95% confidence interval (grey) of the model (obtained through the Monte Carlo procedure). The dashed lines contain the 95% confidence interval defined by the ACF of a white noise process, i.e. outside this interval the ACF of the contributing variables Y is significant.

Monte Carlo procedure. The Brier skill score (BSS) measures the relative accuracy of the model under validation over a reference model, and is defined as:

$$BSS = 1 - \frac{BS}{BS_{ref}} \tag{A.8}$$

where BS_{ref} is the Brier score of the reference model. Here we consider the climatology of h as the reference model, i.e. an empirical model such that $p_{\mathrm{t}} = 0.05 \ \ \forall\, t$. A significant positive value of BSS indicates that when predicting extreme values, the model under validation is more accurate - according to the BS - than the reference model.

For soil moisture drought, the same procedure is applied, but the extremes are defined as values below the 15-percentile of h^{obs}. Also here the climatology of h is used as reference model, i.e. we use an empirical model where $p_{\mathrm{t}} = 0.15 \ \ \forall\, t$.

A.8 Cross-validation procedure

To assess the quality of the conditional model, avoiding overfitting, we perform a 6-fold cross-validation. Therefore, the original sample of data $(\vec{X}, \vec{Y})$ is randomly partitioned into 6 equally sized subsamples. Of the 6 subsamples, 5 subsamples (the training data) are used in fitting the model that is then validated against the remaining subsample. For each training subsample we fit (1) new predictors X for the contributing variables Y, (2) a new joint pdf $f_{\vec{Y}|\vec{X}}(\vec{Y}|\vec{X})$ and (3) a new h-function. For each validation subsample, we simulated 10^4 realizations of the $\vec{Y}$ values through conditioning on the concurring predictors. Finally, by combining the simulations of each validation subsample, 10^4 cross-validation time series of the contributing variables Y and the impact h are obtained.

B. Appendix

B.1 Relative sea level rise influence on extreme sea level

Most of the places experience an important increase of extreme sea level (larger than 1-year return level) days due to relative sea level rise (RSLR). Relative sea level rise is defined as the superposition of sea level rise (SLR) with land uplift/subsidence projections[121]. Here, we use SLR projections based on three land-ice scenarios of water contributions from ice sheets and glaciers[64]. Fig. B.1 shows the probability of a day experiencing extreme sea level as it would occur when adding relative sea level rise (RSLR) projections to the historical sea level time series (i.e., the superposition of astronomical tides and surges, including waves). For example, according to the medium land-ice scenario, along the Mediterranean Sea the probability of a day with extreme sea level is 40-100% (it is higher than 60% for the 90% of locations) (Fig. B.1b). This probability is lower along the Atlantic coast, however it is still very large when compared with that expected when not taking RSLR into account, i.e. 0.3% (Fig. B.1b). The northern part of the Baltic Sea is the only region where - due to uplift[121] - a reduction of the probability of extreme sea level occurrence is projected (Fig. B.1). SLR data from Hinkel et al. (2014)[64] combine SLR from four CMIP5 models (HadGEM2-ES, IPSL-CM5A-LR, MIROC-ESM-CHEM, and NorESM1-M CMIP5) with three land-ice scenarios of water contributions from ice sheets and glaciers[195].

B.2 Bivariate validation

The individual surge, wave and astronomical tide models have been evaluated in refs.[112,161,195,197]. The performance of ERA-Interim to represent precipitation extremes has been evaluated by Hertig et al.[62]. Here we evaluate the covariability of surge levels and precipitation. We find an overall good agreement between ERA-Interim and observation based compound flood probability (Fig. B.2 and B.3). Although the comparison of the model with observations for the single stations shows some biases, the

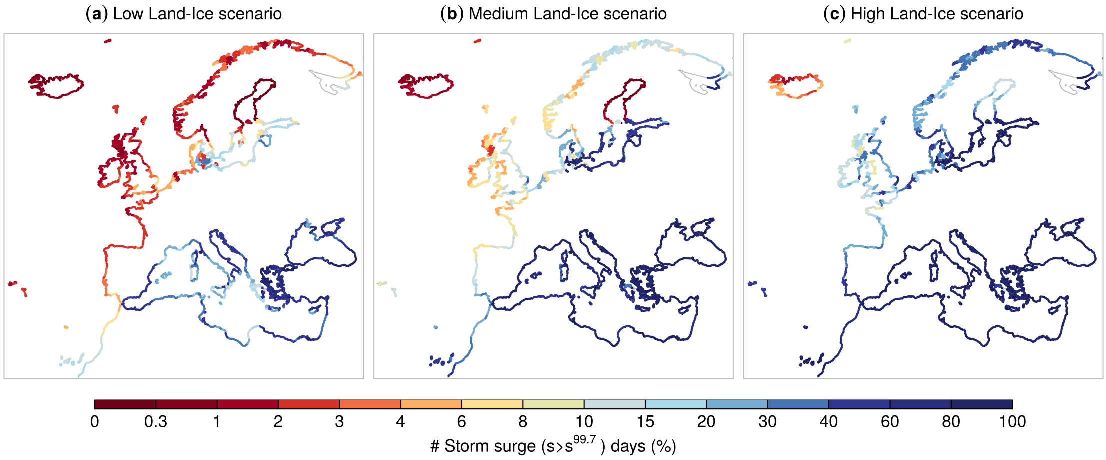

Figure B.1: **Percentage of days experiencing extreme sea level due relative sea level rise (RSLR).** Multi-model mean of probability of a day experiencing extreme sea level (larger than the 1-year return level) as it would occur when adding mean RSLR projections at the end of the century (2099-12-31) to the historical sea level time series (1970-2004). Computed for (**a**) low, (**b**) medium, and (**c**) high land-ice scenarios[64]. Values larger than 0.3% indicate RSLR-driven increasing probability of extreme sea level occurrence.

general geographical pattern of the covariability is captured by the model. The model seems to slightly overestimate the highest Spearman correlations between surges and precipitation (see Fig. B.2c); this might be due to non-linear surge-tide interactions that are not represented by the model. However, this model shortcoming does not affect our assessment of CF return periods (Fig. B.3f). The model reproduces the large-scale pattern of the CF hazard, e.g. the tendency to higher CF probability along the western rather than eastern coasts of UK and Sweden. In both data sets, the astronomical tides reduce the meteorological-driven dependence between precipitation and storm surges (compare panel a with d, and b with e, in Fig. B.2), and the effective CF probability is reduced as well (Fig. B.3). The confidence we have about the bivariate probability density function of more rare precipitation and sea level pairs decrease with the length of the available data. Therefore, given the shortness of the station data (Fig. B.2 and B.3), we computed return periods for potential CF defining precipitation and sea level extremes as values larger than the individual 99^{th} percentiles. This is slightly different from the 1-year return levels ($\sim 99.7^{th}$ percentiles) used for getting the results of the main text, but there the length of the data is $\sim$30 years. Here, we do not consider the wave component of the sea level, as its short-term variability is not properly captured by the sea level stations, unless they are located off shore[195,197]. Data sources used for validation are: E-OBS (resolution 0.5°) for precipitation[59]; the JRC tide gauge database for sea level; astronomical tides were filtered out from the observed data via the UTide[28] Matlab package.

In Fig. B.4 we compare the CMIP5 and renalysis based CF return periods (without

Table B.1: **Information about used CMIP5 models.**

Institute ID	Model Name	Ensemble member
CSIRO-BOM	ACCESS1-0	r1i1p1
CSIRO-BOM	ACCESS1-3	r1i1p1
EC-EARTH	EC-EARTH	r8i1p1
NOAA GFDL	GFDL-ESM2M	r1i1p1
NOAA GFDL	GFDL-ESM2G	r1i1p1
CSIRO-QCCCE	CSIRO-Mk3-6-0	r1i1p1

including the astronomical tides, to focus more on the meteorological component). All of the models show an higher probability of CF along the Mediterranean coast. In this case, due to the natural variability, a comparison of the return period estimated from different models at the individual grid-point is misleading. Therefore, we compare the CF return periods of the different models aggregated over regions. As a result, the CMIP5 based return periods are usually inside the sampling uncertainty of the reanalysis based return periods (Fig. B.4h). However, it appears that CMIP5 models tends to systematically slightly overestimate the return periods with respect to ERA-Interim. Additional analyses indicate that this overestimation might be explained by the lower resolution of the CMIP5 models (not shown). We note that using the delta change approach for estimating the CF return periods in the future, we only employ the climate change signal from the CMIP5 models, rather than the CF return periods in the present climate.

B.3 Supplementary figures

B.3.1 Univariate return periods

To estimate the (univariate) return periods (Fig. B.7b, B.7c, and B.8), we fit the cumulative distribution function F (employing a Generalized Pareto Distribution (GPD)) to threshold excesses over the present 95^{th} percentile (computed over wet days for precipitation). Clusters of threshold excesses separated by less than three days were replaced by a unique event which assumes the maximum observed value during the cluster. The return period of extreme events (1-year return levels, i.e. the $\sim 99.7^{th}$ percentile $x_{99.7}$), is $T_{99.7} = \mu/(1-F(x_{99.7}))$, where μ is the average time elapsing between the events used for the fit of the GPD. The GPD was fitted as explained in the Methods section of the main text.

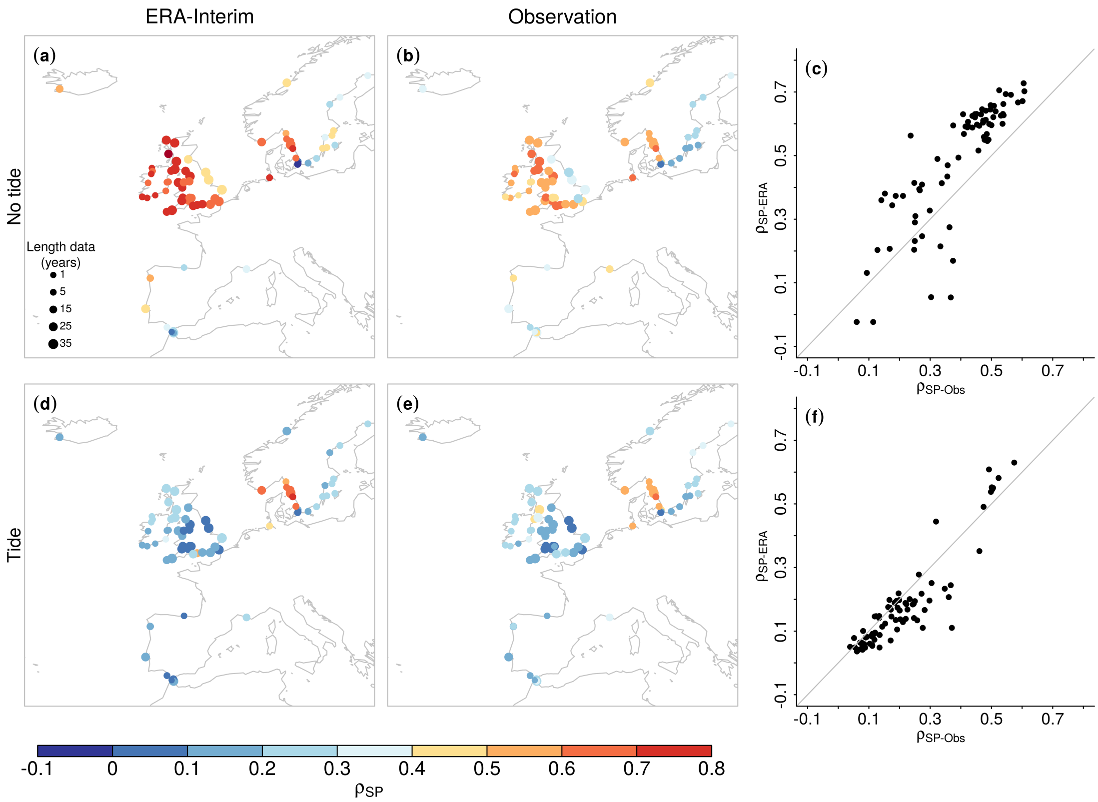

Figure B.2: **Comparison of the dependence between sea level and precipitation based on ERA-Interim and observation data.** Spearman correlation ρ_{SP} between sea level and daily precipitation, based on (**a**) ERA-Interim and (**b**) observations, where sea level time series do not include the astronomical tide component (it was filtered out from the observations via the UTide[28] Matlab package). Correlations based on (**d**) ERA-Interim and (**e**) observations, where the sea level time series include astronomical tides (here, tides obtained from the observed data were added to the ERA-Interim sea level data). Panel (**c**) shows the scatterplot of ρ_{SP} based on ERA-Interim and observations in the case without tides (accordingly, the case including tides is shown in panel (**f**)). The Spearman correlation is computed over time periods where observations intersect ERA-Interim data. The dimension of the dots indicates the length of the time series employed for the analysis, as indicated in the bottom left corner of panel (**a**).

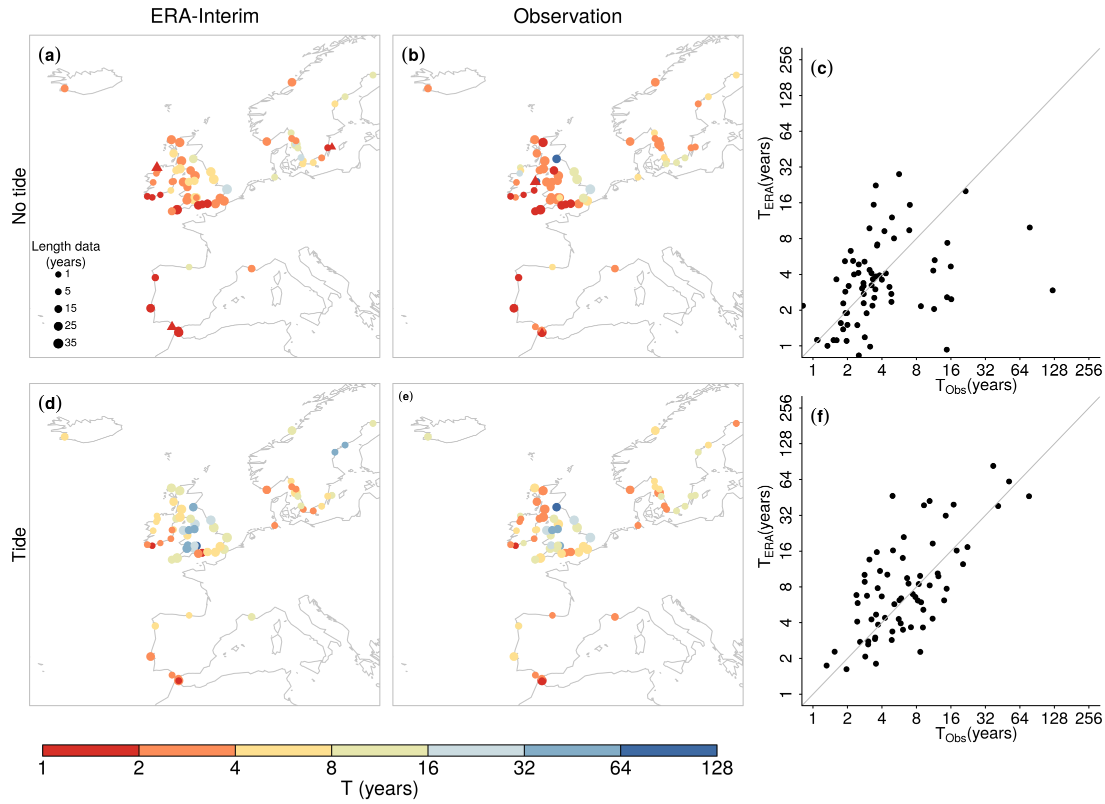

Figure B.3: **Comparison of the return periods of potential compound flooding (CF) based on ERA-Interim and observation data.** Similar to Fig. B.2, but for return periods T of CF (co-occurring sea level and precipitation extremes, i.e. $> 99^{th}$ percentile). The return periods are computed considering time periods where observations intersect ERA-Interim data. Bordeaux triangles indicate values smaller than the legend range.

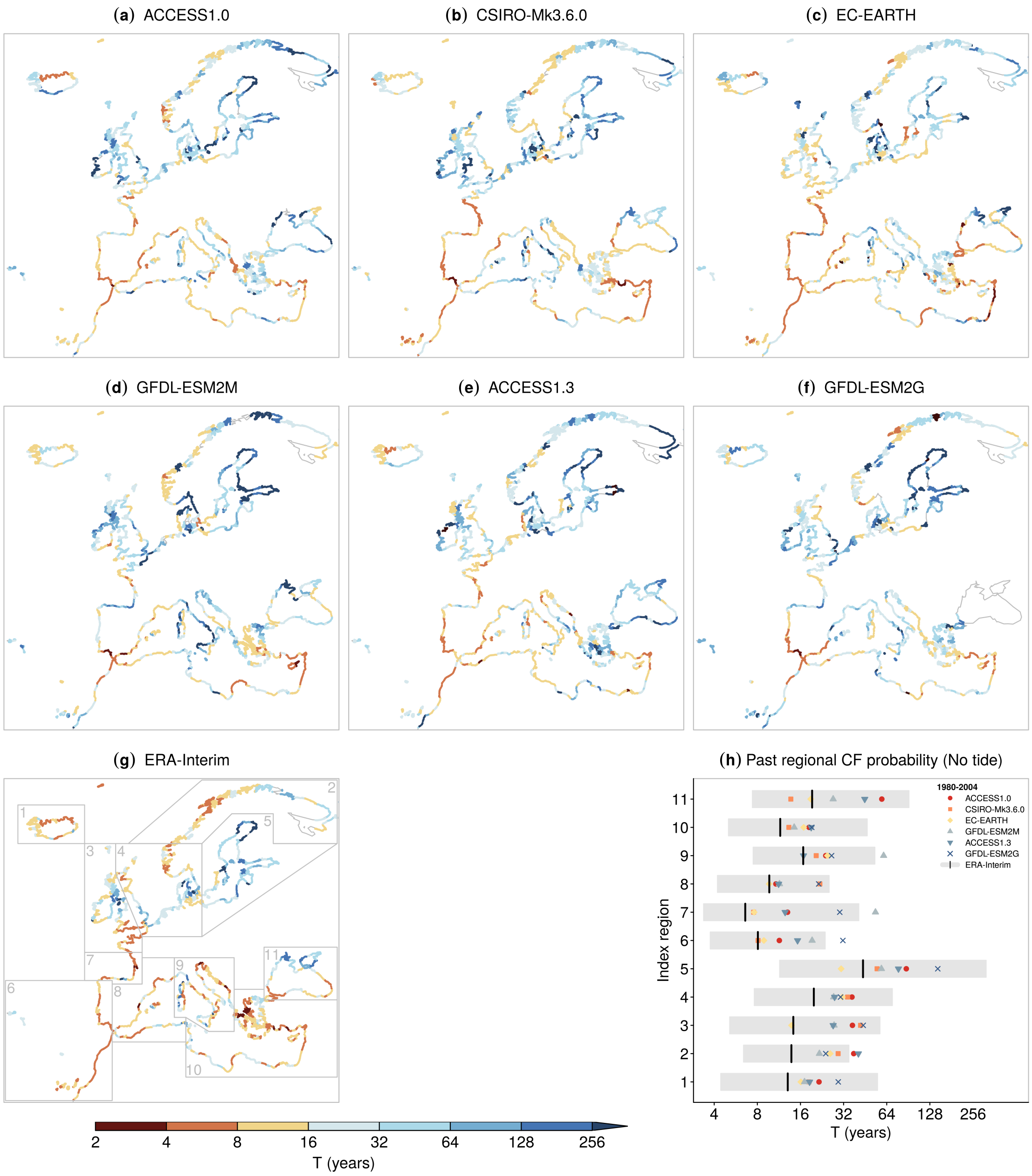

Figure B.4: **Probability of potential compound flood (CF) based on individual models.** Return periods of CF (co-occurring sea level and precipitation extremes, i.e. larger than the individual 1-year return levels). The return periods are based on the period 1980-2004, i.e. the intersection of the model time domains. To focus on the meteorological component only, astronomical tides are not considered here. (**h**) Median value of CF return periods in regions defined in (**g**), based on individual models. For ERA-Interim, grey shading illustrates the sampling uncertainty 95% range (computed as explained in the Methods, but without considering tides).

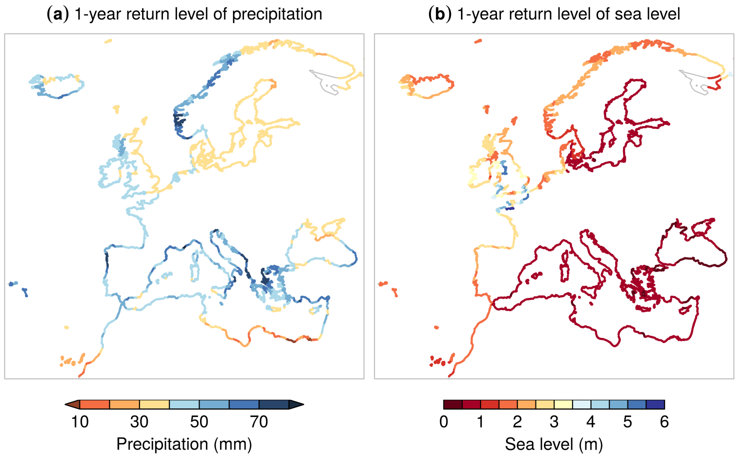

Figure B.5: **Extreme values of sea level and precipitation.** 1-Year return levels of (**a**) precipitation accumulated within a time range ±1 days and (**b**) maximum daily sea level. Based on ERA-Interim data (period 1980-2014).

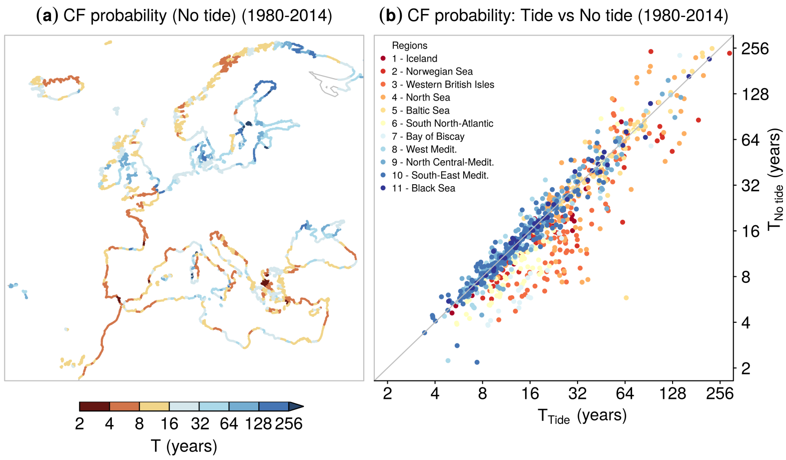

Figure B.6: **Changes in probability of potential compound flood (CF) driven by the astronomical tides.** Return periods of CF (co-occurring sea level and precipitation extremes, i.e. larger than the individual 1-year return levels); based on ERA-Interim data. (**a**) To isolate the effect of astronomical tides on the resulting CF return periods, here sea level does not include astronomical tides. (**b**) Scatterplot of the return periods of CF in the individual locations of the analysed domain, where sea level includes astronomical tides (x-axis, shown in Fig. 5.1), and where sea level does not include astronomical tides (y-axis, shown in panel (**a**)). The colours indicates the geographical region where the locations belong (the regions are defined in Fig. 5.2b).

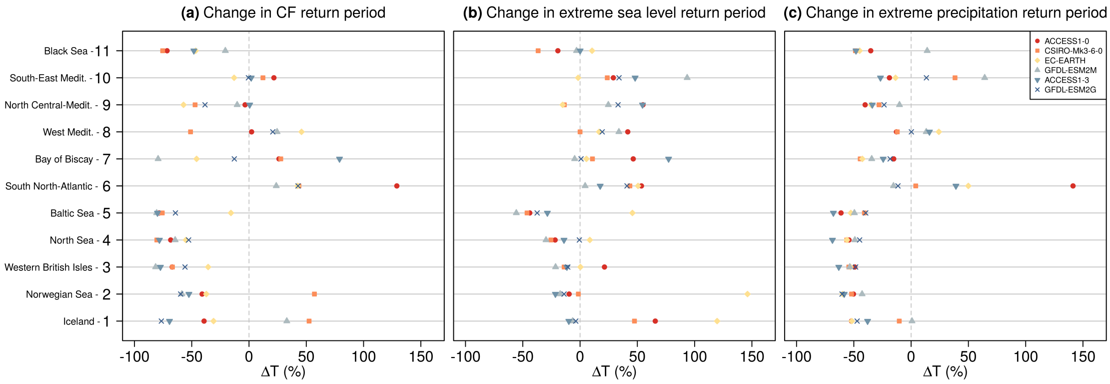

Figure B.7: **Regional changing probability of potential compound flood (CF), extreme sea level and precipitation.** Regional median value of projected change of (**a**) CF, extreme sea level (**b**) and precipitation (**c**) return periods between future (2070-2099) and present (1970-2004), separately for individual models and regions (the latter are defined in Fig. B.4g). SLR is not considered in the definition of future sea levels (see main text). The sea return period change in region 8 is larger than the x-axis, i.e. ~ 180 % (for the ACCESS1-3 model). Similarly, the CF return period change in regions 6, 8, and 10 is ~ 620 %, 480 % (ACCESS1-3 model), and 200 % (GFDL-ESM2M) respectively. See Fig. B.10 for maps of change in CF return periods based on individual CMIP5 models.

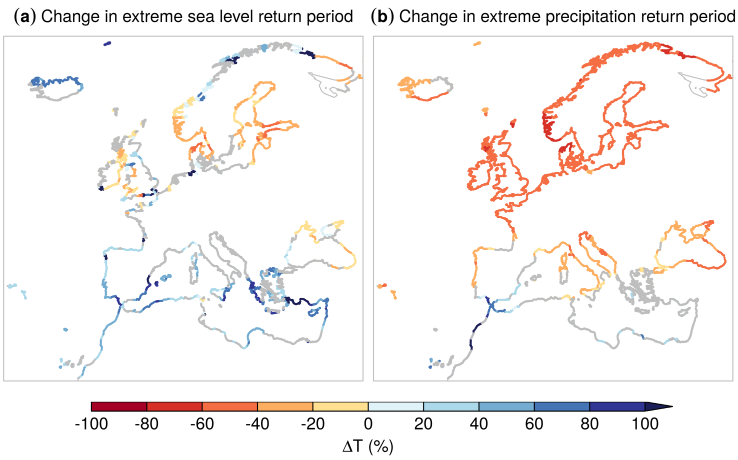

Figure B.8: **Changing return periods of extreme sea level (no SLR), and precipitation.** Multi-model mean of projected change (%) of return periods, between future (2070-2099) and present (1970-2004). Return periods of (**a**) extreme sea level (no SLR) and (**b**) extreme precipitation. Grey points indicate locations where only 4 or fewer out of 6 models agree on the sign of the return period change (3 or less out of 5 models in the Black Sea).

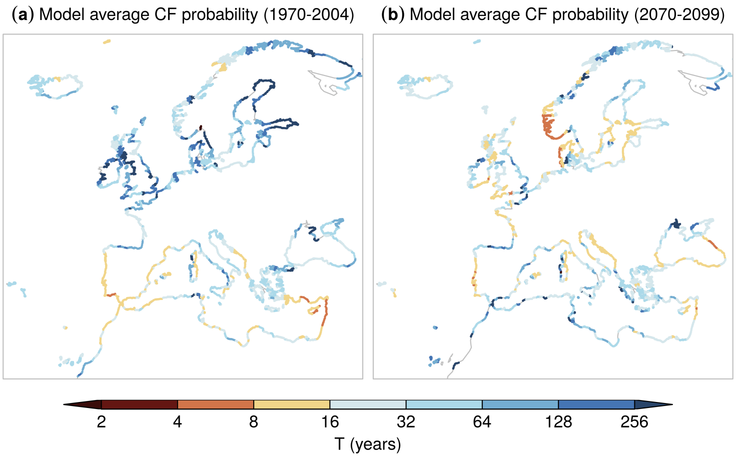

Figure B.9: **Probability of potential compound flood (CF) for present and future periods, based on CMIP5 models.** Multi-model mean of CF return periods (co-occurring sea level (no SLR) and precipitation extremes, i.e. larger than the individual 1-year return levels) for (**a**) present (1970-2004), and (**b**) future (2070-2099).

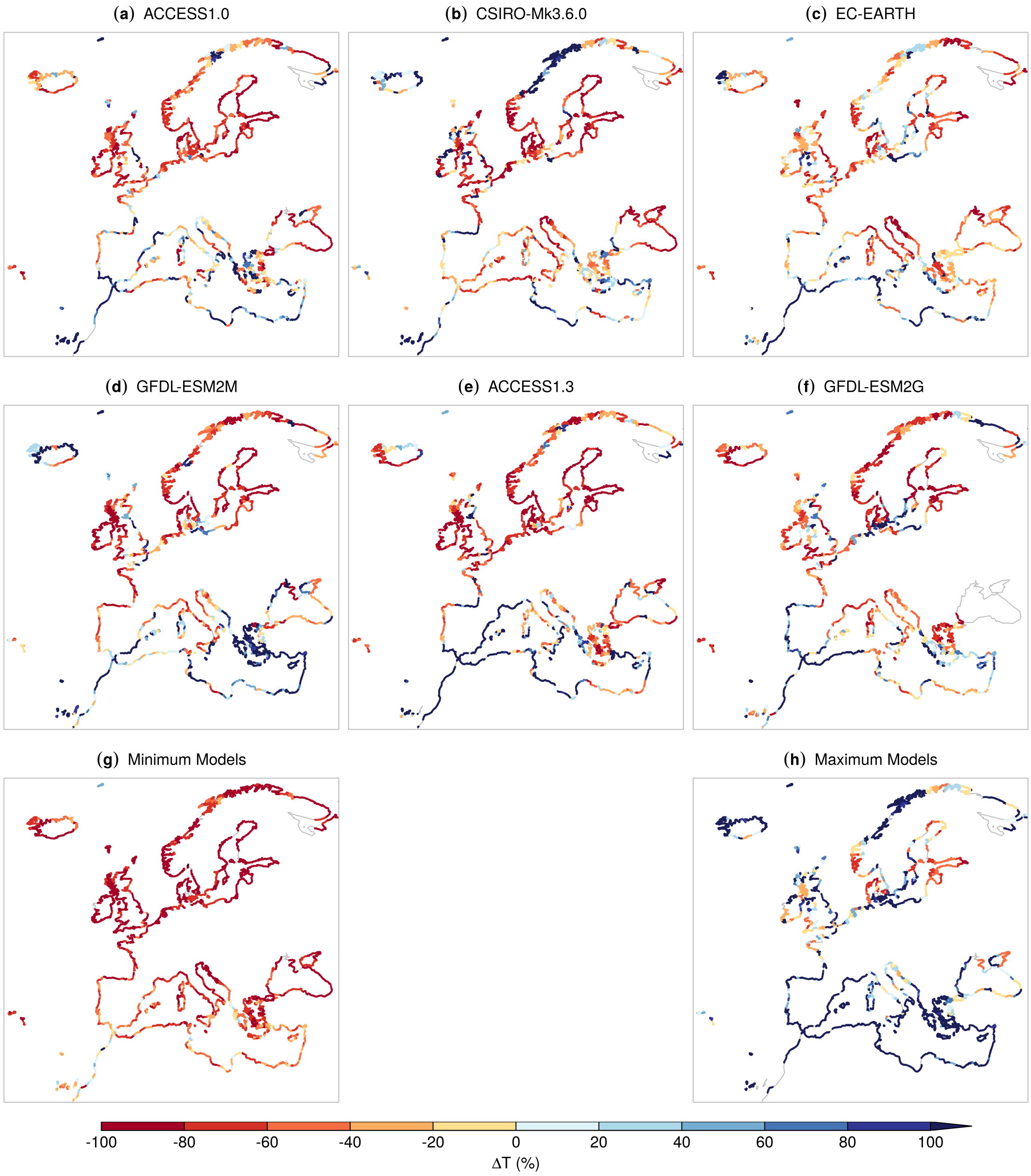

Figure B.10: **Future change of compound flooding (CF) return periods based on individual models.** Projected change (%) of return periods, between future (2070-2099) and present (1970-2004) for individual models (**a-f**). Minimum (**g**) and maximum (**h**) change of the return periods based on the model ensemble.

C. Appendix

C.1 Statistical inference of the multivariate probability density function

Throughout the study in chapter 6, we employ a 4-dimensional D-Vine. For a 4-dimensional D-vine, there are totally twelve possible decompositions. We employ the vine for conditional simulations of h given (Y_3,Y_2,Y_1), and we select the best vine among the six which allows for conditioning sampling following the approach described in section 3.2.3.1. In particular, for convenience we employ a unique decomposition to be applied throughout the study at all sites; the procedure we follow for this selection is outlined later. The used vine is given as:

$$\begin{aligned} f_{3,2,1,h}(y_3, y_2, y_1, h) = {} & f_3(y_3) \cdot f_2(y_2) \cdot f_1(y_1) \cdot f_h(h) \\ & \cdot c_{32}(u_3, u_2) \cdot c_{21}(u_2, u_1) \cdot c_{1h}(u_1, u_h) \\ & \cdot c_{31|2}(u_{3|2}, u_{1|2}) \cdot c_{2h|1}(u_{2|1}, u_{h|1}) \\ & \cdot c_{3h|21}(u_{3|21}, u_{h|21}). \end{aligned} \tag{C.1}$$

The parameters of each bivariate copula in eq. (C.1) are estimated based on the marginal variables $\mathrm{u_i}$ drawn from the marginal CDFs F_i. We use a kernel density estimate for all marginal distributions. The use of kernel density estimates provides a convenient way of estimating the marginal distribution of h. Soil moisture has natural upper and lower bounds, according to its wilting and saturation points respectively, and can also exhibit a bimodal distribution[36,127]. All marginal densities are estimated using the ks R package[39] which employs the bandwidth selector of Wand and Jones[200].

We follow the approach used in ref.[125] to remove ties from the $\mathrm{u_i}$ values were the copulas are fitted to. Through this approach, a small random noise is drawn from a uniform distribution on [-0.001,0.001] and added to $\mathrm{Y}_{1_{\mathrm{PS}}}$ and $\mathrm{Y}_{2_{\mathrm{PL}}}$ values greater than zero. For values equal to zero, we add a random noise drawn from the uniform distribution on [0,0.001].

The selection of the D-vine decomposition in eq. (C.1) is based on an initial test in which we assess the performance of each of the six possible decompositions in their ability to represent h when conditioning on observed Y. At all sites we fit a PCC for each of the six decompositions and use the AIC criterion when selecting the type of copulas to be used. The selection of copula families and the estimation of their parameters is carried out at each site separately. Each copula is chosen from a range of copulas provided by the VineCopula R package[140]. To assess each of the six possible decompositions, a probabilistic forecast of h consisting of 1000 members is produced at all sites. These are compared with observed soil moisture using the root mean squared error. We then select the decomposition that generally shows the highest explanatory power of h at all sites.

After selecting the decomposition to apply, the goodness of fit (GoF) of the selected copulas is tested. Here, copulas initially selected according to the AIC did not always provide a satisfactory fit. For this reason we use two criteria in the selection of a copula for each pair in the PCC. This procedure is carried out sequentially, unconditional copulas are first selected followed by the conditional copulas. We firstly select the top three copulas of the vine according to the AIC and secondly test the GoF of each copula using K-plots[19,49]. We then select the highest ranked copula according to the AIC that shows satisfactory compliance in the K-plots (K-plots are described in appendix A.3 and[19]). Most selected copulas show good agreement according to the K-plots (not shown) where parametric $K(\mathrm{w})$ values generally follow the mean of the empirical values and mostly remain within the uncertainty intervals calculated from 1000 simulations. Some small problems are found with the copulas at sites (e) and (f) which may limit the strength of conclusions drawn from these sites.

List of Figures

1 Introduction **3**
1.1 Atmospheric conditions during a compound flooding in Ravenna 4

2 Modelling of compound events **9**
2.1 Physical evidence of climate change 10
2.2 Historical global mean surface temperature anomalies 11
2.3 Representative Concentration Pathways (RCPs) 12
2.4 Synoptic weather conditions driving extreme events on coastal locations . 15

3 Methods **23**
3.1 Schematic representation of the developed conceptual model 26
3.2 Procedure for computing compound flood bivariate (AND) return periods 32

4 Multivariate statistical modelling of CF in Ravenna (Italy) **33**
4.1 Representation of the hydraulic system of the Ravenna catchment 34
4.2 Impact-model validation based on Q-Q plot 38
4.3 Scatter plots of predictands and predictors driving compound flooding . . 39
4.4 Regression map employed to develop the sea level predictor 41
4.5 Scatter plots of the observed against simulated compound flooding contributing variables 42
4.6 Return levels of compound flooding based on the unconditional model . . 43
4.7 Validation of the conditional model time series 43
4.8 Return levels of compound flooding based on the conditional model 46

5 Higher CF probability in Europe under anthropogenic climate change **49**
5.1 Present probability of potential compound flood 55
5.2 Future probability of potential compound flood 56
5.3 Attribution of probability change in potential compound flood to changes in dependence and marginal distribution of sea level and precipitation . . 57

6 Soil moisture drought in Europe: a CE of precipitation and PET **59**
6.1 Location of the employed Fluxnet sites 61
6.2 Schematic of the variables employed in the soil moisture model 61
6.3 Validation of the modelled soil moisture time series 66
6.4 Assessment of contributing variables to soil moisture 69

6.5 Assessment of contributing variables to soil moisture during 2003 and 2006 heat waves . . . 70
6.6 Assessment of the contributing variable dependencies to soil moisture . . 71
6.7 Sensitivity of soil moisture to the integration period of potential evapotranspiration . . . 73

A Appendix 87
A.1 Graphical representation of D-vines . . . 91
A.2 K-plots of the pair-copula families used in the conditional model . . . 93
A.3 Validation of the unconditional model based on the autcorrelation function 98

B Appendix 99
B.1 Percentage of days experiencing extreme sea level due relative sea level rise 100
B.2 Comparison of the dependence between sea level and precipitation based on ERA-Interim and observation data . . . 102
B.3 Comparison of the return periods of potential compound flooding based on ERA-Interim and observation data . . . 103
B.4 Probability of potential compound flood based on individual models . . . 104
B.5 Extreme values of sea level and precipitation . . . 105
B.6 Changes in probability of potential compound flood driven by the astronomical tides . . . 105
B.7 Regional changing probability of potential compound flood, extreme sea level and precipitation . . . 106
B.8 Changing return periods of extreme sea level (no SLR), and precipitation 106
B.9 Probability of potential compound flood for present and future periods, based on CMIP5 models . . . 107
B.10 Future change of compound flooding return periods based on individual models . . . 108

List of Tables

6 Soil moisture drought in Europe: a CE of precipitation and PET 59
6.1 Information about the FLUXNET sites 60
6.2 Assessment of contributing variables to soil moisture (statistics) 67

B Appendix 99
B.1 Information about used CMIP5 models 101

List of Acronyms

CE Compound Event

CF Compound Flooding

CMIP Coupled Model Intercomparison Project

CMIP5 phase 5 of the Coupled Model Intercomparison Project

CORDEX Coordinated Regional Climate Downscaling Experiment

E-OBS European high-resolution observational gridded data set

ECMWF European Centre for Medium-Range Weather Forecasts

ENSO El Niño-Southern Oscillation

ERA-Interim ECMWF Interim reanalysis

GCM General Circulation Model

GHG Greenhouse gas

IPCC Intergovernmental Panel on Climate Change

PCC Pair Copula Construction

RCM Regional Climate Model

SLP Sea Level Pressure

SLR Sea Level Rise

UNEP United Nations Environment Programme

WCRP World Climate Research Programme

WMO World Meteorological Organization

Bibliography

[1] Aas, K., Czado, C., Frigessi, A., and Bakken, H. (2009). Pair-copula constructions of multiple dependence. *Insurance: Mathematics and Economics*, 44(2):182–198.

[2] Acar, E. F., Genest, C., and NešLehová, J. (2012). Beyond simplified pair-copula constructions. *Journal of Multivariate Analysis*, 110:74–90.

[3] Agarwal, N., Jungclaus, J. H., Köhl, A., Mechoso, C., and Stammer, D. (2015). Additional contributions to cmip5 regional sea level projections resulting from greenland and antarctic ice mass loss. *Environmental Research Letters*, 10(7):074008.

[4] Agenzia per la sicurezza territoriale e la protezione civile (2016). LIFE PRIMES. *http://protezionecivile.regione.emilia-romagna.it/life-primes/progetto/progetto-life-primes/il-progetto-life-primes (last access: 6 December 2016).*

[5] Agenzia regionale per la sicurezza territoriale e la protezione civile - Regione Emilia-Romagna (2015). LIFE PRIMES: Preventing flooding RIsks by Making resilient communitiES (project reference number: LIFE14 CCA/IT/001280). *http://ec.europa.eu/environment/life/project/Projects/index.cfm?fuseaction=search.dspPage&n_proj_id=5247 (last access: 6 December 2016).*

[6] AghaKouchak, A., Cheng, L., Mazdiyasni, O., and Farahmand, A. (2014). Global warming and changes in risk of concurrent climate extremes: Insights from the 2014 California drought. *Geophysical Research Letters*, 41(24):2014GL062308.

[7] Arns, A., Dangendorf, S., Jensen, J., Talke, S., Bender, J., and Pattiaratchi, C. (2017). Sea-level rise induced amplification of coastal protection design heights. *Scientific reports*, 7:40171.

[8] Arns, A., Wahl, T., Dangendorf, S., and Jensen, J. (2015). The impact of sea level rise on storm surge water levels in the northern part of the german bight. *Coastal Engineering*, 96:118–131.

[9] Arpa Emilia-Romagna (2015). Rapporto dellevento meteorologico del 5 e 6 febbraio 2015. *Bologna, Italy.*

[10] Bader, B. and Yan, J. (2016). eva: Extreme value analysis with goodness-of-fit testing. *R package version*, 0.2.4.

[11] Baldocchi, D., Falge, E., Gu, L., Olson, R., Hollinger, D., Running, S., Anthoni, P., Bernhofer, C., Davis, K., Evans, R., et al. (2001). Fluxnet: A new tool to study the temporal and spatial variability of ecosystem–scale carbon dioxide, water vapor, and energy flux densities. *Bulletin of the American Meteorological Society*, 82(11):2415–2434.

[12] Barton, Y., Giannakaki, P., Von Waldow, H., Chevalier, C., Pfahl, S., and Martius, O. (2016). Clustering of regional-scale extreme precipitation events in southern switzerland. *Monthly Weather Review*, 144(1):347–369.

[13] Bedford, T. and Cooke, R. (2001a). Monte carlo simulation of vine dependent random variables for applications in uncertainty analysis. *European Conference on Safety and Reliability 2001.*

[14] Bedford, T. and Cooke, R. M. (2001b). Probability density decomposition for conditionally dependent random variables modeled by vines. *Annals of Mathematics and Artificial intelligence*, 32(1-4):245–268.

[15] Bedford, T. and Cooke, R. M. (2002). Vines: A new graphical model for dependent random variables. *Annals of Statistics*, pages 1031–1068.

[16] Berg, A., Sheffield, J., and Milly, P. C. (2017). Divergent surface and total soil moisture projections under global warming. *Geophysical Research Letters*, 44(1):236–244.

[17] Bernier, N. and Thompson, K. (2007). Tide-surge interaction off the east coast of canada and northeastern united states. *Journal of Geophysical Research: Oceans*, 112(C6).

[18] Bevacqua, E. (2017). *CDVineCopulaConditional: Sampling from Conditional C- and D-Vine Copulas.* R package version 0.1.0.

[19] Bevacqua, E., Maraun, D., Haff, I. H., Widmann, M., and Vrac, M. (2017). Multivariate statistical modelling of compound events via pair-copula constructions: analysis of floods in ravenna (italy). *Hydrology and Earth System Sciences*, 21(6):2701.

[20] Bevacqua, E., Maraun, D., Vousdoukas, M. I., Voukouvalas, E., Vrac, M., Mentaschi, L., and Widmann, M. (2018). Higher potential compound flood risk in northern europe under anthropogenic climate change. *Submitted to Nature Climate Change.*

[21] Bordbar, M. H., Martin, T., Latif, M., and Park, W. (2015). Effects of long-term variability on projections of twenty-first century dynamic sea level. *Nature Climate Change*, 5(4):343.

[22] Brechmann, E. C., Hendrich, K., and Czado, C. (2013). Conditional copula simulation for systemic risk stress testing. *Insurance: Mathematics and Economics*, 53(3):722–732.

[23] Camargo, S. J. (2013). Global and regional aspects of tropical cyclone activity in the cmip5 models. *Journal of Climate*, 26(24):9880–9902.

[24] Carbognin, L., Teatini, P., Tosi, L., Strozzi, T., and Tomasin, A. (2011). Present relative sea level rise in the northern adriatic coastal area.

[25] Carrère, L., Lyard, F., Cancet, M., Guillot, A., and Roblou, L. (2013). Fes 2012: a new global tidal model taking advantage of nearly 20 years of altimetry. In *20 Years of Progress in Radar Altimetry*, volume 710.

[26] Church, J. A., Clark, P. U., Cazenave, A., Gregory, J. M., Jevrejeva, S., Levermann, A., Merrifield, M. A., Milne, G. A., Nerem, R. S., Nunn, P. D., et al. (2013). Sea level change. in: Climate change 2013: The physical science basis. contribution of working group i to the fifth assessment report of the intergovernmental panel on climate change. Technical report.

[27] Ciais, P., Reichstein, M., Viovy, N., Granier, A., Oge, J., Allard, V., Aubinet, M., Buchmann, N., Bernhofer, C., Carrara, A., Chevallier, F., De Noblet, N., Friend, A. D., Friedlingstein, P., Grnwald, T., Heinesch, B., Keronen, P., Knohl, A., Krinner, G., Loustau, D., Manca, G., Matteucci, G., Miglietta, F., Ourcival, J. M., Papale, D., Pilegaard, K., Rambal, S., Seufert, G., Soussana, J. F., Sanz, M. J., Schulze, E. D., Vesala, T., and Valentini, R. (2005). Europe-wide reduction in primary productivity caused by the heat and drought in 2003. *Nature*, 437(7058):529–533.

[28] Codiga, D. L. (2011). Unified tidal analysis and prediction using the utide matlab functions. technical report 2011-01. graduate school of oceanography, university of rhode island, narragansett, ri. 59pp.

[29] Coles, S., Bawa, J., Trenner, L., and Dorazio, P. (2001). *An introduction to statistical modeling of extreme values*, volume 208. Springer.

[30] Collins, M., Knutti, R., Arblaster, J., Dufresne, J.-L., Fichefet, T., Friedlingstein, P., Gao, X., Gutowski, W., Johns, T., Krinner, G., et al. (2013). Long-term climate change: projections, commitments and irreversibility.

[31] Coumou, D., Petoukhov, V., Rahmstorf, S., Petri, S., and Schellnhuber, H. J. (2014). Quasi-resonant circulation regimes and hemispheric synchronization of extreme weather in boreal summer. *Proceedings of the National Academy of Sciences*, 111(34):12331–12336.

[32] Cubasch, U., D. W. D. C. M. F. D. F. N. M. and Winther, J.-G. (2013). Introduction. in: Climate change 2013: The physical science basis. contribution of working group i to the fifth assessment report of the intergovernmental panel on climate change. Technical report.

[33] Dai, A. (2011). Drought under global warming: a review. *Wiley Interdisciplinary Reviews: Climate Change*, 2(1):45–65.

[34] Dai, A. (2013). Increasing drought under global warming in observations and models. *Nature Climate Change*, 3(1):52–58.

[35] Dai, A., Trenberth, K. E., and Qian, T. (2004). A Global Dataset of Palmer Drought Severity Index for 18702002: Relationship with Soil Moisture and Effects of Surface Warming. *Journal of Hydrometeorology*, 5(6):1117–1130.

[36] D'Andrea, F., Provenzale, A., Vautard, R., and De Noblet-Decoudr, N. (2006). Hot and cool summers: Multiple equilibria of the continental water cycle. *Geophysical Research Letters*, 33(24):L24807.

[37] Dee, D. P., Uppala, S., Simmons, A., Berrisford, P., Poli, P., Kobayashi, S., Andrae, U., Balmaseda, M., Balsamo, G., Bauer, P., et al. (2011). The era-interim reanalysis: Configuration and performance of the data assimilation system. *Quarterly Journal of the royal meteorological society*, 137(656):553–597.

[38] Du, J., Shen, J., Zhang, Y. J., Ye, F., Liu, Z., Wang, Z., Wang, Y. P., Yu, X., Sisson, M., and Wang, H. V. (2018). Tidal response to sea-level rise in different types of estuaries: the importance of length, bathymetry, and geometry. *Geophysical Research Letters*.

[39] Duong, T. (2017). *ks: Kernel Smoothing*. R package version 1.10.7.

[40] Economou, T., Stephenson, D. B., Pinto, J., Shaffrey, L., and Zappa, G. (2015). Serial clustering of extratropical cyclones in a multi-model ensemble of historical and future simulations. *Quarterly Journal of the Royal Meteorological Society*, 141(693):3076–3087.

[41] Emanuel, K. A. (2013). Downscaling cmip5 climate models shows increased tropical cyclone activity over the 21st century. *Proceedings of the National Academy of Sciences*, 110(30):12219–12224.

[42] Feynman, R. P. (1955). The value of science. *Engineering and Science*, 19(3):13–15.

[43] Fischer, E. M. and Knutti, R. (2013). Robust projections of combined humidity and temperature extremes. *Nature Climate Change*, 3(2):126.

[44] Fischer, E. M. and Knutti, R. (2016). Observed heavy precipitation increase confirms theory and early models. *Nature Climate Change*, 6(11):986.

[45] Fischer, E. M., Seneviratne, S. I., Vidale, P. L., Lüthi, D., and Schär, C. (2007). Soil moisture–atmosphere interactions during the 2003 european summer heat wave. *Journal of Climate*, 20(20):5081–5099.

[46] Flannigan, M. D., Krawchuk, M. A., de Groot, W. J., Wotton, B. M., and Gowman, L. M. (2009). Implications of changing climate for global wildland fire. *International journal of wildland fire*, 18(5):483–507.

[47] Flato, G., Marotzke, J., Abiodun, B., Braconnot, P., Chou, S. C., Collins, W. J., Cox, P., Driouech, F., Emori, S., Eyring, V., et al. (2013). Evaluation of climate models. in: climate change 2013: the physical science basis. contribution of working group i to the fifth assessment report of the intergovernmental panel on climate change. *Climate Change 2013*, 5:741–866.

[48] Gambolati, G., Teatini, P., and Gonella, M. (2002). Gis simulations of the inundation risk in the coastal lowlands of the northern adriatic sea. *Mathematical and Computer Modelling*, 35(9-10):963–972.

[49] Genest, C. and Favre, A.-C. (2007). Everything you always wanted to know about copula modeling but were afraid to ask. *Journal of hydrologic engineering*, 12(4):347–368.

[50] Genest, C., Ghoudi, K., and Rivest, L.-P. (1995). A semiparametric estimation procedure of dependence parameters in multivariate families of distributions. *Biometrika*, 82(3):543–552.

[51] Genest, C., Rémillard, B., and Beaudoin, D. (2009). Goodness-of-fit tests for copulas: A review and a power study. *Insurance: Mathematics and economics*, 44(2):199–213.

[52] Giorgi, F., Jones, C., Asrar, G. R., et al. (2009). Addressing climate information needs at the regional level: the cordex framework. *World Meteorological Organization (WMO) Bulletin*, 58(3):175.

[53] Gräler, B., Petroselli, A., Grimaldi, S., De Baets, B., and Verhoest, N. (2016). An update on multivariate return periods in hydrology. *Proceedings of the International Association of Hydrological Sciences*, 373:175–178.

[54] Gräler, B., van den Berg, M., Vandenberghe, S., Petroselli, A., Grimaldi, S., De Baets, B., and Verhoest, N. (2013). Multivariate return periods in hydrology: a critical and practical review focusing on synthetic design hydrograph estimation. *Hydrology and Earth System Sciences*, 17(4):1281–1296.

[55] Gudmundsson, L., Rego, F., Rocha, M., and Seneviratne, S. I. (2014). Predicting above normal wildfire activity in southern europe as a function of meteorological drought. *Environmental Research Letters*, 9(8):084008.

[56] Haigh, I. D., Wadey, M. P., Wahl, T., Ozsoy, O., Nicholls, R. J., Brown, J. M., Horsburgh, K., and Gouldby, B. (2016). Spatial and temporal analysis of extreme sea level and storm surge events around the coastline of the uk. *Scientific data*, 3:160107.

[57] Hallegatte, S., Green, C., Nicholls, R. J., and Corfee-Morlot, J. (2013). Future flood losses in major coastal cities. *Nature climate change*, 3(9):802–806.

[58] Halwatura, D., McIntyre, N., Lechner, A. M., and Arnold, S. (2017). Capability of meteorological drought indices for detecting soil moisture droughts. *Journal of Hydrology: Regional Studies*, 12:396–412.

[59] Haylock, M., Hofstra, N., Klein Tank, A., Klok, E., Jones, P., and New, M. (2008). A european daily high-resolution gridded data set of surface temperature and precipitation for 1950–2006. *Journal of Geophysical Research: Atmospheres*, 113(D20).

[60] Hazeleger, W., Van den Hurk, B., Min, E., Van Oldenborgh, G., Petersen, A., Stainforth, D., Vasileiadou, E., and Smith, L. (2015). Tales of future weather. *Nature Climate Change*, 5(2):107–113.

[61] Heffernan, J., Stephenson, A., and Gilleland, E. (2016). Ismev: an introduction to statistical modeling of extreme values. *R package version*, 1.41.

[62] Hertig, E., Maraun, D., Bartholy, J., Pongracz, R., Vrac, M., Mares, I., Gutiérrez, J. M., Wibig, J., Casanueva, A., and Soares, P. M. (2018). Comparison of statistical downscaling methods with respect to extreme events over europe: Validation results from the perfect predictor experiment of the cost action value. *International Journal of Climatology*.

[63] Hillier, J. K., Macdonald, N., Leckebusch, G. C., and Stavrinides, A. (2015). Interactions between apparently primary weather-driven hazards and their cost. *Environmental Research Letters*, 10(10):104003.

[64] Hinkel, J., Lincke, D., Vafeidis, A. T., Perrette, M., Nicholls, R. J., Tol, R. S., Marzeion, B., Fettweis, X., Ionescu, C., and Levermann, A. (2014). Coastal flood damage and adaptation costs under 21st century sea-level rise. *Proceedings of the National Academy of Sciences*, 111(9):3292–3297.

[65] Hirabayashi, Y., Mahendran, R., Koirala, S., Konoshima, L., Yamazaki, D., Watanabe, S., Kim, H., and Kanae, S. (2013). Global flood risk under climate change. *Nature Climate Change*, 3(9):816–821.

[66] Hirschi, M., Seneviratne, S. I., Alexandrov, V., Boberg, F., Boroneant, C., Christensen, O. B., Formayer, H., Orlowsky, B., and Stepanek, P. (2011). Observational evidence for soil-moisture impact on hot extremes in southeastern Europe. *Nature Geoscience*, 4(1):17–21.

[67] Hobæk Haff, I. (2012). Comparison of estimators for pair-copula constructions. *Journal of Multivariate Analysis*, 110:91–105.

[68] Hobæk Haff, I., Aas, K., and Frigessi, A. (2010). On the simplified pair-copula constructionsimply useful or too simplistic? *Journal of Multivariate Analysis*, 101(5):1296–1310.

[69] Hobæk Haff, I. et al. (2013). Parameter estimation for pair-copula constructions. *Bernoulli*, 19(2):462–491.

[70] Hobæk Haff, I., Frigessi, A., and Maraun, D. (2015). How well do regional climate models simulate the spatial dependence of precipitation? an application of pair-copula constructions. *Journal of Geophysical Research: Atmospheres*, 120(7):2624–2646.

[71] Horsburgh, K. and Wilson, C. (2007). Tide-surge interaction and its role in the distribution of surge residuals in the north sea. *Journal of Geophysical Research: Oceans*, 112(C8).

[72] Howard, T., Lowe, J., and Horsburgh, K. (2010). Interpreting century-scale changes in southern north sea storm surge climate derived from coupled model simulations. *Journal of Climate*, 23(23):6234–6247.

[73] Hydraulics, WL Delft (2014). Delft3D-FLOW, Simulation of multi-dimensional hydrodynamic flows and transport phenomena, including sediments. *User Manual, Delft, Holanda*.

[74] Ikeuchi, H., Hirabayashi, Y., Yamazaki, D., Muis, S., Ward, P. J., Winsemius, H. C., Verlaan, M., and Kanae, S. (2017). Compound simulation of fluvial floods and storm surges in a global coupled river-coast flood model: Model development and its application to 2007 cyclone sidr in bangladesh. *Journal of Advances in Modeling Earth Systems*.

[75] Joe, H. (1996). Families of m-variate distributions with given margins and m (m-1)/2 bivariate dependence parameters. *Lecture Notes-Monograph Series*, pages 120–141.

[76] Joe, H. (1997). *Multivariate models and multivariate dependence concepts*. CRC Press.

[77] Kew, S., Selten, F., Lenderink, G., and Hazeleger, W. (2013). The simultaneous occurrence of surge and discharge extremes for the rhine delta. *Natural hazards and earth system sciences*, 13(8):2017–2029.

[78] Klerk, W.-J., Winsemius, H., van Verseveld, W., Bakker, A., and Diermanse, F. (2015). The co-incidence of storm surges and extreme discharges within the rhine–meuse delta. *Environmental Research Letters*, 10(3):035005.

[79] Kossin, J. P. (2018). A global slowdown of tropical-cyclone translation speed. *Nature*, 558:104.

[80] Kumbier, K., Carvalho, R. C., Vafeidis, A. T., and Woodroffe, C. D. (2018). Investigating compound flooding in an estuary using hydrodynamic modelling: a case study from the shoalhaven river, australia. *Natural Hazards and Earth System Sciences*, 18(2):463.

[81] Kurowicka, D. and Cooke, R. M. (2007). Sampling algorithms for generating joint uniform distributions using the vine-copula method. *Computational statistics & data analysis*, 51(6):2889–2906.

[82] Lefevre, F., Lyard, F., Le Provost, C., and Schrama, E. J. (2002). Fes99: a global tide finite element solution assimilating tide gauge and altimetric information. *Journal of Atmospheric and Oceanic Technology*, 19(9):1345–1356.

[83] Lenderink, G. and Van Meijgaard, E. (2008). Increase in hourly precipitation extremes beyond expectations from temperature changes. *Nature Geoscience*, 1(8):511.

[84] Leonard, M., Westra, S., Phatak, A., Lambert, M., van den Hurk, B., McInnes, K., Risbey, J., Schuster, S., Jakob, D., and Stafford-Smith, M. (2014). A compound event framework for understanding extreme impacts. *Wiley Interdisciplinary Reviews: Climate Change*, 5(1):113–128.

[85] Liu, Z., Cheng, L., Hao, Z., Li, J., Thorstensen, A., and Gao, H. (2018). A framework for exploring joint effects of conditional factors on compound floods. *Water Resources Research*, 54(4):2681–2696.

[86] Liu, Z., Zhou, P., Chen, X., and Guan, Y. (2015). A multivariate conditional model for streamflow prediction and spatial precipitation refinement. *Journal of Geophysical Research: Atmospheres*, 120(19).

[87] Losada, I., Reguero, B., Méndez, F., Castanedo, S., Abascal, A., and Mínguez, R. (2013). Long-term changes in sea-level components in latin america and the caribbean. *Global and Planetary Change*, 104:34–50.

[88] Lowe, J. and Gregory, J. (2005). The effects of climate change on storm surges around the united kingdom. *Philosophical Transactions of the Royal Society of London A: Mathematical, Physical and Engineering Sciences*, 363(1831):1313–1328.

[89] Luo, L., Apps, D., Arcand, S., Xu, H., Pan, M., and Hoerling, M. (2017). Contribution of temperature and precipitation anomalies to the California drought during 20122015. *Geophysical Research Letters*, 44(7):2016GL072027.

[90] Mailier, P. J., Stephenson, D. B., Ferro, C. A., and Hodges, K. I. (2006). Serial clustering of extratropical cyclones. *Monthly weather review*, 134(8):2224–2240.

[91] Mann, M. (2017). It's a fact: climate change made hurricane harvey more deadly. *The Guardian*, 28.

[92] Mann, M. E., Rahmstorf, S., Kornhuber, K., Steinman, B. A., Miller, S. K., and Coumou, D. (2017). Influence of anthropogenic climate change on planetary wave resonance and extreme weather events. *Scientific Reports*, 7:45242.

[93] Manning, C., Widmann, M., Bevacqua, E., Van Loon, A. F., Maraun, D., and Vrac, M. (2018a). Soil moisture drought in europe: a compound event of precipitation and potential evapotranspiration on multiple timescales. *Journal of Hydrometeorology, Under review.*

[94] Manning, C., Widmann, M., Bevacqua, E., Van Loon, A. F., Maraun, D., and Vrac, M. (2018b). Title title title title title title title title title title title title title title. *In preparation.*

[95] Maraun, D. (2013). When will trends in european mean and heavy daily precipitation emerge? *Environmental Research Letters*, 8(1):014004.

[96] Maraun, D., Shepherd, T. G., Widmann, M., Zappa, G., Walton, D., Gutiérrez, J. M., Hagemann, S., Richter, I., Soares, P. M., Hall, A., et al. (2017). Towards process-informed bias correction of climate change simulations. *Nature Climate Change*, 7(11):764.

[97] Maraun, D., Wetterhall, F., Ireson, A., Chandler, R., Kendon, E., Widmann, M., Brienen, S., Rust, H., Sauter, T., Themeßl, M., et al. (2010). Precipitation downscaling under climate change: Recent developments to bridge the gap between dynamical models and the end user. *Reviews of Geophysics*, 48(3).

[98] Maraun, D. and Widmann, M. (2018). *Statistical Downscaling and Bias Correction for Climate Research.* Cambridge University Press.

[99] Martius, O., Pfahl, S., and Chevalier, C. (2016). A global quantification of compound precipitation and wind extremes. *Geophysical Research Letters*, 43(14):7709–7717.

[100] Martius, O., Sodemann, H., Joos, H., Pfahl, S., Winschall, A., Croci-Maspoli, M., Graf, M., Madonna, E., Mueller, B., Schemm, S., et al. (2013). The role of upper-level dynamics and surface processes for the pakistan flood of july 2010. *Quarterly Journal of the Royal Meteorological Society*, 139(676):1780–1797.

[101] Masina, M., Lamberti, A., and Archetti, R. (2015). Coastal flooding: A copula based approach for estimating the joint probability of water levels and waves. *Coastal Engineering*, 97:37–52.

[102] Materia, S., Dirmeyer, P. A., Guo, Z., Alessandri, A., and Navarra, A. (2010). The sensitivity of simulated river discharge to land surface representation and meteorological forcings. *Journal of Hydrometeorology*, 11(2):334–351.

[103] Mazdiyasni, O. and AghaKouchak, A. (2015). Substantial increase in concurrent droughts and heatwaves in the united states. *Proceedings of the National Academy of Sciences*, 112(37):11484–11489.

[104] Melet, A., Meyssignac, B., Almar, R., and Le Cozannet, G. (2018). Underestimated wave contribution to coastal sea-level rise. *Nature Climate Change*, 8(3):234.

[105] Mentaschi, L., Vousdoukas, M. I., Voukouvalas, E., Dosio, A., and Feyen, L. (2017). Global changes of extreme coastal wave energy fluxes triggered by intensified teleconnection patterns. *Geophysical Research Letters*, 44(5):2416–2426.

[106] Meredith, E. P., Semenov, V. A., Maraun, D., Park, W., and Chernokulsky, A. V. (2015). Crucial role of black sea warming in amplifying the 2012 krymsk precipitation extreme. *Nature Geoscience*, 8(8):615.

[107] Michele, C., Salvadori, G., Vezzoli, R., and Pecora, S. (2013). Multivariate assessment of droughts: Frequency analysis and dynamic return period. *Water Resources Research*, 49(10):6985–6994.

[108] Mo, K. C. and Lettenmaier, D. P. (2016). Precipitation deficit flash droughts over the united states. *Journal of Hydrometeorology*, 17(4):1169–1184.

[109] Moftakhari, H. R., Salvadori, G., AghaKouchak, A., Sanders, B. F., and Matthew, R. A. (2017). Compounding effects of sea level rise and fluvial flooding. *Proceedings of the National Academy of Sciences*, 114(37):9785–9790.

[110] Mora, C., Dousset, B., Caldwell, I. R., Powell, F. E., Geronimo, R. C., Bielecki, C. R., Counsell, C. W., Dietrich, B. S., Johnston, E. T., Louis, L. V., et al. (2017). Global risk of deadly heat. *Nature Climate Change*, 7(7):501.

[111] Moseley, C., Hohenegger, C., Berg, P., and Haerter, J. O. (2016). Intensification of convective extremes driven by cloud–cloud interaction. *Nature Geoscience*, 9(10):748.

[112] Muis, S., Verlaan, M., Winsemius, H. C., Aerts, J. C., and Ward, P. J. (2016). A global reanalysis of storm surges and extreme sea levels. *Nature communications*, 7.

[113] NASA (2017). Deadly tropical storm Kai-tak examined with IMERG and GPM satellite. *Extreme Weather News, https://pmm.nasa.gov/extreme-weather/deadly-tropical-storm-kai-tak-examined-imerg-and-gpm-satellite.*

[114] Nelsen, R. (2006). An introduction to copulas, ser. *Lecture Notes in Statistics. New York: Springer.*

[115] NOAA (2017). Tides & Currents. *https://tidesandcurrents.noaa.gov/ (last access: 14 March 2017).*

[116] Orth, R. and Seneviratne, S. I. (2015). Introduction of a simple-model-based land surface dataset for europe. *Environmental Research Letters*, 10(4):044012.

[117] Palmer, W. C. (1965). *Meteorological drought*, volume 30. US Department of Commerce, Weather Bureau Washington, DC.

[118] Paprotny, D., Morales-Nápoles, O., and Jonkman, S. N. (2017). Hanze: a pan-european database of exposure to natural hazards and damaging historical floods since 1870. *Earth System Science Data Discussions.*

[119] Paprotny, D., Vousdoukas, M. I., Morales-Nápoles, O., Jonkman, S. N., and Feyen, L. (2018). Compound flood potential in europe. *Hydrol. Earth Syst. Sci. Discuss*, 2018:1–34.

[120] Pathiraja, S., Westra, S., and Sharma, A. (2012). Why continuous simulation? the role of antecedent moisture in design flood estimation. *Water Resources Research*, 48(6).

[121] Peltier, W., Argus, D., and Drummond, R. (2015). Space geodesy constrains ice age terminal deglaciation: The global ice-6g_c (vm5a) model. *Journal of Geophysical Research: Solid Earth*, 120(1):450–487.

[122] Perez, J., Menendez, M., Mendez, F. J., and Losada, I. J. (2014). Evaluating the performance of cmip3 and cmip5 global climate models over the north-east atlantic region. *Climate dynamics*, 43(9-10):2663–2680.

[123] Pfahl, S., OGorman, P., and Fischer, E. (2017). Understanding the regional pattern of projected future changes in extreme precipitation. *Nature Climate Change*, 7(6):423–427.

[124] Pfahl, S. and Wernli, H. (2012). Quantifying the relevance of cyclones for precipitation extremes. *Journal of Climate*, 25(19):6770–6780.

[125] Pham, M. T., Vernieuwe, H., De Baets, B., Willems, P., and Verhoest, N. (2016). Stochastic simulation of precipitation-consistent daily reference evapotranspiration using vine copulas. *Stochastic Environmental Research and Risk Assessment*, 30(8):2197–2214.

[126] Pinto, J. G., Bellenbaum, N., Karremann, M. K., and Della-Marta, P. M. (2013). Serial clustering of extratropical cyclones over the north atlantic and europe under recent and future climate conditions. *Journal of geophysical research: Atmospheres*, 118(22).

[127] Porporato, A. and DOdorico, P. (2004). Phase Transitions Driven by State-Dependent Poisson Noise. *Physical Review Letters*, 92(11):110601.

[128] Randall, D. A., Wood, R. A., Bony, S., Colman, R., Fichefet, T., Fyfe, J., Kattsov, V., Pitman, A., Shukla, J., Srinivasan, J., et al. (2007). Climate models and their evaluation. In *Climate change 2007: The physical science basis. Contribution of Working Group I to the Fourth Assessment Report of the IPCC (FAR)*, pages 589–662. Cambridge University Press.

[129] Rebel, K. T., de Jeu, R. A. M., Ciais, P., Viovy, N., Piao, S. L., Kiely, G., and Dolman, A. J. (2012). A global analysis of soil moisture derived from satellite observations and a land surface model. *Hydrol. Earth Syst. Sci.*, 16(3):833–847.

[130] Rebetez, M., Dupont, O., and Giroud, M. (2009). An analysis of the july 2006 heatwave extent in europe compared to the record year of 2003. *Theoretical and Applied Climatology*, 95(1):1–7.

[131] Rockström, J., Steffen, W., Noone, K., Persson, Å., Chapin III, F. S., Lambin, E. F., Lenton, T. M., Scheffer, M., Folke, C., Schellnhuber, H. J., et al. (2009). A safe operating space for humanity. *nature*, 461(7263):472.

[132] Ruffault, J., Moron, V., Trigo, R., and Curt, T. (2016). Objective identification of multiple large fire climatologies: an application to a mediterranean ecosystem. *Environmental Research Letters*, 11(7):075006.

[133] Saghafian, B. and Mehdikhani, H. (2014). Drought characterization using a new copula-based trivariate approach. *Natural hazards*, 72(3):1391–1407.

[134] Salvadori, G. and De Michele, C. (2007). On the use of copulas in hydrology: theory and practice. *Journal of Hydrologic Engineering*, 12(4):369–380.

[135] Salvadori, G., De Michele, C., Kottegoda, N. T., and Rosso, R. (2007). *Extremes in nature: an approach using copulas*, volume 56. Springer Science & Business Media.

[136] Salvadori, G., Durante, F., and De Michele, C. (2011). On the return period and design in a multivariate framework. *Hydrology and Earth System Sciences*, pages 3293–3305.

[137] Salvadori, G., Durante, F., De Michele, C., Bernardi, M., and Petrella, L. (2016). A multivariate copula-based framework for dealing with hazard scenarios and failure probabilities. *Water Resources Research*, 52(5):3701–3721.

[138] Salvadori, G., Durante, F., Tomasicchio, G., and D'alessandro, F. (2015). Practical guidelines for the multivariate assessment of the structural risk in coastal and off-shore engineering. *Coastal Engineering*, 95:77–83.

[139] Sawyer, J. (1972). Man-made carbon dioxide and the greenhouse effect. *Nature*, 239(5366):23.

[140] Schepsmeier, U., Stoeber, J., Brechmann, E. C., Graeler, B., Nagler, T., and Erhardt, T. (2017). *VineCopula: Statistical Inference of Vine Copulas.* R package version 2.1.1.

[141] Schoelzel, C. and Friederichs, P. (2008). Multivariate non-normally distributed random variables in climate research–introduction to the copula approach. *Nonlinear Processes in Geophysics*, 15(5):761–772.

[142] Seneviratne, S. I. (2012). Climate science: Historical drought trends revisited. *Nature*, 491(7424):338–339.

[143] Seneviratne, S. I., Corti, T., Davin, E. L., Hirschi, M., Jaeger, E. B., Lehner, I., Orlowsky, B., and Teuling, A. J. (2010a). Investigating soil moisture–climate interactions in a changing climate: A review. *Earth-Science Reviews*, 99(3-4):125–161.

[144] Seneviratne, S. I., Corti, T., Davin, E. L., Hirschi, M., Jaeger, E. B., Lehner, I., Orlowsky, B., and Teuling, A. J. (2010b). Investigating soil moistureclimate interactions in a changing climate: A review. *Earth-Science Reviews*, 99(34):125–161.

[145] Seneviratne, S. I., Lehner, I., Gurtz, J., Teuling, A. J., Lang, H., Moser, U., Grebner, D., Menzel, L., Schroff, K., Vitvar, T., and Zappa, M. (2012a). Swiss prealpine Rietholzbach research catchment and lysimeter: 32 year time series and 2003 drought event. *Water Resources Research*, 48(6):W06526.

[146] Seneviratne, S. I., Lthi, D., Litschi, M., and Schr, C. (2006). Landatmosphere coupling and climate change in Europe. *Nature*, 443(7108):205–209.

[147] Seneviratne, S. I., Nicholls, N., Easterling, D., Goodess, C. M., Kanae, S., Kossin, J., Luo, Y., Marengo, J., Innes, K. M., Rahimi, M., Reichstein, M., Sorteberg, A., Vera, C., Zhang, X., Rusticucci, M., Semenov, V., Alexander, L. V., Allen, S., Benito, G., Cavazos, T., Clague, J., Conway, D., Della-Marta, P. M., Gerber, M., Gong, S., Goswami, B. N., Hemer, M., Huggel, C., den Hurk, B. V., Kharin, V. V., Kitoh, A., Tank, A. M. G. K., Li, G., Mason, S., Guire, W. M., Oldenborgh, G. J. V., Orlowsky, B., Smith, S., Thiaw, W., Velegrakis, A., Yiou, P., Zhang, T., Zhou, T., and Zwiers, F. W. (2012b). Changes in climate extremes and their impacts on the natural physical environment. In *Managing the Risks of Extreme Events and Disasters to Advance Climate Change Adaptation*, pages 109–230. Cambridge University Press, Cambridge.

[148] Serinaldi, F. (2016). Can we tell more than we can know? the limits of bivariate drought analyses in the united states. *Stochastic environmental research and risk assessment*, 30(6):1691–1704.

[149] Serinaldi, F., Bonaccorso, B., Cancelliere, A., and Grimaldi, S. (2009). Probabilistic characterization of drought properties through copulas. *Physics and Chemistry of the Earth, Parts A/B/C*, 34(1012):596–605.

[150] Sharma, S. and Mujumdar, P. (2017). Increasing frequency and spatial extent of concurrent meteorological droughts and heatwaves in india. *Scientific reports*, 7(1):15582.

[151] Sheffield, J., Wood, E. F., Chaney, N., Guan, K., Sadri, S., Yuan, X., Olang, L., Amani, A., Ali, A., Demuth, S., et al. (2014). A drought monitoring and forecasting system for sub-sahara african water resources and food security. *Bulletin of the American Meteorological Society*, 95(6):861–882.

[152] Sheffield, J., Wood, E. F., and Roderick, M. L. (2012). Little change in global drought over the past 60 years. *Nature*, 491(7424):435–438.

[153] Shepherd, T. G. (2014). Atmospheric circulation as a source of uncertainty in climate change projections. *Nature Geoscience*, 7(10):703.

[154] Shepherd, T. G. (2016). A common framework for approaches to extreme event attribution. *Current Climate Change Reports*, 2(1):28–38.

[155] Shiau, J. (2003). Return period of bivariate distributed extreme hydrological events. *Stochastic environmental research and risk assessment*, 17(1-2):42–57.

[156] Shiau, J.-T., Feng, S., and Nadarajah, S. (2007). Assessment of hydrological droughts for the yellow river, china, using copulas. *Hydrological Processes*, 21(16):2157–2163.

[157] Sklar, M. (1959). Fonctions de repartition an dimensions et leurs marges. *Publ. Inst. Statist. Univ. Paris*, 8:229–231.

[158] Sousa, P. M., Trigo, R. M., Pereira, M. G., Bedia, J., and Gutiérrez, J. M. (2015). Different approaches to model future burnt area in the iberian peninsula. *Agricultural and Forest Meteorology*, 202:11–25.

[159] Stadtherr, L., Coumou, D., Petoukhov, V., Petri, S., and Rahmstorf, S. (2016). Record balkan floods of 2014 linked to planetary wave resonance. *Science advances*, 2(4):e1501428.

[160] Stagge, J. H., Kingston, D. G., Tallaksen, L. M., and Hannah, D. M. (2017). Observed drought indices show increasing divergence across europe. *Scientific Reports*, 7(1):14045.

[161] Stammer, D., Ray, R., Andersen, O. B., Arbic, B., Bosch, W., Carrère, L., Cheng, Y., Chinn, D., Dushaw, B., Egbert, G., et al. (2014). Accuracy assessment of global barotropic ocean tide models. *Reviews of Geophysics*, 52(3):243–282.

[162] Sterl, A., Brink, H. v. d., Vries, H. d., Haarsma, R., and Meijgaard, E. v. (2009). An ensemble study of extreme storm surge related water levels in the north sea in a changing climate. *Ocean Science*, 5(3):369–378.

[163] Stöber, J., Joe, H., and Czado, C. (2013). Simplified pair copula constructionslimitations and extensions. *Journal of Multivariate Analysis*, 119:101–118.

[164] Stocker, T., Qin, D., Plattner, G., Tignor, M., Allen, S., Boschung, J., Nauels, A., Xia, Y., Bex, V., and Midgley, P. (2013). Ipcc, 2013: summary for policymakers in climate change 2013: the physical science basis, contribution of working group i to the fifth assessment report of the intergovernmental panel on climate change.

[165] Svensson, C. and Jones, D. A. (2004). Dependence between sea surge, river flow and precipitation in south and west britain. *Hydrology and Earth System Sciences Discussions*, 8(5):973–992.

[166] Switanek, M. B., Maraun, D., and Bevacqua, E. (2018). Multivariate statistical downscaling of precipitation and temperature fields. *In preparation.*

[167] Takayabu, I., Hibino, K., Sasaki, H., Shiogama, H., Mori, N., Shibutani, Y., and Takemi, T. (2015). Climate change effects on the worst-case storm surge: a case study of typhoon haiyan. *Environmental Research Letters*, 10(6):064011.

[168] Taylor, K. E., Stouffer, R. J., and Meehl, G. A. (2012). An overview of cmip5 and the experiment design. *Bulletin of the American Meteorological Society*, 93(4):485–498.

[169] Team, C. W., Pachauri, R., and Reisinger, A. (2007). Climate change 2007: Synthesis report. contribution of working groups i, ii and iii to the fourth assessment report of the intergovernmental panel on climate change. *IPCC, Geneva, Switzerland.*

[170] Team, R. C. (2016). R: A language and environment for statistical computing. r foundation for statistical computing, vienna, austria. 2014.

[171] Teuling, A. J., Van Loon, A. F., Seneviratne, S. I., Lehner, I., Aubinet, M., Heinesch, B., Bernhofer, C., Grnwald, T., Prasse, H., and Spank, U. (2013). Evapotranspiration amplifies European summer drought. *Geophysical Research Letters*, 40(10):2071–2075.

[172] Tisseuil, C., Vrac, M., Lek, S., and Wade, A. J. (2010). Statistical downscaling of river flows. *Journal of Hydrology*, 385(1-4):279–291.

[173] Tolman, H. (2014). The wavewatch iii development group, user manual and system documentation version 4.18. Technical report, NOAA/NWS/NCEP/MMAB.

[174] Törnros, T. and Menzel, L. (2014). Addressing drought conditions under current and future climates in the Jordan River region. *Hydrol. Earth Syst. Sci.*, 18(1):305–318.

[175] Trenberth, K. E., Dai, A., Schrier, G. v. d., Jones, P. D., Barichivich, J., Briffa, K. R., and Sheffield, J. (2014). Global warming and changes in drought. *Nature Climate Change*, 4(1):17–22.

[176] Trenberth, K. E., Fasullo, J. T., and Shepherd, T. G. (2015). Attribution of climate extreme events. *Nature Climate Change*, 5(8):725.

[177] Trigo, R. M., Ramos, C., Pereira, S. S., Ramos, A. M., Zêzere, J. L., and Liberato, M. L. (2016). The deadliest storm of the 20th century striking portugal: Flood impacts and atmospheric circulation. *Journal of Hydrology*, 541:597–610.

[178] Tsakiris, G. and Vangelis, H. (2005). Establishing a drought index incorporating evapotranspiration. *European Water*, 9(10):3–11.

[179] Tsimplis, M. and Woodworth, P. (1994). The global distribution of the seasonal sea level cycle calculated from coastal tide gauge data. *Journal of Geophysical Research: Oceans*, 99(C8):16031–16039.

[180] Van den Brink, H., Können, G., Opsteegh, J., Van Oldenborgh, G., and Burgers, G. (2005). Estimating return periods of extreme events from ecmwf seasonal forecast ensembles. *International Journal of Climatology*, 25(10):1345–1354.

[181] Van den Brink, H., Können, G., Opsteegh, J., van Oldenborgh, G. J., and Burgers, G. (2004). Improving 104-year surge level estimates using data of the ecmwf seasonal prediction system. *Geophysical Research Letters*, 31(17).

[182] van den Hurk, B., van Meijgaard, E., de Valk, P., van Heeringen, K.-J., and Gooijer, J. (2015). Analysis of a compounding surge and precipitation event in the netherlands. *Environmental Research Letters*, 10(3):035001.

[183] van Oldenborgh, G. J., van der Wiel, K., Sebastian, A., Singh, R., Arrighi, J., Otto, F., Haustein, K., Li, S., Vecchi, G., and Cullen, H. (2017). Attribution of extreme rainfall from hurricane harvey, august 2017. *Environmental Research Letters*, 12(12):124009.

[184] Van Vuuren, D. P., Edmonds, J., Kainuma, M., Riahi, K., Thomson, A., Hibbard, K., Hurtt, G. C., Kram, T., Krey, V., Lamarque, J.-F., et al. (2011). The representative concentration pathways: an overview. *Climatic change*, 109(1-2):5.

[185] Vandenberghe, S., Verhoest, N., Onof, C., and De Baets, B. (2011). A comparative copula-based bivariate frequency analysis of observed and simulated storm events: A case study on bartlett-lewis modeled rainfall. *Water Resources Research*, 47(7).

[186] Vautard, R., Yiou, P., D'andrea, F., De Noblet, N., Viovy, N., Cassou, C., Polcher, J., Ciais, P., Kageyama, M., and Fan, Y. (2007). Summertime european heat and drought waves induced by wintertime mediterranean rainfall deficit. *Geophysical Research Letters*, 34(7).

[187] Vicente-Serrano, S. M., Beguería, S., Lorenzo-Lacruz, J., Camarero, J. J., López-Moreno, J. I., Azorin-Molina, C., Revuelto, J., Morán-Tejeda, E., and Sanchez-Lorenzo, A. (2012). Performance of drought indices for ecological, agricultural, and hydrological applications. *Earth Interactions*, 16(10):1–27.

[188] Vicente-Serrano, S. M., Beguera, S., and Lpez-Moreno, J. I. (2009). A Multi-scalar Drought Index Sensitive to Global Warming: The Standardized Precipitation Evapotranspiration Index. *Journal of Climate*, 23(7):1696–1718.

[189] Vicente-Serrano, S. M., Lopez-Moreno, J.-I., Beguería, S., Lorenzo-Lacruz, J., Sanchez-Lorenzo, A., García-Ruiz, J. M., Azorin-Molina, C., Morán-Tejeda, E., Revuelto, J., Trigo, R., et al. (2014). Evidence of increasing drought severity caused by temperature rise in southern europe. *Environmental Research Letters*, 9(4):044001.

[190] Villarini, G., Smith, J. A., Baeck, M. L., Vitolo, R., Stephenson, D. B., and Krajewski, W. F. (2011). On the frequency of heavy rainfall for the midwest of the united states. *Journal of Hydrology*, 400(1-2):103–120.

[191] Vitolo, R., Stephenson, D. B., Cook, I. M., and Mitchell-Wallace, K. (2009). Serial clustering of intense european storms. *Meteorologische Zeitschrift*, 18(4):411–424.

[192] Volosciuk, C., Maraun, D., Semenov, V. A., Tilinina, N., Gulev, S. K., and Latif, M. (2016). Rising mediterranean sea surface temperatures amplify extreme summer precipitation in central europe. *Scientific reports*, 6:32450.

[193] Volpi, E. and Fiori, A. (2014). Hydraulic structures subject to bivariate hydrological loads: return period, design, and risk assessment. *Water Resources Research*, 50(2):885–897.

[194] Vousdoukas, M. I., Almeida, L. P. M., and Ferreira, Ó. (2012). Beach erosion and recovery during consecutive storms at a steep-sloping, meso-tidal beach. *Earth Surface Processes and Landforms*, 37(6):583–593.

[195] Vousdoukas, M. I., Mentaschi, L., Voukouvalas, E., Verlaan, M., and Feyen, L. (2017). Extreme sea levels on the rise along europe's coasts. *Earth's Future*, 5(3):304–323.

[196] Vousdoukas, M. I., Mentaschi, L., Voukouvalas, E., Verlaan, M., Jevrejeva, S., Jackson, L., and Feyen, L. (2018). Global probabilistic projections of extreme sea levels. *Submitted to Nature Communications*.

[197] Vousdoukas, M. I., Voukouvalas, E., Annunziato, A., Giardino, A., and Feyen, L. (2016). Projections of extreme storm surge levels along europe. *Climate Dynamics*, 47(9-10):3171–3190.

[198] Wahl, T., Jain, S., Bender, J., Meyers, S. D., and Luther, M. E. (2015). Increasing risk of compound flooding from storm surge and rainfall for major us cities. *Nature Climate Change*, 5(12):1093–1097.

[199] Wahl, T., Ward, P. J., Winsemius, H. C., AghaKouchak, A., Bender, J., Haigh, I. D., Jain, S., Leonard, M., Veldkamp, T. I. E., and Westra, S. (2018). When environmental forces collide. *Eos*, 99.

[200] Wand, M. P. and Jones, M. C. (1994). Multivariate plug-in bandwidth selection. *Computational Statistics*, 9(2):97–116.

[201] Ward, P. J., Jongman, B., Aerts, J. C., Bates, P. D., Botzen, W. J., Loaiza, A. D., Hallegatte, S., Kind, J. M., Kwadijk, J., Scussolini, P., et al. (2017). A global framework for future costs and benefits of river-flood protection in urban areas. *Nature climate change*, 7(9):642.

[202] Weisse, R., von Storch, H., Niemeyer, H. D., and Knaack, H. (2012). Changing north sea storm surge climate: An increasing hazard? *Ocean & coastal management*, 68:58–68.

[203] Widmann, M. (2005). One-dimensional cca and svd, and their relationship to regression maps. *Journal of Climate*, 18(14):2785–2792.

[204] Wu, W., McInnes, K., O'grady, J., Hoeke, R., Leonard, M., and Westra, S. (2018). Mapping dependence between extreme rainfall and storm surge. *Journal of Geophysical Research: Oceans*, 123(4):2461–2474.

[205] Zappa, G. and Shepherd, T. G. (2017). Storylines of atmospheric circulation change for european regional climate impact assessment. *Journal of Climate*, 30(16):6561–6577.

[206] Zarch, M. A. A., Sivakumar, B., and Sharma, A. (2015). Droughts in a warming climate: A global assessment of standardized precipitation index (spi) and reconnaissance drought index (rdi). *Journal of Hydrology*, 526:183–195.

[207] Zhang, X., Hegerl, G., Seneviratne, S., Stewart, R., Zwiers, F., and Alexander, L. (2014). Wcrp grand challenge: Understanding and predicting weather and climate extremes. Technical report, Tech. rep., World Climate Research Program, http://www. wcrp-climate. org/images/documents/grand_challenges/GC_Extremes_v2. pdf, White Paper.

[208] Zheng, F., Leonard, M., and Westra, S. (2015). Efficient joint probability analysis of flood risk. *Journal of Hydroinformatics*, 17(4):584–597.

[209] Zheng, F., Westra, S., Leonard, M., and Sisson, S. A. (2014). Modeling dependence between extreme rainfall and storm surge to estimate coastal flooding risk. *Water Resources Research*, 50(3):2050–2071.

[210] Zheng, F., Westra, S., and Sisson, S. A. (2013). Quantifying the dependence between extreme rainfall and storm surge in the coastal zone. *Journal of hydrology*, 505:172–187.

[211] Zijl, F., Verlaan, M., and Gerritsen, H. (2013). Improved water-level forecasting for the northwest european shelf and north sea through direct modelling of tide, surge and non-linear interaction. *Ocean Dynamics*, 63(7):823–847.

[212] Zotarelli, L., Dukes, M. D., Romero, C. C., Migliaccio, K. W., and Morgan, K. T. (2010). Step by step calculation of the penman-monteith evapotranspiration (fao-56 method). *Institute of Food and Agricultural Sciences. University of Florida.*

[213] Zscheischler, J., Orth, R., and Seneviratne, S. I. (2017). Bivariate return periods of temperature and precipitation explain a large fraction of European crop yields. *Biogeosciences Discuss.*, 2017:1–18.

[214] Zscheischler, J. and Seneviratne, S. I. (2017). Dependence of drivers affects risks associated with compound events. *Science Advances*, 3(6):e1700263.

[215] Zscheischler, J., Westra, S., Hurk, B. J., Seneviratne, S. I., Ward, P. J., Pitman, A., AghaKouchak, A., Bresch, D. N., Leonard, M., Wahl, T., et al. (2018). Future climate risk from compound events. *Nature Climate Change*, page 1.